Millennial-length tree-ring records: A basis for climate reconstruction and assessment of climate extremes and trends at local to global scales

Dissertation

zur Erlangung des Grades

"Doktor der Naturwissenschaften"

im Promotionsfach Geographie

am Fachbereich Chemie, Pharmazie und Geowissenschaften

der Johannes Gutenberg-Universität Mainz

Lara Klippel

geb. in Mainz

Mainz, den 4. April 2019

Tag der mündlichen Prüfung:

25. Juni 2019

Betreuer der Dissertation

Not available online

Summary

Over the last two decades, tree-rings have become one of the most important paleoclimatic archives in terms of studying high-resolution climate over the Common Era (CE) in the mid-to-high latitudes. Such analyses are crucial, not only to put current temperature and hydroclimatic changes in a long-term context, but also to assess the full range of natural and anthropogenic climate forcing. However, estimates of the first millennium remain poorly constrained due to a paucity of millennial-length tree-ring records, causing a spatial under-representation of some regions in larger-scale climate reconstructions and increasing uncertainty in the interpretation of climatic trends and extremes. Thus, a major activity towards the assessment of long-term climate dynamics at local to regional scales is the development of new millennial-length proxy records. This thesis addresses the aforementioned topic by (i) developing two millennial-length climate reconstructions based on tree-ring width (TRW) and maximum latewood density (MXD) measurements from *Pinus heldreichii* trees growing in the high-elevation environment at the tree line of Mount Smolikas in the Pindus Mountains in northern Greece and by (ii) assessing millennial-length temperature trends in tree-ring records in a global proxy database compiled by the PAGES 2k consortium to identify potential drivers that limit long-term temperature trends in tree-ring data. Calibration studies showed that *P. heldreichii* TRW is controlled by June-July precipitation and April temperatures, with differences in the climate signal of four sites arising from varying meltwater supply and exposure effects. MXD formation is controlled by summer temperatures. Climate signal strength of both parameters is particularly strong in the high-frequency spectrum, mirroring inter-annual climate variability patterns and thus allowing for a detection of climate extremes. Based on the standardized precipitation index and TRW, regional summer drought variability is reconstructed over the period 730-2015 CE. MXD of the trees is translated in an August-September temperature reconstruction covering the period 738-2014 CE. Regional high-resolution, annually resolved climate information is extended for the first time back into the first millennium, thus both reconstructions fill a temporal and spatial gap in a larger-scale hydroclimate and temperature reconstruction network in Europe. The records help to advance our understanding of climate variability over Europe, associated atmospheric processes, and external forcings. The PAGES 2k multiproxy database offers a new and unique opportunity to study the lack of long-term cooling trends in tree-ring data which can be expected in Northern Hemisphere summers, particularly in the high latitudes, due to orbitally driven changes in solar irradiance. Tests of different influencing factors reveal that preserving millennial-scale cooling trends related to orbital forcing is not feasible in most tree-ring datasets. This result is of great importance as it touches the current debate by showing that tree-ring data do not lack this trend as a consequence of inappropriate tree-ring standardization. Evaluation of the database provides a basis not only to improve future climate reconstructions, but also to enhance our understanding of long-term climate variations as well as to reduce associated uncertainties.

Zusammenfassung

Informationen aus Baumjahrringen haben sich in den letzten zwei Jahrzehnten zu einem wichtigen Paläoklimaarchiv in den gemäßigten und hohen Breiten entwickelt. Durch die annuelle Auflösung der Messungen können Klimaveränderungen mit einer hohen Präzision datiert und detektiert werden und sowohl längerfristige Klimatrends als auch abrupte Klimaveränderungen und -extreme identifiziert werden. Paläoklimatische Analysen sind nicht nur notwendig, um den gegenwärtigen Erderwärmungsprozess und die Zunahme von Trockenperioden zu studieren, sondern auch, um die Ausprägung dieser Entwicklungen im zeitlichen Kontext der letzten 2000 Jahre beurteilen zu können. Bislang beruhen globale oder hemisphärische Klimarekonstruktionen auf nur wenigen tausendjährigen Proxyzeitreihen, weshalb die Verlässlichkeit der Daten im ersten Jahrtausend n. Chr. reduziert ist. Einige Regionen sind nicht mehr im globalen Mittelwert vertreten und durch die Abnahme der Anzahl der Messungen nimmt die Unsicherheit in der Interpretation von Trends und Extremen zu. Rekonstruktionen müssen daher stetig weiterentwickelt und verbessert werden. Dies kann unter anderem durch die Entwicklung neuer Rekonstruktionen aus im globalen Mittel unterrepräsentierten Regionen sowie durch ein besseres Verständnis von bestehenden Datensätzen erreicht werden. Im Rahmen dieser Arbeit werden daher zwei neue tausendjährige Klimarekonstruktionen basierend auf Jahrringbreitemessungen und Jahrringdichtemessungen von *Pinus heldreichii,* die an der Waldgrenze von Mt. Smolikas im Pindosgebirge in Griechenland wachsen, entwickelt. Darüber hinaus wird anhand einer globalen Multiproxydatenbank (PAGES 2k) untersucht, warum Jahrringzeitenreihen gegenüber anderen Proxyarchiven, wie z.B. Eisbohrkernen, reduzierte Langzeittrends aufweisen.

Kalibrationsstudien haben gezeigt, dass das Jahrringbreitewachstum von *P. heldreichii* maßgeblich von den Niederschlägen im Juni-Juli und den Temperaturen im April bestimmt wird, wobei die Stärke des Klimasignals zwischen verschiedenen Standorten durch expositionsbedingte Strahlungsunterschiede sowie Schmelzwassereinflüsse variiert. Die Bildung der maximalen Spätholzdichte wird hingegen von der Sommertemperatur kontrolliert. Basierend auf einer hohen und zeitlich stabilen Kalibration wird die Jahrringbreitechronologie genutzt, um über den Zeitraum 730-2015 die regionale Niederschlagsvariabilität und extreme Trockenjahre zu rekonstruieren. Die Spätholzdichtechronologie wird in eine Rekonstruktion der August-September Sommertemperaturen transferiert, um wiederum lokale bis überregionale Temperaturextreme zu identifizieren (738-2014). Beide Zeitreihen leisten einen wesentlichen Beitrag, das Netzwerk an Paläoklimainformationen sowie das Verständnis über zugrundeliegende atmosphärische Muster und Klimaforcings im nordöstlichen Mittelmeerraum in räumlicher und zeitlicher Dimension zu erweitern.

Die Analyse der PAGES 2k Multiproxydatenbank eröffnet die Möglichkeit, das Fehlen eines präindustriellen Abkühlungstrends in zahlreichen Jahrringzeitreihen systematisch in der Nordhemisphäre zu untersuchen. Infolge von orbitalem Forcing, vor allem durch Veränderungen der Erdpräzession, nimmt die Sonneneinstrahlung auf der Nordhalbkugel im Sommer ab, was zu

niedrigeren Sommertemperaturen und damit verringertem Baumwachstum führt. Erwartungsgemäß sollte daher vor allem in sommertemperatursensitiven Proxys, wie den Jahrringen in den hohen nördlichen Breiten, ein Abkühlungstrend sichtbar sein. Verschiedene Tests haben jedoch gezeigt, dass es nicht möglich ist, diesen Trend zu erhalten und, dass nicht, wie allgegenwärtig angenommen wird, die Jahrringstandardisierung für das Fehlen des Trends verantwortlich ist. Durch das Aufzeigen von Stärken und Schwächen des Jahrringproxys wird zudem die Sensibilität erhöht, im Rahmen einer zukünftigen Datenauswahl die spektralen Eigenschaften verschiedener Proxys stärker zu berücksichtigen. Dies soll letztendlich dazu beitragen, eine Reduzierung von Trendunsicherheiten in Klimarekonstruktionen zu erreichen.

Acknowledgements

Not available online

Table of contents

1 | Introduction

Due to a lack of reliable instrumental precipitation and temperature measurements prior to the mid-19th century (Böhm *et al*. 2009), information about annual- to centennial-scale climate dynamics relies on indirect climate recorders, the so-called proxy archives, that store climatic information in their physical and chemical properties. The most abundant proxies (for review, see Wanner *et al*. 2008; Jones *et al*. 2009) are corals (Cooper *et al*. 2012), historical documents (Pfister *et al*. 1999), ice cores (Kinnard *et al*. 2011), lake and marine sediment cores (Nieto-Moreno *et al*. 2013), speleothems (Martín-Chivelet *et al*. 2011), and tree-rings (Esper *et al*. 2012). Proxy-derived high-resolution climate reconstructions over the Common Era, especially the past millennium, are crucial for putting the ongoing Anthropocene warming (Crutzen 2002) in a long-term context of natural climate variability (Büntgen *et al*. 2011) and for assessing whether the global warming of ~0.85 °C since 1880 (Hartmann *et al*. 2013) caused by an increased level of atmospheric greenhouse gases is unprecedented compared to past climatic changes (Morice *et al*. 2012). Proxy data provide independent information to test and evaluate climate simulations (PAGES 2k PMIP3 group 2015) and enable us to better constrain uncertainties in the projections of the predicted 21st century climate change (Braconnot *et al*. 2012; Deser *et al*. 2012). Further, knowledge of temperature variability and extremes during the last two millennia is important for evaluating the relative importance of different climate forcings over time, e.g. orbital, solar, volcanic and greenhouse gas forcing and land-cover changes, and for assessing the interplay between internal climate variability and the response to external forcing (Wanner *et al*. 2008). Multi-proxy temperature reconstructions have been produced at the global scale (Jones *et al*. 1998; Mann and Jones 2003; Loehle 2007; Mann *et al*. 2008) as well as for the Southern *(*Neukom *et al*. 2014) and Northern Hemisphere (Mann *et al*. 1999; Crowley and Lowery 2000; Moberg *et al*. 2005; Hegerl *et al*. 2007; Juckes *et al*. 2007; Ljungqvist 2010; Christiansen and Ljungqvist 2011; Christiansen and Ljungqvist 2012; Shi *et al*. 2013).

1 – 1 The importance of tree-ring data

Tree-rings are the most important proxy to reconstruct extratropical climatic variations in the growing season over the last centuries to millennia because they provide annual resolution and thus allow a very precise dating of climatic events, e.g. volcanic eruptions (Esper *et al*. 2013a). They are the most abundant proxy in the temperate and boreal zone (Fritts 1976), hence providing the basis for the reconstruction of hemispheric means (Schneider *et al*. 2015) as well as the reconstruction of spatial temperature anomaly patterns on annual to centennial scales (Anchukaitis *et al*. 2017).

The International Tree-Ring Data Bank (ITRDB; Grissino-Mayer and Fritts 1997), the community's platform to share proxy data, holds 7689 measurement datasets from 62 countries by December 2018 from Europe (2258), Asia (1583), North America (3330), South America (304), Africa (34), and

Australia (180), which demonstrates the potential inherent to this proxy in terms of global climate reconstruction with a high spatial and temporal resolution (Zhao *et al*. 2018).

Annual tree-ring formation in conifers is associated with seasonal climate fluctuations, inducing periods of cambial activity and dormancy (Fritts 1976). During the growing season (air temperature > 5°C; Rossi *et al*. 2007), cambial cell division, enlargement, and wall thickening (Plomion *et al*. 2001) cause stem diameter and biomass to increase and cells with different anatomical structure and function to form. Cells produced during spring and early summer form the light-coloured, so-called earlywood, which enables an efficient water uptake through less dense and thin-walled cells with a large lumen. The so-called latewood zone comprises thick-walled cells with high lignin content and reduced lumen size, growth which prioritizes structural strength over hydraulic function (Cherubini *et al*. 2004).

The majority of tree-ring data are TRW records produced by measurements of the annual radial increment of the earlywood and latewood. A more complex measure is MXD, determined by the ratio between cell wall thickness and cell size. The highest wood density is found in the latewood established toward the end of the growing season, before the tree enters a state of growth cessation (Rossi *et al*. 2007). MXD measurements are produced using x-ray densitometry. Prepared wood samples (further information in chapter 4) are exposed alongside a stepped calibration wedge of known density, and optical-density measurements obtained from the x-ray film image are transformed into estimates of wood density (Lenz *et al*. 1976; Schweingruber *et al*. 1988).

A robust climate signal can only be retrieved from trees growing in habitats with temperature or precipitation posing the growth-limiting factors (Fritts 1976). In cold environments, temperature regulates the length of the vegetation period (Rossi *et al*. 2007), thus favourable conditions prolong the time for cell production, resulting in wide rings with a very dense latewood. Vice versa, cooler conditions shorten the vegetation period and cause the formation of narrow and less dense rings. In arid environments, water availability and water uptake regulate cell formation processes, causing a growth cessation during phases of water-limitation (Akkemik and Aras 2005; Touchan *et al*. 2005; Akkemik *et al*. 2008). Extreme cold years are hence captured as extremely narrow and/or less dense rings whereas warm climate anomalies are associated with wide rings and a higher density.

Refined knowledge and an improved understanding of the full range of past extratropical Northern Hemisphere summer temperature variability solely based on tree-ring data was contributed by Briffa (2000), Esper *et al*. (2002), D'Arrigo *et al*. (2006), Schneider *et al*. (2015), Stoffel *et al*. (2015), and Wilson *et al*. (2016). At the hemispheric scale, temperature extremes have been studied only in response to volcanic eruptions (Schneider *et al*. 2015), but comprehensive studies about past climatic extremes, associated external forcings and atmospheric patterns, as well as their implications for human societies have been increasingly established at the regional or local scale (Esper *et al*. 2013b, Tejedor *et al*. 2016).

1 – 2 A short review of activities of the PAGES 2k network

Within the context of studying global temperature changes of the past 2000 years, the Past Global Changes community (PAGES; http://www.pages-igbp.org/ini/wg/2k-network/intro) introduced the 2k network project to coordinate and integrate regional efforts to assemble proxy observations and climate reconstructions. In the first phase (2008-2013), nine regional groups, spanning eight continents and the global ocean, were established with the goal of generating a global array of regional temperature reconstructions covering the last 2000 years. It has been shown that at multidecadal to centennial scales past global temperature changes have a strong regional expression and that a global Medieval Warm Period (MWP) or Little Ice Age (LIA) are absent (PAGES 2k 2013 Consortium).

During the second phase (2014-2016), efforts focused on proxy data-model comparisons, large-scale climate analysis, and the evolution of the first database by integrating new proxies and sites to expand the temporal and spatial coverage. A joint analysis of the PAGES 2k regional reconstructions with state-of-the-art model simulations shows that temperature reconstructions and models agree in the Northern Hemisphere, but disagree in the Southern Hemisphere (PAGES 2k PMIP3 group 2015). In a synthesis of 57 marine-origin sea surface temperature reconstructions generated by the regional group Ocean 2k, a global ocean cooling trend over the pre-industrial Common Era has been identified (McGregor *et al*. 2015) and analysis of the regional PAGES 2k temperature reconstructions reveals an onset of industrial-era warming earlier than previously suggested from historical observations (Abram *et al*. 2016). Further, in a unique, community-wide effort, the database was expanded. The updated version is currently the world's largest collection of multiple proxy records covering the Common Era (PAGES 2k Consortium 2017) and integrates 692 temperature-sensitive proxy records from trees (415 records), ice cores (49), lake (42) and marine sediments (58), corals (96), documentary evidence (15), sclerosponges (8), speleothems (4), boreholes (3), bivalves (1), and a tree/borehole hybrid (1) from all continents (PAGES 2k Consortium 2017).

Phase 3 (2017-2020) seeks to further develop collaboration with other research communities and initiatives, such as the World Climate Research Program (WCRP) and the Intergovernmental Panel on Climate Change (IPCC), as well as to reduce uncertainties in the interpretation of paleotemperature information. Further, it is planned to expand joint analysis of climate model simulations and reconstructions and to develop the understanding of mechanism driving regional climate variability (http://www.pastglobalchanges.org).

1 – 3 Objectives and structure of this dissertation

One of those designated PAGES 2k regions is Europe. A European June-August temperature reconstruction, which relies on ten (near) millennial-length temperature sensitive tree-ring records and one documentary index series, was produced at the end of phase I of the network 2k project (PAGES

2k Consortium 2013). Five of the tree-ring records are based on MXD data (Jämtland, Lötschental, NorthScan, Pyrenees, Torneträsk) that contain a substantially enhanced climate signal compared to TRW data (Albania, Carpathians, French Alps, Central Alps, Tatra) as shown by the analysis of the network's temperature sensitivity (Figure 1–1 and Table 1–1). Correlation coefficients with regional instrumental temperature data decline from $r > 0.6$ in northern Scandinavia (MXD) and Central Europe (MXD or TRW) to $r \sim 0.55$ in the western Mediterranean (MXD) and $r < 0.5$ in the eastern Mediterranean region (TRW) (Figure 1–1). However, much shorter eastern Mediterranean MXD chronologies developed for the Mt. Olympus region in Greece (1521-2010; Klesse *et al*. 2015), the Pirin Mountains in Bulgaria (1768-2008; Trouet *et al*. 2012), multiple sites in the northeastern Mediterranean basin (1675-1980; Trouet 2014), and Italy (1650-1980; Leonelli *et al*. 2017), demonstrate that MXD contains a significant summer temperature signal ($r > 0.6$). The spatial patterns clearly indicate the need for developing millennial-length MXD chronologies in southeastern Europe.

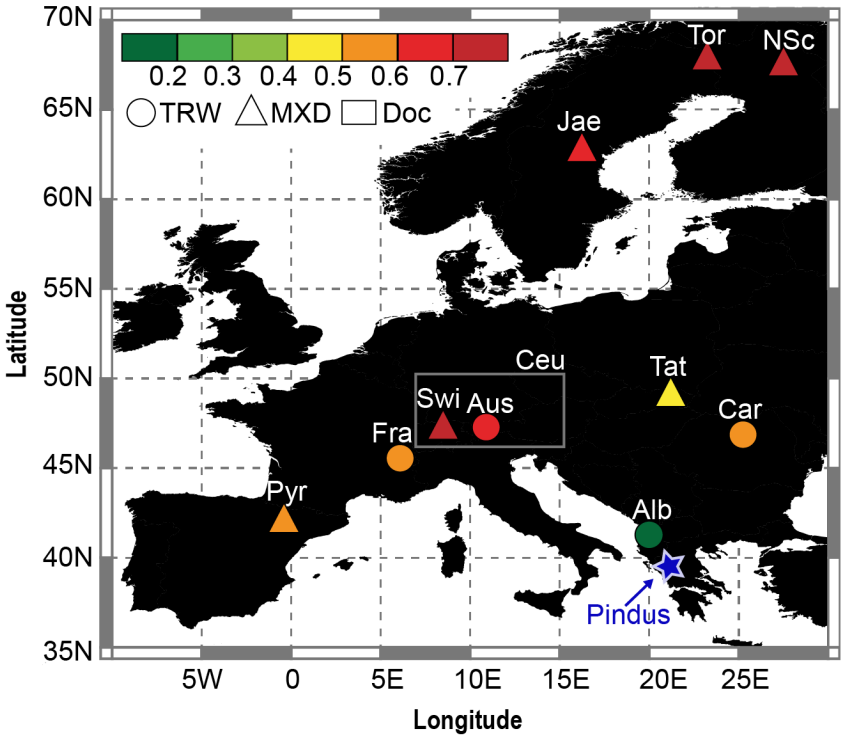

Figure 1–1 | European PAGES 2k network including 10 (near) millennial-length temperature sensitive TRW or MXD chronologies, and one documentary index record (PAGES 2k Consortium 2013). Coloured dots and triangles refer to the correlation with local instrumental summer temperatures provided in the original publications (Table 1–1). The blue star indicates the location of the new study site presented in this dissertation.

In the chapters 2-4, a network of high-elevation *P. heldreichii* sites from Mt. Smolikas, the highest peak in the Pindus Mts. in northern Greece, is presented. The species is abundant in the high mountains of the Balkans and survives in very old stands containing individuals of millennial age

which demonstrates the potential of these sites to contribute to high-resolution paleoclimatology and to expand knowledge of annually resolved natural climate variability in southeastern Europe. One of the main topics of this thesis will be the development of a millennial-length MXD chronology based on *P. heldreichii* samples from the Pindus Mts. and the assessment of inherent climate signals to finally establish a millennial-length summer temperature reconstruction for southern Europe.

Table 1–1 | PAGES 2k network of 10 temperature sensitive tree-ring records and one documentary index record (DOC) used to establish a regional European summer temperature reconstruction (PAGES 2k Consortium 2013).

Site	Code	Country	Proxy	Period	Reference
Albania	**Alb**	Albania	TRW	968-2008	Seim *et al*. 2012
Central Alps	**Aus**	Austria	TRW	-500-2003	Büntgen *et al*. 2011
Carpathians	**Car**	Romania	TRW	1163-2005	Popa and Kern 2009
Central Europe	**Ceu**	Germany, Switzerl., Czech Republic	DOC	1500-2007	Dobrovolný *et al*. 2010
French Alps	**Fra**	France	TRW	969-2007	Büntgen *et al*. 2012
Jämtland	**Jae**	Sweden	MXD	1107-2007	Gunnarson *et al*. 2011
NorthScan	**NSc**	Finland	MXD	-138-2006	Esper *et al*. 2012
Pyrenees	**Pyr**	Spain	MXD	1260-2005	Büntgen *et al*. 2008
Lötschental	**Swi**	Switzerland	MXD	755-2004	Büntgen *et al*. 2006
Tatra	**Tat**	Slovakia	TRW	1040-2011	Büntgen *et al*. 2013
Torneträsk	**Tor**	Sweden	MXD	500-2004	Melvin *et al*. 2013

Chapter 2, "*High-elevation inter-site differences in Mount Smolikas tree-ring width data*", presents the analysis of climate signals preserved in 382 *P. heldreichii* TRW series from Mt. Smolikas. Four site chronologies were developed to detect the influence of slope exposition on tree-growth and on climate sensitivity. Results are discussed in terms of a possible usage for climate reconstruction, because due to the record length, great potential is given to prolong regional climate history for more than 800 years. The analysis is continued in chapter 3 "*A 1286-year hydro-climate reconstruction for the*

Balkan Peninsula". It has been shown that especially summer precipitation has significant growth implications at higher frequencies, thus based on the network of the *P. heldreichii* sites, regional summer drought variability was reconstructed for the period 730-2015 CE. The study's focus on the detection of severe drought events and changes in their magnitude and frequency over the last millennium. In chapter 4, "*A 1200+ year reconstruction of temperature extremes for the northeastern Mediterranean region*", the first millennial-length MXD record is developed because, compared to TRW, MXD shows a substantially enhanced temperature sensitivity at annual to multi-decadal scales. The new record is currently the regionals' best replicated product in the first millennium. The new reconstruction of August-September temperatures focusses on the detection of summer temperature extremes and associated changes in the intensity and frequency over the Common Era.

With the release of the updated PAGES 2k database v2.0.0 in 2017 (PAGES 2k Consortium 2017), new potential for climate reconstructions at continental, hemispheric, and global scales is given. The amount, spatial distribution, and diversity of the data provide an unprecedented opportunity to analyse regional to large-scale temperature patterns over the Common Era. Thus, chapter 5, "*Differing pre-industrial cooling trends between tree-rings and lower-resolution temperature proxies*", shifts the focus from the regional-scale of chronology development to the assessment of Northern Hemisphere millennial-scale temperature trends preserved in best-replicated archives: tree-rings, ice cores, marine and lake sediments over the pre-industrial period 1-1800 CE. From a forcing perspective, we expect cooling trends across the Northern Hemisphere (NH) summers, particularly in the high latitudes, due to orbitally driven changes in solar irradiance. However, long-term cooling trends are only retained in ice cores, glacier ice, and marine sediments, but not in tree-rings. Several hypotheses are tested to explore this difference, including the effects of location (high NH latitudes vs. mid latitudes), season (annual vs. summer), tree-ring detrending (methods to remove non-climatic noise), and varying temperature sensitivity (high vs. low).

2 | High-elevation inter-site differences in Mount Smolikas tree-ring width data

Lara Klippel[1], Paul J. Krusic[2, 3, 4], Robert Brandes[5], Claudia Hartl-Meier[1], Valerie Trouet[6], Matthew Meko[6], Jan Esper[1]

[1]*Department of Geography, Johannes Gutenberg University, Mainz, Germany*

[2]*Department of Geography, University of Cambridge, Cambridge, UK*

[3]*Navarino Environmental Observatory, Messina, Greece*

[4]*Department of Physical Geography, Stockholm University, Stockholm, Sweden*

[5]*Department of Geography, Friedrich-Alexander University, Erlangen, Germany*

[6]*Laboratory of Tree-Ring Research, University of Arizona, Tucson, USA*

Dendrochronologia, 2017, published

2 – 1 Introduction

Tree-ring width (TRW) chronologies are an important proxy for the reconstruction of climate variability over the past millennium (Esper *et al*. 2016). Information about past climate conditions and their implications for society improve our understanding of natural and anthropogenically driven climate variability (Büntgen *et al*. 2011). This is crucial in the development of future climate scenarios and the evaluation of potential social and environmental impacts of climate (Esper *et al*. 2004; Kovats *et al*. 2014). Continuous improvement of the spatial coverage by millennium-length TRW chronologies is needed to assess climate variability patterns and their association with forcings at regional (Köse *et al*. 2011; Trouet *et al*. 2012; Seftigen *et al*. 2013) and hemispheric scales (Esper *et al*. 2002; D'Arrigo *et al*. 2006; Schneider *et al*. 2015; Stoffel *et al*. 2015; Wilson *et al*. 2016). *Pinus heldreichii* CHRIST (or Bosnian pine) is a Tertiary relict tree species, endemic to the high mountains of the Balkans, and is abundant in northern Greece, western Bulgaria, Bosnia-Herzegovina, and Albania (Brandes 2007). The species survives in very old stands with individuals of millennial age (Konter *et al*. 2017) demonstrating the potential of these sites to contribute to high-resolution paleoclimate reconstruction. The wood of *P. heldreichii* is very resinous and consequently resistant to decay and decomposition. This characteristic is beneficial for preserving material from fallen trees, especially in remote areas of the timberline ecotone (Brandes 2007). Numerous Bosnian pine chronologies have been developed from collections in various areas of the species' range. These extant chronologies have two common features: they are typically very long, and the climate signal from their TRW measurements is weak (maximum $r_{1901\text{-}2012} = -0.29$ with June-July temperature in Seim *et al*. (2012); $r_{1925\text{-}2000} = 0.29$ with April Temperature in Todaro *et al*. (2007); $r_{1934\text{-}2004} = 0.38$ with previous August precipitation, and $r_{1985\text{-}1992} = \sim -0.3$ with June temperature in Panayotov *et al*. (2010). The species is resistant to a rough mountain climate and can tolerate harsh winters as well as a certain degree of summer drought. Therefore, the existence of the pure, zonal *P. heldreichii*-stands in northern Greece is explained by the seasonal extremes of a low latitude mountain climate (Brandes 2007).

Theories explaining the low climate sensitivity are diverse and encompass anthropogenic activity, the remoteness of meteorological stations, and mixed climate controls (Todaro *et al*. 2007; Panayotov *et al*. 2010; Seim *et al*. 2012). However, most previous studies did not consider site-specific ecological constraints as influences on climate signals (Holland and Steyn 1975; Schweingruber 1996). Near to the Greek border with Albania, Mount Smolikas (2637m a.s.l.) crowns the mountain range of the northern Pindus Mountains at 40°05´N/20°55´E (Figure 2–1a and Figure 2–1b). The sites in this study are situated around an eastern foothill of Mt. Smolikas and differ in exposure only (Figure 2–1a). Slope aspect alters the amount of received solar radiation and length of insolation period, thus creating a range of microclimates on a small spatial scale (Urban *et al*. 2000; Gallardo-Cruz *et al*. 2009; Hartl-Meier *et al*. 2014; Hartl-Meier *et al*. 2015). Insolation controls evapotranspiration, soil and air temperature, air humidity, soil moisture, and the duration of the growing period that in turn affects the species composition and biomass production (Pook and Morre 1966; Paudel and Vetaas 2014; Måren

et al. 2015). In the Mediterranean, south-facing slopes receive the most sunlight, which supports evapotranspiration and results in drought stress for trees, whereas north-facing slopes retrain more humidity and favour growth (Stenberg and Shoshany 2001).

In this study, we explore the effect of slope exposure on tree growth and the impact on potentially varying climate signals by calibrating the chronologies of four differently exposed, high elevation *P. heldreichii* sites against regional instrumental temperature and precipitation data. We introduce a preliminary millennium-length TRW dataset and evaluate its potential and limitations for establishing a climate reconstruction.

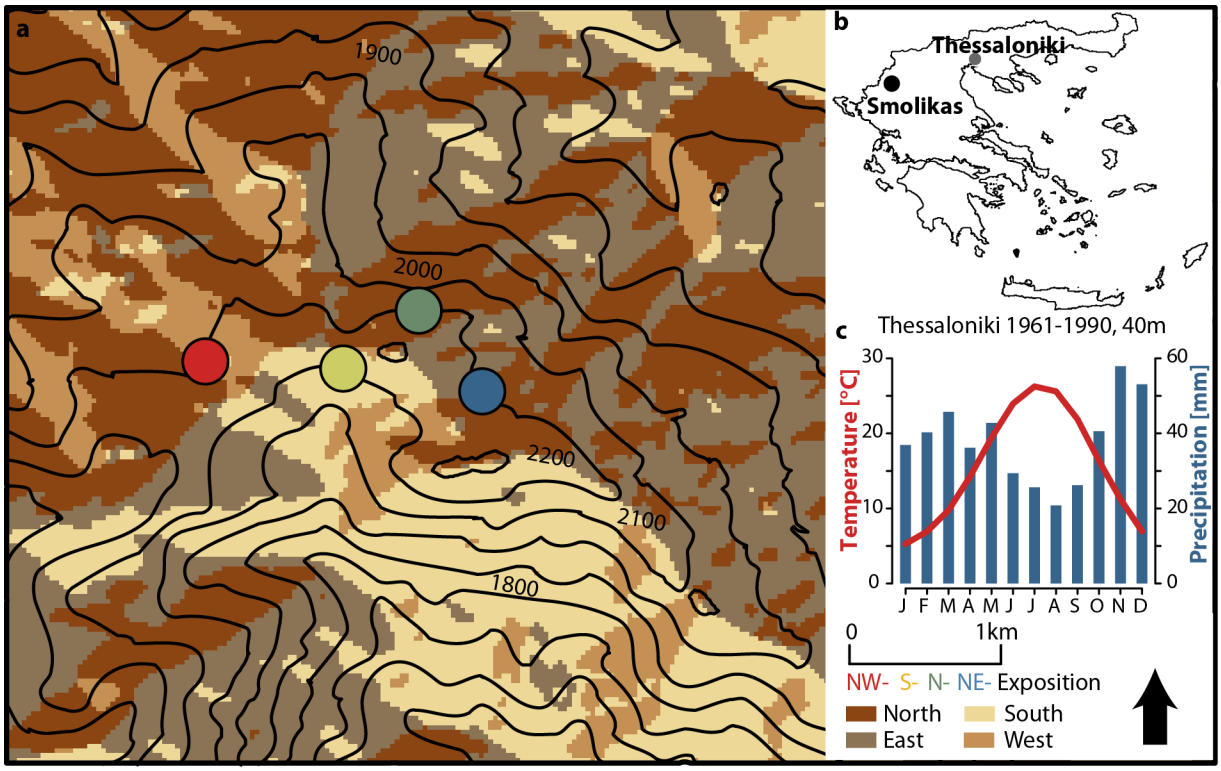

Figure 2–1 | a Contour and site exposure map of the study region and position of the sampling sites; **b** map of Greece indicating the research area and the instrumental station. **c** Climate diagram of the meteorological station in Thessaloniki (40m a.s.l., 1961-1990).

2 – 2 Material and methods

2 – 2.1 Geographical settings and sampling design

In northern Greece, *P. heldreichii* is native to the upper oro-mediterranean vegetation zone and appears first at ca. 1.000m a.s.l. in mixed forests with *Fagus sylvatica* L., *Pinus nigra* J.F. Arnold, and *Abies borisii-regis* Mattf. Between 1.500-2.300m a.s.l., *P. heldreichii* forms pure stands to the timberline, with dwarfed specimens reaching 2.600m a.s.l. on Mt. Olympus (Brandes 2007). The southern distribution limit of the species is near the village Metsovo, in the Pindus Mts., at 39°40´N.

On Mt. Smolikas, the zone of pure *P. heldreichii* stands starts at 1.300-1.500m a.s.l. and transforms into an open timberline ecotone at 1.900-2.400m a.s.l. (Brandes 2007). Anthropogenic impacts are presently constrained to pastoral farming. However, the name Mt. Smolikas, originating from the Slavic word "Smola" (engl. tar), points to a much greater economic importance of the area in the past, when the *P. heldreichii* resins were extracted for tar production (Meiggs 1982). Geologically the higher areas of the mountain are formed by serpentine, a dry bedrock poor in nutrients, but not karstified or fissured (Stevanovic *et al.* 2003; Hughes *et al.* 2006). *P. heldreichii* grows on dry substrate, such as limestone and serpentine rocks.

Between 2011 and 2015, 101 living and 92 dead *P. heldreichii* trees were sampled in this timberline ecotone in 2100-2200m a.s.l. at four differently exposed (NW, S, N, NE) sites on the eastern flanks and foothills of Mt. Smolikas (Figure 2–2a). The climate in this elevation is characterized by hard, snowy winters with intense frost and snow melt occurring only in late spring. Summer dryness, typical for the Mediterranean climate, is reduced in northern Greece to less than three months (June to August). In addition to this, summer storms, which yield heavy rainfall, often moderate the hygrothermic summer conditions on Mt. Smolikas (Fotiadi *et al.* 1999; Loukas *et al.* 2002).

2 – 2.2 Chronology development, standardization and statistics

All disks and cores were prepared following standard dendrochronological techniques to produce fine-sanded surfaces for micrometre measurement (Strokes and Smiley 1968). Tree-ring widths were measured in two labs by two different measuring systems; in Stockholm the Velmex System (Velmex Inc., Bloomfield, NY, USA) with an accuracy of 0.001 mm was used, and in Mainz the Lintab system with an accuracy of 0.01 mm was used (Rinn 2003). Dating and measurement quality control was performed by skeleton plotting (Strokes and Smiley 1968) and statistical cross-dating with the program COFECHA (Holmes 1983). A data adaptive power transformation was applied to reduce the heteroscedastic structure of the TRW series (Cook and Peters 1997; Büntgen *et al.* 2005) and the subsequent series were standardized by calculating residuals from cubic smoothing splines with a 50% frequency-response cut-off at 300 years (Cook and Peters 1981) using the software ARSTAN (Cook 1985; Cook and Krusic 2016). Based on the number of samples and the average correlation coefficients among the individual series (Rbar), variance stabilization was applied to all site chronologies (Frank *et al.* 2007). This standardization approach emphasizes inter-annual to multi-decadal variations, and minimizes centennial and longer trends (Cook *et al.* 1995). The final site TRW chronologies and composite TRW chronology were developed by calculating the robust bi-weight mean of tree-ring indices of each calendar year and truncated at the minimum sample size of < 5 series (Cook 1985). Growth and chronology characteristics were analysed based on several statistical parameters using raw and standardized series. The running Rbar expresses the mean interseries correlation (Fritts 1976) and the expressed population signal (EPS) describes the strength of the common variance within a chronology (Speer 2010). A widely accepted level, indicating the reliability

of the common signal, is 0.85. Both statistics were calculated for 30-year segments with 15 years overlap. Average growth rates (AGR) were analysed for the first 300 years of living trees, which allows an inter-site growth comparison by reducing the influence of different age-structures. The establishment of regional curves (RC), empirically defined biological age/growth stand curves, permits further inter-site growth comparison (Briffa *et al*. 1992).

Climate-growth relationships were assessed using instrumental monthly and seasonal temperature and precipitation data from the Thessaloniki (40.52°N/23.00°E, 40m a.s.l.; Figure 2–1c) and Larissa meteorological stations (39.62°N/22.42°E; 74m a.s.l.). We recognize that the dryer and warmer climate in these eastern cities does not ideally represent the temperature and precipitation of the study site, however, the more proximal stations (e.g. Metsovo and Ioannina) could not be used for analysis due to their low data coverage. A spatial correlation analysis was computed between tree-ring chronologies and high-resolution 0.25° gridded E-OBS climate data (1950-2014; Horvat *et al*. 1974) to explore the local and regional climate responses. All meteorological data were retrieved from the Royal Netherlands Meteorological Institute's (KNMI) Climate Explorer (https://climexp.knmi.nl; van Oldenborgh 2005; Trouet and van Oldenborgh 2013).

High-frequency climate signal tests were performed to verify the strength of the tree-growth/climate relationship (Büntgen *et al*. 2008; Konter *et al*. 2015). A high-pass filter was applied by calculating the residuals between the standardized TRW, temperature, and precipitation time series and their corresponding 10-year cubic smoothing splines. Correlations between site chronologies and instrumental data were computed from the previous-year June to the current-year September, as well as for seasonal means of two, three, and four months (not all displayed). To test the climate signals' temporal stability, 31-year moving window correlations, between the maximum responding months or seasons and tree-ring indices, were calculated. Correlation maps were produced based on the original and first-differenced climate data to evaluate the spatial signal patterns at high and low frequencies.

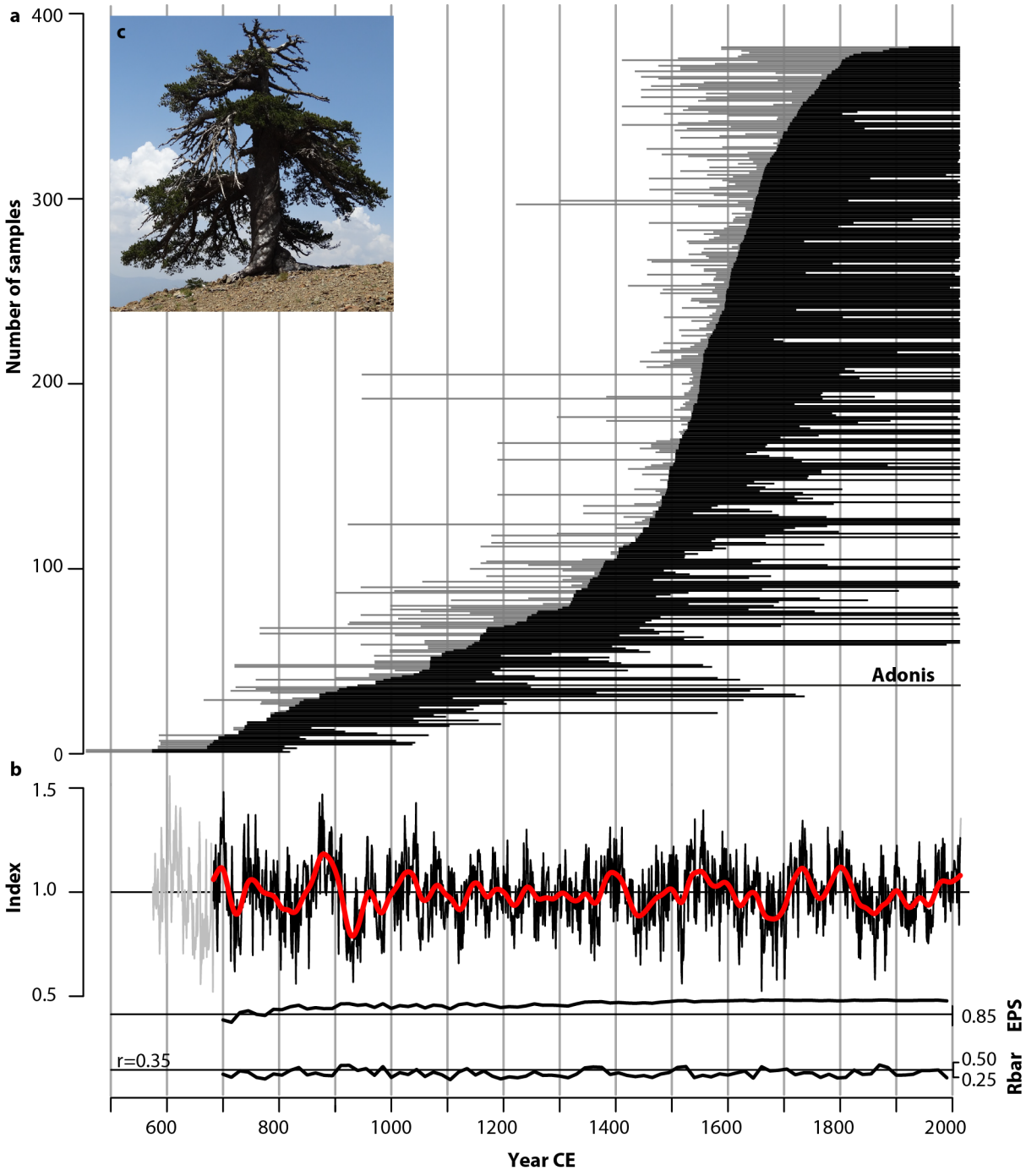

Figure 2–2 | Chronology characteristics: **a** temporal distribution of 382 core and disk samples encompassing 133017 measured tree rings from 4 sites. One bar represents an individual sample; the black section indicates the measured length and the grey section displays a pith-offset estimate; **b** power transformed 300-year spline detrended Smolikas *P. heldreichii* TRW chronology (black, n < 5 grey) and corresponding 50-year spline (red) with EPS and Rbar statistics computed for 30-year segments with 15 years of overlap in the bottom panels and **c** *Adonis*, a Bosnian pine, dendrochronologically dated to be 1075 years old and therefore currently the oldest living inhabitant in Europe.

2 – 3 Results

2 – 3.1 Intra- and inter-site growth characteristics

The Mt. Smolikas composite chronology contains annual to multi-decadal scale fluctuations (Figure 2–2b). The number of single TRW measurement series integrated in this record changes considerably through time, from only ≤ 5 series in 683 to 31 series in 1000, and 185 series in 2014. Coherency among the individual TRW measurement series, expressed by the inter-series correlation, is moderate (mean Rbar = 0.35) but temporally robust, and indicates the potential of the Smolikas record for high-resolution climate reconstruction back to the first millennium. Mean chronology age calculated for each year over the period 575-2014 is fairly balanced prior to 1700, but increases towards the present, largely due to the integration of artificially younger remnant samples, a consequence of weathering, and consideration of samples from relatively old living trees. Biologically young trees, between 50 and 200 years, are underrepresented in the chronologies (Esper *et al*. 2016). Of the 15 cores with more than 700 rings, the longest is a living tree series containing 1075 rings, spanning the period 941 to 2015, and the longest relict series contained 865 rings, spanning the period 873-1737 (Figure 2–2a). On multi-decadal scales, TRW index values increase during 920-1050, 1420-1540, 1650-1740 and 1850-2014, and decrease during 880-920, 1550-1690, and 1800-1850. The multi-decadal intervals of above-average growth characterizing the mid-16th century coincide with an increased regeneration, as many trees started growing in this period, likely indicating favourable climatic conditions (Figure 2–2a).

Table 2–1 | Descriptive statistics of the four Mt. Smolikas site chronologies.

Site	Period CE	Chrono CE	MSL (yrs)	n tree	n core	AGR	EPS (yrs)	AC[a]	SD[a]	MS[a]	Rbar[a]
NW	673-2014	740-2014	427	67	126	0.94	980	0.76	0.30	0.23	0.38
S	575-2014	1070-2014	316	57	111	0.75	1315	0.73	0.32	0.27	0.36
N	1425-2014	1550-2014	296	23	46	0.84	1610	0.73	0.32	0.22	0.33
NE	685-2014	1414-2014	308	47	99	0.70	1440	0.73	0.30	0.29	0.42
all	575-2014	683-2014	348	194	382	0.82	730	0.74	0.31	0.23	0.34

MSL: mean segment length, AGR: average growth rate of the first 300 years of growth from living trees, year until EPS is > 0.85, AC: first-order autocorrelation, SD: standard deviation, MS: mean sensitivity, Rbar: interseries correlation, [a] common period n > 5.

The lengths of site chronologies (n > 5 samples) range from 464 years at the N-exposed site to 1274 years at the NW-exposed site. Mean segment length varies between 296 years at the N- and 427 years at the NW-exposed site (Table 2–1). The sites are robust (EPS ≥ 0.85) after 980 at the NW-exposed

site, 1315 at the S-exposed site, 1610 at the N-exposed, and 1440 at the NE-exposed site. Trees at the NE-exposed site display the highest mean sensitivity, the highest Rbar, and the lowest average growth rate, which suggests a strong preservation of climatic information in high-frequency TRW variations. The opposite is true for trees at the N-exposed site, where the average growth rate is highest but the mean sensitivity and Rbar are lowest. In addition, moderate inter-site correlations ranging from r = 0.56 to 0.89 among the raw chronologies, and from r = 0.65 to r = 0.87 among the standardized chronologies over the 1550-2014 common period, point to substantial site-specific growth variations. The NW-, S- and N-exposed stands show an overall strong inter-site agreement, whereas their correspondence with the NE-exposed stand is surprisingly low.

The existence of heterogeneous growth rates, despite similar segment lengths, suggests there exists non-age-related inter- and intra-site differences (Figure 2–3a). Biological growth rates for the first 300 years differ remarkably among sites despite the removal of remnant wood with uncertain pith-offset estimates (Figure 2–3b). At the NW- and N-facing stands, the median and mean growth rates are significantly higher than at the S- and NE-facing stands. Intra-site variance of AGR is lower than inter-site variance, but single values largely overlap. The cambial age-alignment and subsequent averaging of the individual series to regional curves exhibits pronounced site differences, however (Figure 2–3c). The regional curves have the same decreasing course through time, except for the first 150 years of growth at the NW-facing site, and the first 100 years of growth at the S-facing site. The absolute growth level differs at every point of cambial age, whereas it is persistently higher at the N- and NW- facing stands, and lower at the S- and NE- facing stands. The decline through time is a lifelong phenomenon and is still apparent after more than 800 years (Figure 2–3c).

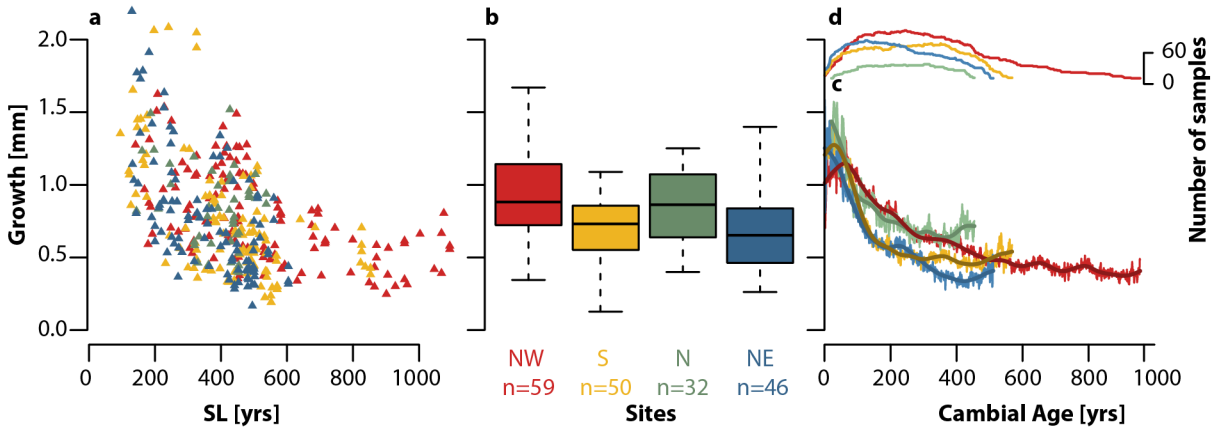

Figure 2–3 | Site-related growth characteristics: **a** growth rate to segment length (SL) ratio and **b** growth rates over the first 300-years of living trees and **c** RCs (thin) and corresponding 100-year splines (bold) when n> 10 series and **d** number of samples incorporated in RCs.

2 – 3.2 Climate signals

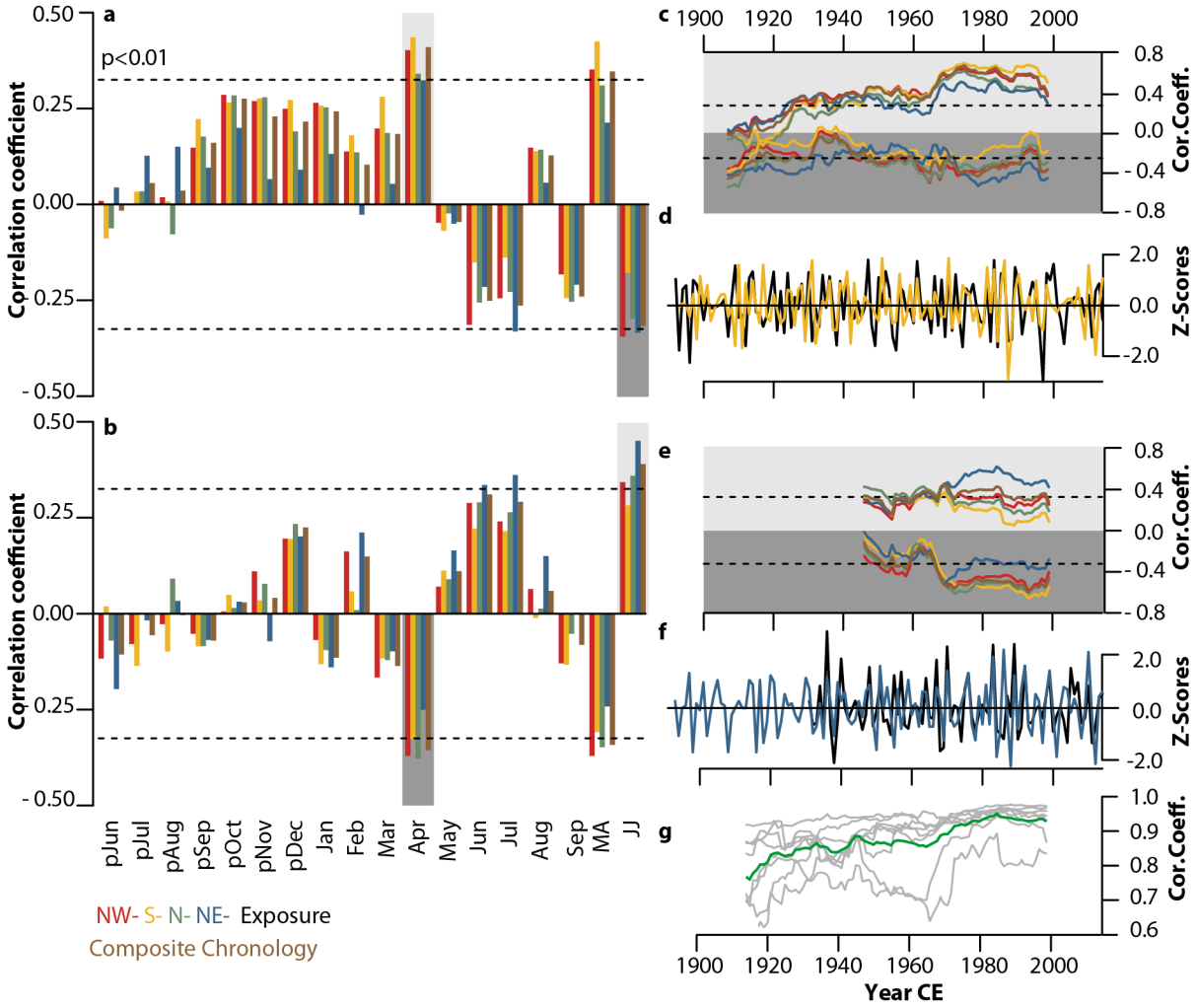

Figure 2–4 | Correlation coefficients of power transformed 300-year spline detrended and 10-year high-pass filtered site chronologies with 10-year high-pass filtered monthly **a** temperature and **b** precipitation data from the meteorological station in Thessaloniki (40.52°N/23.00°E; 40m a.s.l.) for the period 1931-2014. Dashed lines indicate $p < 0.01$; 31-year moving window correlations for the maximum responding month April and season June-July respectively for **c** temperature and **e** precipitation; Z-Scores of the maximum responding site chronology and **d** April temperatures (black) and **f** June-July precipitation (black); **g** 31-year moving window correlation coefficients between monthly temperature data (March to October, grey lines) from the meteorological stations in Thessaloniki and Larissa (39.63°N/22.42°E; 74m a.s.l.) and its mean (green).

In the high-frequency domain (high-pass filtered data), tree growth at the four sites at Mt. Smolikas is significantly controlled by climate in April and June-July (Figure 2–4). The climatic responses synchronize seasonally between the four sites: inter-site differences are relatively small compared to monthly and seasonal differences. At all sites, TRW is positively correlated with early summer (June-July) precipitation and negatively with early summer temperatures, whereas in spring (April) the signs are reversed. Previous years' precipitation and summer temperatures, as well as the current years'

May, August, and September's climate, have no significant growth control. Though the relationships are not significant, temperatures in the previous years' autumn and winter are positively correlated with TRW. Despite the synchronized growth/climate response pattern, some site-specific differences exist: The S-facing stand shows greatest response, and the NE-facing stand weakest response, to April temperatures ($r_{1931\text{-}2014} = 0.32$ to 0.44). These tendencies are reversed in June and July, when the S-facing stand shows the lowest and the NE-facing stand the highest response to June-July precipitation ($r_{1931\text{-}2014} = 0.28$ to 0.45). Precipitation in April ($r_{1931\text{-}2014} = -0.25$ to -0.38) and temperature in June-July ($r_{1931\text{-}2014} = -0.18$ to -0.34) are significantly anticorrelated with growth (Figure 2–4a and Figure 2–4c). The post 1950 climate correlation coefficients are temporally stable (Figure 2–4c to Figure 2–4f).

A period of relatively weak correlations prior to this date is followed by strengthened relationships; a systematic shift that occurs independently of the site and month. Splitting the 1931-2014 period into two equal sized windows, the correlation coefficient between April temperatures and the S-facing chronology improves from $r = 0.37$ to $r = 0.49$. Likewise, for June-July precipitation at the NE-facing site the correlations increase from $r = 0.41$ to $r = 0.50$. In addition, moving window correlations between average temperatures recorded at the stations in Thessaloniki and Larissa during the growing season, display an increasing synchronicity through time (Figure 2–4g).

Spatial correlations between the site chronologies and E-OBS gridded June-July precipitation and April temperatures are weak, and little variance is explained by values from grids close to the study site (Figure 2–5; insets). Correlation coefficients improve in the high-frequency domain, which underscores the strong growth/climate relationship at the inter-annual timescale. Positive significant correlation coefficients between TRW indices and June-July precipitation, and April temperatures are stable from central Italy, over large areas of the Balkan Peninsula, to the eastern Mediterranean (Figure 2–5). Weaker, but still significant negative correlations occur over the British Isles, Spain, Scandinavia, Poland, and Ukraine. Even though all sites roughly share the same spatial temperature and precipitation patterns (only most diverse sites displayed in Figure 2–5), site differences in spatial signal strength do occur. The S-exposed stand, with highest April temperature signal, is highly responsive to temperatures over large areas of the Balkan Peninsula but shows the least spatial connection to June-July precipitation. In contrast, the NE-exposed stand shows the weakest correlations with April temperatures, but the strongest correlations with June-July precipitation (Figure 2–5).

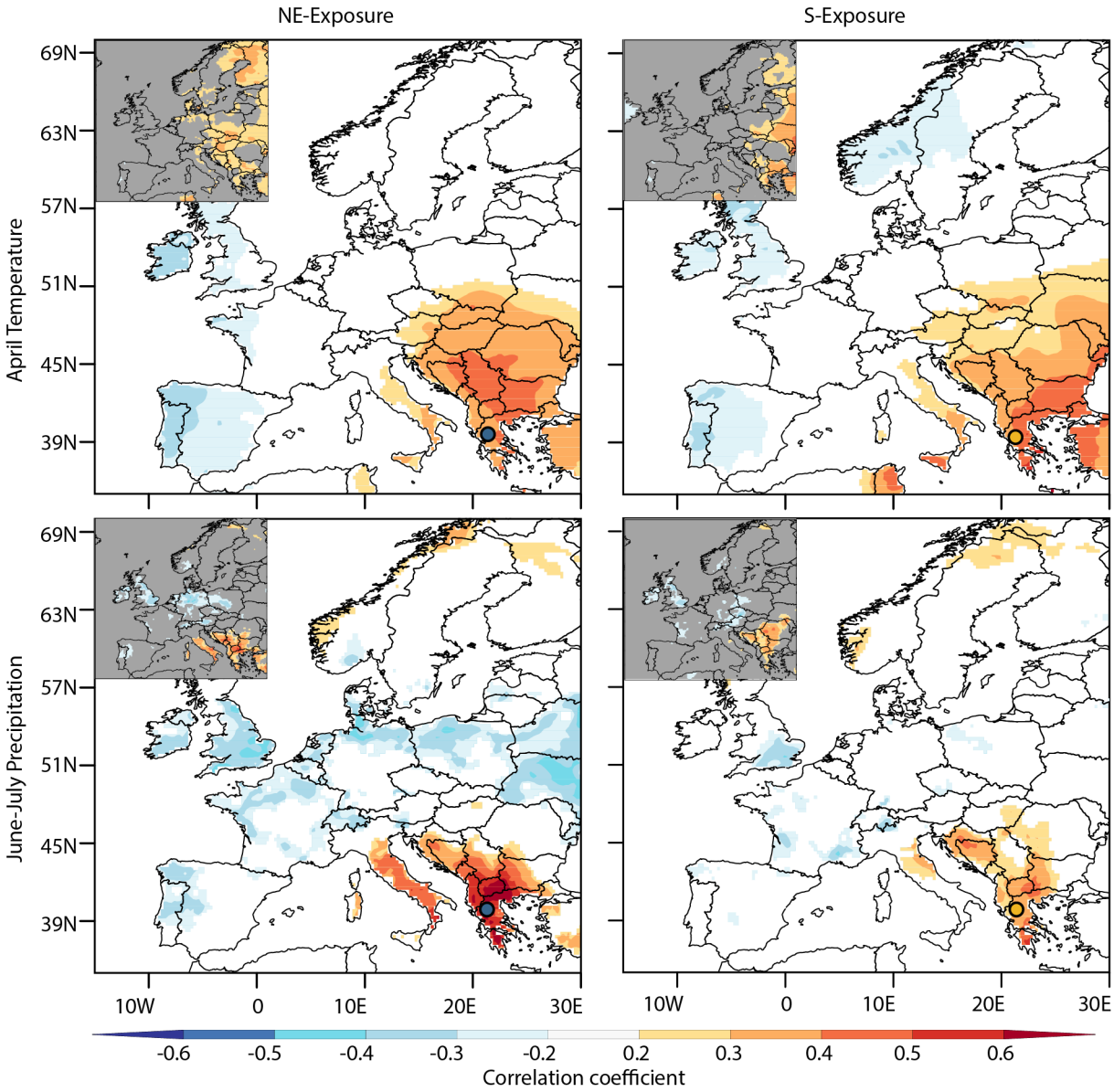

Figure 2–5 | Spatial correlations between gridded E-OBS 0.25° first differenced April temperature (upper panels) and June-July precipitation (lower panels) data with 300-year spline detrended chronologies of the NE-facing (left panels) and S-facing (right panels) stand when $p < 10\%$. Insets refer to original data and yellow and blue dots to the NE- and S-facing site respectively.

2 – 4 Discussion

2 – 4.1 Evaluation of intra- and inter-site growth characteristics

The Smolikas *P. heldreichii* TRW compilation, dating back to 575, is potentially one of the most important natural-historical archives from the eastern Mediterranean due to its discrete provenance, length, and constantly high sample depth ($n > 5$ samples in 683). The living trees on Smolikas are exceptionally capable of producing a millennial-length chronology possessing a high degree of low-frequency climate variation (Esper *et al*. 2004; Esper *et al*. 2012). The most notable example is *Adonis*

(Figure 2–2c), a Bosnian pine that dendrochronologically dated to be over 1075 years old (Konter *et al*. 2017) making it the current, oldest known living tree in Europe providing a valuable history of past environmental conditions. Combining information from these living trees with remnant wood from the same site, we are able to extend the Smolikas chronology back in time with a high degree of sample replication.

Low inter-site correlations, the application of standardization techniques that stress different frequencies, and high site-specific Rbar values confirm the existence of site differences at multiple timescales (Düthorn *et al*. 2013). Young living trees between 50 and 200 years in age are underrepresented in our dataset, likely because agricultural activities throughout the 18th and 19th century have led to a reduced regeneration rate (Todaro *et al*. 2007). Due economic reasons the population decrease in the village Samarina, located at the foot of Mt. Smolikas, from 3000 inhabitants in 1890 to only 500 in 1960 (Beuermann 1967), led to a reduction of free-range herd sizes. This supported a recovery of the forest stocks in the 20th and 21st centuries (McNeill 1992). The absolute number of inhabitants in the region differs with the historical archive, but all reports note a remarkable decrease of population in the 20th century and subsequent reduction of grazing pressure (Beuermann 1967; McNeill 1992; Brandes 2007).

Diverse growth levels and low inter-site correlations indicate substantial site differences. The wide range of growth rates between sites, despite identical ages, cannot be explained by age-effects alone. It is apparent that the differently exposed stands do not belong to the same biological growth population (Esper *et al*. 2003). The N- and NW- facing, versus the S- and NE-facing exposures are, respectively, the upper and lower range of growth extremes; the least growth-limited and least climatic-sensitive; and the most growth-limited and most climatic-sensitive (Fritts 1976). In the NW-/S-facing stands the increase in growth over the first 150/100 years is related to biological forces. We find groups of trees standing relatively close together, competing for resources. Under such stand conditions the competitive power and growth rate of young trees is reduced (Chi *et al*. 2015). These findings suggest, that if applying RCS, the analysis of subsamples is highly recommended. Incorporating all series into a single Smolikas growth population might bias the resulting chronology and interpretation (Esper *et al*. 2003).

2 – 4.2 Climate signals

The seasonally uniform response of the differently exposed sites to temperature and precipitation demonstrates how the Mediterranean climate regime enforces growth synchronicity, whereas exposure only causes minor differences (Loukas *et al*. 2002; Bolle 2003; Luterbacher *et al*. 2012; Seim *et al*. 2015). The site-independent positive shift in climate sensitivity post-1950s, and the temporally coinciding increase in station synchronicity of temperature data from Larissa and Thessaloniki, points to biases in the pre-1950 instrumental record. Caution must be exercised when considering these early data for calibration and reconstruction trials (Mamara *et al*. 2012; Dienst *et al*. 2017). The inverse

response between tree growth and April temperature (positive) and precipitation (negative) suggests dry and warm conditions favour growth in spring. These conditions enable a faster snowmelt and earlier start of cambial activity resulting in a longer growing season (Deslauriers *et al*. 2008). In contrast, high precipitation and colder temperatures affect a longer lasting snow cover, thereby delaying the onset of growth (Vaganov *et al*. 1999). The climate signal strength in April is associated with exposure effects: S-facing stands receive the strongest insolation and are most sensitive to April temperature. On the other hand, N- and NE-facing stands receive less solar radiation and are least sensitive to this parameter. A more intense and longer lasting daily insolation period on the S-facing slope enables larger warming and faster snowmelt, which in turn positively affects growth onset. N- and NE- facing slopes retain more moisture because lower insolation rates slow the thawing process (Holland and Steyn 1975; Måren *et al*. 2015).

The positive association with previous autumn and winter temperatures, a period when the trees are dormant, has been found in previous studies (Panayotov *et al*. 2010; Trouet *et al*. 2012), but cannot be explained by cambial activity (Plomion *et al*. 2001). Cold and dry versus wet and warm conditions over southern Europe are associated with the strength of the North Atlantic Oscillation (Hurell 2003). During warm winters, snowfall is partially replaced by rainfall, resulting in a reduced snow pack and favouring an early growth onset (Vaganov *et al*. 1999). In addition to this, in warm winters the trees are less exposed to frost. Consequently, the likelihood of damage to roots and needles is reduced (Tranquillini *et al*. 1979; Panayotov *et al*. 2010; Hartl-Meier *et al*. 2015). In summer, drought stress, high temperatures, and water depletion induce a reduction of the metabolic and photosynthetic activity of trees that slows their growth (Chaves 2002; Vieira *et al*. 2013). Anomalously wet and cool summers favour metabolic activity, whereas anomalously dry and warm summers increases drought stress and has the opposite effect (Touchan *et al*. 2008; Levanic *et al*. 2012).

Over a predominantly dry growing season, tree growth is simultaneously favoured in spring and limited in summer. As a result, the absolute strength of the preserved climatic information in a tree ring is reduced. We suggest that the S-facing stand in particular shows a reduced response to summer precipitation because the stand greatly benefits from an early growth onset. The early start of the vegetation period enables the development of wide rings in spring (Rossi *et al*. 2007). The suggestion that early biomass gains may compensate losses by summer drought stress (Esper *et al*. 2007; Tejedor *et al*. 2016) cannot be properly defended as total ring-widths have only annual resolution (Fritts 1976). By contrast those trees living in the NE-facing stand, without the benefit of early cell formation in spring, do capture a clear June-July climate signal. The N- and NE-facing stands are nearest to each other, yet display a different sensitivity to summer precipitation. The character of ground and surface meltwater flows effect on growth is one possible explanation. In the Mt. Smolikas sampling sites, the NW-, S- and N-facing slopes, meltwater likely infiltrates directly into the ground, thus making the trees less prone to summer droughts. On the NE-facing slope, water runoff through erosion channels

causes fast depletion of poor soil water reserves. Such efficient drainage increases the tree's dependency on summer precipitation and drought exposure (King *et al*. 2013; Vieira *et al*. 2013).

The spatial correlation maps of gridded April temperature and June-July precipitation show strong climatic signals over the Balkan Peninsula related to common forcings, climate regimes, and synoptic patterns (Xoplaki *et al*. 2004; Xoplaki *et al*. 2012; Trouet *et al*. 2012; Trouet *et al*. 2014). The patterns are similar to those produced using the Thessaloniki climate data, underscoring the potential to reconstruct climate for different seasons and variables, using different site chronologies on Mt. Smolikas. The spatial correlation analysis also reveals a distinct dipole pattern across Europe that is consistent with the summer North Atlantic Oscillation (sNAO) mode (Folland *et al*. 2009); responsible for annual and decadal summer temperature and drought variability over Greece (Xoplaki *et al*. 2003; Oikonomou *et al*. 2010). Temperature reconstructions using *P. heldreichii* MXD data from the Pirin Moutains in Bulgaria (Trouet *et al*. 2012) and Mt. Olympus in Greece (Klesse *et al*. 2015), are reported to have a strong and consistent anti-phase relationship with the sNAO (Folland *et al*. 2009), suggesting the sNAO is an important driver of the teleconnection between summer temperatures in northwestern versus southeastern Europe. In this analysis, we find some coherence with the sNAO, however, values are mostly insignificant. The weak sNAO signal is arguably related to the use of TRW which, compared to MXD, has a lower climatic signal strength, due to TRW's higher auto-correlation (Melvin *et al*. 2013).

In contrast to previous studies of *P. heldreichii* TRW data, that report climate signals of variable strength (Todaro *et al*. 2007; Panayotov *et al*. 2010; Seim *et al*. 2012), we find temporally robust signals after 1950. The significant and temporally robust April temperature correlations across all sites, and the statistically significant June-July precipitation signal in the NE-facing trees, suggests the TRW data from Mt. Smolikas have great potential for reconstructing climate. We hypothesize that the notable signal strength found, in comparison to previous *P. heldreichii* studies, is related to i) the standardization method used ii) slope exposure effects (Holland and Steyn 1975; Hartl-Meier *et al*. 2014; Hartl-Meier *et al*. 2015), iii) higher site elevation with generally stronger growth limitations (Körner 2007; Hartl-Meier *et al*. 2014), and iv) ecological effects including geomorphological modulated water supply (Fritts 1976). Reduced signal strength, inherent to this and all previously mentioned studies, might be a consequence of the poorly representative meteorological station data used for analysis. Lowland station data tend to underestimate precipitation, and desiccation extremes at higher elevations (Fotiadi *et al*. 1999). The detection of distinct site differences in climate signal strength, on even small spatial scales, demonstrates the importance of careful site selection when performing dendroclimatological studies (Fritts 1976).

2 – 5 Conclusions

We present an assessment of the site-specific climate signals in a new millennium-length TRW chronology from the Pindus Mts. of Greece that extends back to 575. We find inter-site differences in climate signal strength that appear to be related to slope exposure, biological memory effects, and meltwater supply. The strongest growth limitation is found at the S-facing site where trees are most sensitive to April temperatures, as well as at the NE-facing site where trees respond stronger to June-July precipitation. At the NW- and N-facing stands, *P. heldreichii* growth is least limited and contains a weaker climate signal. Due to opposing growth/climate relationships, manifest by warm and dry conditions supporting growth in spring but limiting growth in summer, biological memory effects arise and the initiation of cell formation in spring likely affects climate sensitivity in summer. If site differences are strictly considered, the climate of two seasons (April and June-July) could be reconstructed using only trees from S-exposed sites for temperature, and only trees from NE-exposed sites for precipitation. Further work will focus on (i) increasing sample replication through the inclusion of additional sites, (ii) investigating low-frequency trends in the millennial-length chronology, (iii) performing a TRW-based climate reconstruction, and (iv) producing MXD measurements to further explore the potential of reconstructing summer temperature variability in this Mediterranean environment.

2 – 6 Acknowledgements

Supported by the German Research Foundation (DFG, ES 161/9-1) and National Science Foundation CAREER grant (AGS-1349942). We are thankful to Soumaya Belmecheri, Tilman Büttner, Manuel Dienst, Markus Kochbeck, Oliver Konter, Amarita Krusic, Anna Krusic, Jonas Krusic, Fredrik C. Ljungqvist, Sam Williams and Hakan Grudd for valuable assistance in the field.

2 – 7 References

Beuermann A. 1967. *Fernweidewirtschaft in Südosteuropa: ein Beitrag zur Kulturgeographie des östlichen Mittelmeergebietes*. Westermann: Braunschweig, Germany.

Bolle HJ. 2003. *Mediterranean Climate*. Springer: Heidelberg, Germany.

Brandes R. 2007. *Waldgrenzen griechischer Hochgebirge: Unter besonderer Berücksichtigung des Taygetos, Südpeloponnes*. Friedrich-Alexander-Universität Erlangen-Nürnberg: Erlangen, Germany.

Briffa KR, Jones PD, Bartholin TS, Eckstein D, Schweingruber FH, Karlen W, Zetterberg P, Eronen M. 1992. Fennoscandian summers from AD 500 - temperature changes on short and long timescales. *Clim. Dyn.* **7**: 111-119.

Büntgen U, Esper J, Frank DC, Nicolussi K, Schmidhalter M. 2005. A 1052-year tree-ring proxy for Alpine summer temperatures. *Clim. Dyn.* **25**: 141-153.

Büntgen U, Frank D, Wilson R, Carrer M, Urbinati C, Esper J. 2008. Testing for tree-ring divergence in the European Alps. *Glob. Chang. Biol.* **14**: 2443-2453.

Büntgen U, Tegel W, Nicolussi K, McCormick M, Frank D, Trouet V, Kaplan JO, Herzig F, Heussner KU, Wanner H, Luterbacher J, Esper J. 2011. 2500 years of European climate variability and human susceptibility. *Science* **331**: 578-582.

Chaves MM. 2002. How plants cope with water stress in the field? Photosynthesis and growth. *Ann. Bot.* **89**: 907-916.

Chi XL, Tang ZY, Xie ZQ, Guo Q, Zhang, M, Ge JL, Xiong GM, Fang JY. 2015. Effects of size, neighbors, and site condition on tree growth in a subtropical evergreen and deciduous broad-leaved mixed forest, China. *Ecol. Evol.* **5**: 5149-5161.

Cook ER, Peters K. 1981. The smoothing spline: a new approach to standardizing forest interior tree-ring width series for dendroclimatic studies. *Tree-Ring Bulletin* **41**: 45-53.

Cook ER. 1985. *A time series analysis approach to tree ring standardization (PhD thesis)*. University of Arizona: Tucson, USA.

Cook E, Briffa KR, Meko DM, Graybill D, Funkhouser G. 1995. The 'segment length curse' in long tree-ring chronology development for palaeoclimatic studies. *Holocene* **5**: 229-237.

Cook ER, Peters K. 1997. Calculating unbiased tree-ring indices for the study of climatic and environmental change. *Holocene* **7**: 361-370.

Cook ER, Krusic PJ. 2016. *Program ARSTAN: a tree-ring standardization program based on detrending and autoregressive time series modeling, wit interactive graphs*. Lamont-Doherty Earth Observatory Columbia University: New York, USA.

D'Arrigo R, Wilson R, Jacoby G. 2006. On the long-term context for late twentieth century warming. *J. Geophys. Res.* **111**: D03103, doi: 10.1029/2005JD006352.

Deslauriers A, Rossi S, Anfodillo T, Saracino A. 2008. Cambial phenology, wood formation and temperature thresholds in two contrasting years at high altitude in southern Italy. *Tree Physiol.* **28**: 863-871.

Dienst M, Linden J, Engstrom E, Esper J. 2017. Removing the relocation bias from the 155-year Haparanda temperature record in Northern Europe. *Int. J. Climatol.* **37**: 4015-4026.

Düthorn E, Holzkämper S, Timonen M, Esper J. 2013. Influence of micro-site conditions on tree-ring climate signals and trends in central and northern Sweden. *Trees* **27**: 1395-1404.

Esper J, Cook ER, Krusic PJ, Peters K, Schweingruber FH. 2003. Tests of the RCS method for preserving low-frequency variability in long tree-ring chronologies. *Tree-Ring Res.* **59**: 81-98.

Esper J, Treydte K, Frank DC, Gärtner H, Büntgen U. 2004. Temperaturvariationen und Jahrringe | Temperature variation and tree rings. *Schweiz. Z. Forstwes.* **155**: 213-221.

Esper J, Frank D, Büntgen U, Verstege A, Luterbacher J. 2007. Long-term drought severity variations in Morocco. *Geophys. Res. Lett.* **34**: L17702, doi: 10.1029/2007GL030844.

Esper J, Büntgen U, Timonen M, Frank DC. 2012. Variability and extremes of northern Scandinavian summer temperatures over the past two millennia. *Glob. Planet. Chang.* **88-89**: 1-9.

Esper J, Krusic PJ, Ljungqvist FC, Luterbacher J, Carrer M, Cook E, Davi NK, Hartl-Meier C, Kirdyanov A, Konter O, Myglan V, Timonen M, Treydte K, Trouet V, Villalba R, Yang B, Büntgen U. 2016. Ranking of tree-ring based temperature reconstructions of the past millennium. *Quat. Sci. Rev.* **145**: 134-151.

Folland CK, Knight J, Linderholm HW, Fereday D, Ineson S, Hurrell JW. 2009. The Summer North Atlantic Oscillation: Past, Present, and Future. *J. Clim.* **22**: 1082-1103.

Fotiadi AK, Metaxas DA, Bartzokas A. 1999. A statistical study of precipitation in northwest Greece. *Int. J. Climatol.* **19**: 1221-1232.

Frank D, Esper J, Cook ER. 2007. Adjustment for proxy number and coherence in a large-scale temperature reconstruction. *Geophys. Res. Lett.* **34**: L16709, doi: 10.1029/2007GL030571.

Fritts HC. 1976. *Tree rings and climate*. Blackburn Press: Caldwell, USA.

Gallardo-Cruz JA, Pérez-García EA, Meave JA. 2009. β-Diversity and vegetation structure as influenced by slope aspect and altitude in a seasonally dry tropical landscape. *Landsc. Ecol.* **24**: 473-482.

Hartl-Meier C, Dittmar C, Zang C, Rothe A. 2014. Mountain forest growth response to climate change in the Northern Limestone Alps. *Trees* **28**: 819-829.

Hartl-Meier C, Zang C, Büntgen U, Esper J, Rothe A, Gottlein A, Dirnbock T, Treydte K. 2015. Uniform climate sensitivity in tree-ring stable isotopes across species and sites in a mid-latitude temperate forest. *Tree Physiol.* **35**: 4-15.

Haylock MR, Hofstra N, Tank A, Klok EJ, Jones PD, New M. 2008. A European daily high-resolution gridded data set of surface temperature and precipitation for 1950-2006. *J. Geophys Res. Atmos.* **113**:D20119, doi:10.1029/2008JD010201.

Holland PG, Steyn DG. 1975. Vegetational responses to latitudinal variations in slope angle and aspect. *J. Biogeogr.* **2**: 179-183.

Holmes RL. 1983. Computer-assisted quality control in tree-ring dating and measurement. *Tree-Ring Bulletin* **43**: 69-78.

Horvat I, Glavač V, Ellenberg H. 1974. *Vegetation Südosteuropas; Vegetation of Southeast-Europe*. Fischer: Stuttgart, Germany.

Hughes PD, Woodward JC, Gibbard PL. 2006. Late Pleistocene glaciers and climate in the Mediterranean. *Glob. Planet. Chang.* **50**: 83-98.

Hurrell JW. 2003. *The North Atlantic oscillation: Climatic significance and environmental impact, Geophysical monograph*. American Geophysical Union: Washington, USA.

King G, Fonti P, Nievergelt D, Büntgen U, Frank D. 2013. Climatic drivers of hourly to yearly tree radius variations along a 6 degrees C natural warming gradient. *Agric. For. Meteorol.* **168**: 36-46.

Klesse S, Ziehmer M, Rousakis G, Trouet, Frank D. 2015. Synoptic drivers of 400 years of summer temperature and precipitation variability on Mt. Olympus, Greece. *Clim. Dyn.* **45**: 807-824.

Konter O, Rosner K, Kyncl T, Esper J, Büntgen U. 2015. Spatiotemporal variations in the climatic response of *Larix decidua* from the Slovakian Tatra Mountains. In: *Proceedings of the DENDROSYMPOSIUM 2014,* Wilson R, Helle G, Gaertner H (eds). Deutsches GeoForschungsZentrum GFZ, Potsdam pp. 62-69.

Konter O, Krusic PJ, Trouet V, Esper J. 2017. Meet Adonis, Europe's oldest dendrochronologically dated tree. *Dendrochronologia* ***42***: 12.

Körner C. 2007. The use of altitude in ecological research. *Trends Ecol. Evol.* **22**: 569-574.

Köse N, Akkemik Ü, Dalfes HN, Özeren MS. 2011. Tree-ring reconstructions of May-June precipitation for western *Anatolia. Quat. Res.* **75**: 438-450.

Kovats RS, Valentini R, Bouwer LM, Georgopoulou E, Jacob D, Martin E, Rounsevell M, Soussana JF. 2014. Europe. In *Climate Change 2014: Impacts, Adaptation, and Vulnerability. Part B: Regional Aspects. Contribution of Working Group II to the Fifth Assessment Report of the Intergovernmental Panel of Climate Change,* Barros VR, Field CB, Dokken DJ, Mastrandrea MD, Mach KJ, Bilir TE, Chatterjee M, Ebi KL, Estrada YO, Genova RC, Girma B, Kissel ES, Levy AN, MacCracken S, Mastrandrea PR, White LL (eds). Cambridge University Press, Cambridge, pp. 1267-1326.

Levanic T, Popa I, Poljansek S, Nechita C. 2012. A 323-year long reconstruction of drought for SW Romania based on black pine (*Pinus nigra*) tree-ring widths. *Int. J. Biometeorol.* **57**: 703-714.

Loukas A, Vasiliades L, Dalezios NR. 2002. Hydroclimatic variability of regional droughts in Greece using the palmer moisture anomaly index. *Nord. Hydrol.* **33**: 425-442.

Luterbacher J, García-Herrera R, Akcer-On S, Allan R, Alvarez-Castro MC, Benito G, Booth J, Büntgen U, Cagatay N, Colombaroli D, Davis B, Esper J, Felis T, Fleitmann D, Frank D, Gallego D, Garcia-Bustamante E, Glaser R, Gonzalez-Rouco FJ, Goosse H, Kiefer T, Macklin MG, Manning SW, Montagna P, Newman L, Power MJ, Rath V, Ribera P, Riemann D, Roberts N, Sicre MA, Silenzi S, Tinner W, Tzedakis PC, Valero-Garcés B, van der Schrier G, Vannière B, Vogt S, Wanner H, Werner JP, Willett G, Williams MH, Xoplaki E, Zerefos CS, Zorita E. 2012. A review of 2000 years of paleoclimatic evidence in the Mediterranean. In *The climate of the Mediterranean region*: *From the past to the future*, Lionello P (ed). Elsevier, Amsterdam, pp. 87-185.

Mamara A, Argiriou AA, Anadranistakis M. 2012. Homogenization of mean monthly temperature time series of Greece. *Int. J. Climatol.* **33**: 2649-2666.

Måren IE, Karki S, Prajapati C, Yadav RK, Shrestha BB. 2015. Facing north or south: Does slope aspect impact forest stand characteristics and soil properties in a semiarid trans-Himalayan valley? *J. Arid Environ.* **121**: 112-123.

McNeill JR. 1992. *The mountains of the Mediterranean world: An environmental history*. Cambridge University Press: Cambridge, United Kingdom.

Meiggs R. 1982. *Trees and timber in the ancient Mediterranean world*. Clarendon Press: Oxford, United Kingdom.

Melvin TM, Grudd H, Briffa KR. 2013. Potential bias in 'updating' tree-ring chronologies using regional curve standardisation: Re-processing 1500 years of Tornetrask density and ring-width data. *Holocene* **23**: 364-373.

Oikonomou C, Flocas HA, Hatzaki M, Nisantzi A, Asimakopoulos DN. 2010. Relationship of extreme dry spells in Eastern Mediterranean with large-scale circulation. *Theor. Appl. Climatol.* **100**: 137-151.

Panayotov M, Bebi P, Trouet V, Yurukov S. 2010. Climate signal in tree-ring chronologies of *Pinus peuce* and *Pinus heldreichii* from the Pirin Mountains in Bulgaria. *Trees* **24**: 479-490.

Paudel S, Vetaas OR. 2014. Effects of topography and land use on woody plant species composition and beta diversity in an arid Trans-Himalayan landscape, Nepal. *J. Mt. Sci.* **11**: 1112-1122.

Plomion C, Leprovost G, Stokes A. 2001. Wood formation in trees. *Plant Physiol.* **127**: 1513-1523.

Pook E, Moore C. 1966. The influence of aspect on the composition and structure of dry sclerophyll forest on black mountain Canberra. *Aust. J. Bot.* **14**: 223-242.

Rinn F. 2003. Time series analysis and presentation for dendrochronology and related applications, URL http://www.rimatech.com.

Rossi S, Deslauriers A, Anfodillo T, Carraro V. 2007. Evidence of threshold temperatures for xylogenesis in conifers at high altitudes. *Oecologia* **152**: 1-12.

Schneider L, Smerdon JE, Büntgen U, Wilson RJS, Myglan VS, Kirdyanov AV, Esper J. 2015. Revising midlatitude summer temperatures back to A.D. 600 based on a wood density network. *Geophys. Res. Lett.* **42**: 4556-4562.

Schweingruber FH. 1996. *Tree rings and environment dendroecology*. Haupt: Vienna, Austria.

Seftigen K, Linderholm HW, Drobyshev I, Niklasson M. 2013. Reconstructed drought variability in southeastern Sweden since the 1650s. *Int. J. Climatol.* **33**, 2449-2458.

Seim A, Büntgen U, Fonti P, Haska H, Herzig F, Tegel W, Trouet V, Treydte, K. 2012. Climate sensitivity of a millennium-long pine chronology from Albania. *Clim. Res.* **51**: 217-228.

Seim A, Treydte K, Trouet V, Frank D, Fonti P, Tegel W, Panayotov M, Fernandez-Donado L, Krusic P, Büntgen U. 2015. Climate sensitivity of Mediterranean pine growth reveals distinct east-west dipole. *Int. J. Clim.* **35**: 2503-2513.

Speer JH. 2010. *Fundamentals of tree-ring research*. University of Arizona Press: Tucson, USA.

Sternberg M, Shoshany M. 2001. Influence of slope aspect on Mediterranean woody formations: Comparison of a semiarid and an arid site in Israel. *Ecol. Res.* **16**: 335-345.

Stevanovic V, Tan K, Iatrou G. 2003. Distribution of the endemic Balkan flora on serpentine - I. obligate serpentine endemics. *Plant Syst. Evol.* **242**: 149-170.

Stoffel M, Khodri M, Corona C, Guillet S, Poulain V, Bekki S, Guiot J, Luckman BH, Oppenheimer C, Lebas N, Beniston M, Masson-Delmotte V. 2015. Estimates of volcanic-induced cooling in the Northern Hemisphere over the past 1,500 years. *Nature Geosci.* **8**: 784-788.

Strokes MA, Smiley TL. 1968. *An introduction to tree ring dating*. The University of Chicargo Press: Chigargo, USA.

Tejedor E, de Luis M, Cuadrat JM, Esper J, Saz MA. 2016. Tree-ring-based drought reconstruction in the Iberian Range (east of Spain) since 1694. *Int. J. Biometeorol.* **60**: 361-72.

Todaro L, Andreu L, D'Alessandro CM, Gutirrez E, Cherubinic P, Saracino A. 2007. Response of *Pinus leucodermis* to climate and anthropogenic activity in the National Park of Pollino (Basilicata, Southern Italy). *Biol. Conserv.* **137**: 507-519.

Touchan R, Meko DM, Aloui A. 2008. Precipitation reconstruction for Northwestern Tunisia from tree rings. *J. Arid Environ.* **72**: 1887-1896.

Tranquillini W, Billings WD, Golley F, Lange OL, Olson JS. 1979. *Physiological Ecology of the Alpine Timberline*. Springer: Berlin, Germany.

Trouet V, Panayotov MP, Ivanova A, Frank D. 2012. A pan-European summer teleconnection mode recorded by a new temperature reconstruction from the northeastern Mediterranean (AD 1768-2008). *Holocene* **22**: 887-898.

Trouet V, van Oldenborgh GJ. 2013. KNMI Climate Explorer: A web-based research tool for high-resolution paleoclimatology. *Tree-Ring Res.* **69**: 3-13.

Trouet V. 2014. A tree-ring based late summer temperature reconstruction (AD 1675-1980) for the northeastern Mediterranean. *Radiocarbon* **56**: 69-78.

Urban DL, Miller C, Halpin PN, Stephenson NL. 2000. Forest gradient response in Sierran landscapes: the physical template. *Landsc. Ecol.* **15**: 603-620.

Vaganov EA, Hughes MK, Kirdyanov AV, Schweingruber FH, Silkin PP. 1999. Influence of snowfall and melt timing on tree growth in subarctic Eurasia. *Nature* **400**: 149-151.

van Oldenborgh GJ. 2005. Searching for decadal variations in ENSO precipitation teleconnections. *Geophys Res. Lett.* **32**: L15701, doi: 10.1029/2005GL023110.

Vieira J, Rossi S, Campelo F, Freitas H, Nabais C. 2013. Seasonal and daily cycles of stem radial variation of *Pinus pinaster* in a drought-prone environment. *Agric. For. Meteorol.* **180**: 173-181.

Wilson R, Anchukaitis K, Briffa KR, Büntgen U, Cook E, D'Arrigo R, Davi N, Esper J, Frank D, Gunnarson B, Hegerl G, Helama S, Klesse S, Krusic PJ, Linderholm HW, Myglan V, Osborn TJ, Rydval M, Schneider L, Schurer A, Wiles G, Zhang P, Zorita E. 2016. Last millennium northern hemisphere summer temperatures from tree rings: Part I: The long term context. *Quat. Sci. Rev.* **134**: 1-18.

Xoplaki E, Luterbacher J, González-Rouco JF, Wanner H. 2003. Mediterranean summer air temperature variability and its connection to the large-scale atmospheric circulation and SSTs. *Clim. Dyn.* **20**: 723-739.

Xoplaki E, Gonzalez-Rouco JF, Luterbacher J, Wanner H. 2004. Wet season Mediterranean precipitation variability: influence of large-scale dynamics and trends. *Clim. Dyn.* ***23***: 63-78.

Xoplaki E, Trigo RM, García-Herrera R, Barriopedro D, D'Andrea F, Fischer EM, Gimeno L, Gouveia C, Hernández E, Kuglitsch FG, Mariotti A, Nieto R, Pinto JG, Pozo-Vázquez D, Saaroni H, Toreti A, Trigo IF, Vicente-Serrano SM, Yiou P, Ziv B. 2012. Large-scale atmospheric circulation driving extreme climate events in the Mediterranean and its related impacts. In *The climate of the Mediterranean region: From the past to the future*, Lionello P (ed). Elsevier, Amsterdam, pp. 87-185.

3 | A 1286-year hydro-climate reconstruction for the Balkan Peninsula

Lara Klippel[1], Paul J. Krusic[2,3,4], Robert Brandes[5], Claudia Hartl[1], Soumaya Belmecheri[6], Manuel Dienst[1], Jan Esper[1]

[1]*Department of Geography, Johannes Gutenberg University, Mainz, Germany*

[2]*Department of Geography, University of Cambridge, Cambridge, UK*

[3]*Navarino Environmental Observatory, Messina, Greece*

[4]*Department of Physical Geography, Stockholm University, Stockholm, Sweden*

[5]*Department of Geography, Friedrich-Alexander University, Erlangen, Germany*

[6]*Laboratory of Tree-Ring Research, University of Arizona, Tucson, USA*

Boreas, 2018, published

3 – 1 Introduction

Across the Mediterranean climate models predict, in forthcoming decades, a summer temperature increase, and a summer precipitation reduction (Giorgi and Lionello 2008; Diffenbaugh and Giorgi 2012). In terms of spatial distribution, the largest temperature increase is expected for the Iberian and Balkan Peninsulas (Dubrovský *et al*. 2013), accompanied by an amplification in the frequency, intensity and duration of summer droughts (Gao and Giorgi 2008) and heatwaves (Fischer and Schar 2010; Nastos and Kapsomenakis 2015). Meteorological records reveal a precipitation decrease in the recent decades in the eastern Mediterranean (Maheras and Anagnostopoulou 2003; García-Herrera *et al*. 2007), and extreme drought episodes have become more frequent and persistent (Xoplaki *et al*. 2004). To place the recent and predicted conditions in a long-term context, paleoclimate reconstructions are needed (Esper *et al*. 2007; Schneider *et al*. 2015; Ljungqvist *et al*. 2016; Wilson *et al*. 2016).

Along the Balkan Peninsula, including the Pindus Mountain range in Greece, we find very old *Pinus heldreichii* (PIHE; Brandes 2007) stands with several individuals reaching millennial age. The oldest individual named *Adonis* is dendrochronologically dated to be over 1075 years old (Konter *et al*. 2017). This makes it currently the oldest known living tree in Europe, and provides a history of climatic and environmental conditions going back into the first millennium. This long-lived species has been used in several dendrochronological studies (e.g. Todaro *et al*. 2007; Panayotov *et al*. 2010; Seim *et al*. 2012; Trouet *et al*. 2012; Klesse *et al*. 2015). Recent studies relying on maximum latewood density (MXD) have successfully reconstructed past temperature variations using PIHE (Trouet *et al*. 2012; Klesse *et al*. 2015), but there has been no attempt yet to reconstruct changes in past climate by means of total tree-ring width (TRW) measurements. It has been shown that the low frequency climate signal in TRW measurements is not stable (Seim *et al*. 2012), though at higher frequencies temperature and precipitation have significant growth implications (Klippel *et al*. 2017). PIHE growth at Mt. Smolikas is significantly controlled by temperature in April and precipitation in June-July, which emphasizes the overall importance of an early growth onset and subsequent moisture conditions (Klippel *et al*. 2017).

There are several high-resolution reconstructions of hydro-climatic conditions from the eastern Mediterranean, derived from TRW of other species, e.g., *Juniperus excels* (Touchan *et al*. 2005), *Pinus nigra* (Akkemik and Aras 2005; Köse *et al*. 2011; Levanic *et al*. 2012; Poljanšek *et al*. 2013; Klesse *et al*. 2015) and *Quercus sp*. (Akkemik *et al*. 2005; Griggs *et al*. 2007; Cufar *et al*. 2008). However, our understanding of the spatiotemporal patterns and magnitude of precipitation changes, particularly prior to the Little Ice Age (LIA), is still limited due to an increasing data paucity back in time (Esper *et al*. 2016). Based on the stable climate signal in the high-frequency domain, this work aims to develop for the first time a PIHE TRW based summer precipitation reconstruction extending

back to the first millennium. We focus on interannual variability in hydro-climate and the identification of extreme dry and pluvial events.

3 – 2 Data and methods

3 – 2.1 Study area and tree-ring data

Tree-ring data used in this study comprise 207 821 annual ring width measurements, from 133 relict and 185 living PIHE trees, sampled between the years 2011 and 2016. We compiled a composite TRW chronology from eight different locations (Table 3–1) in the timberline ecotone of Mt. Smolikas at 1950-2200m a.s.l. (the highest peak of the Pindus Range in northern Greece) (Figure 3–1a). Conditions, such as rocky shallow soils, summer dryness, snow cover in winter (Fotiadi *et al*. 1999; Loukas *et al*. 2002) and decay resistant resinous wood (Lange *et al*. 1994), permits the preservation of relict material. PIHE is native to the oro-mediterranean vegetation belt (Brandes 2007), a region characterized by large seasonal temperature and precipitation changes, including heavy winter frosts and snow, and intense dryness during the summer period (Bolle 2003).

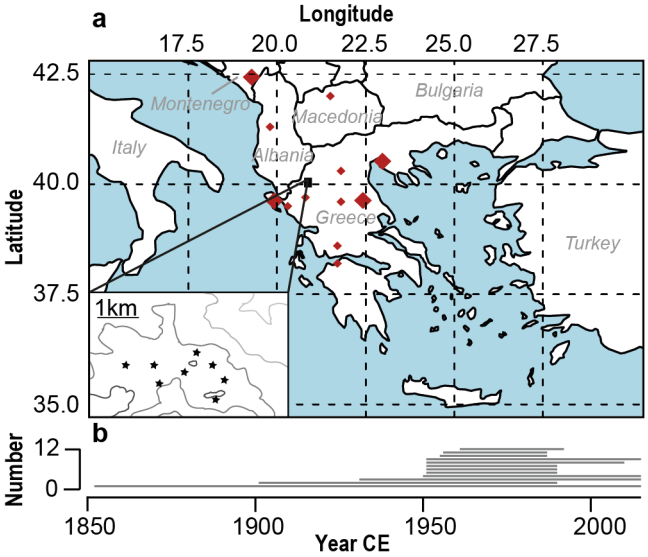

Figure 3–1 | Site characteristics **a** Location of the study area in the Pindus Mountains (black square) and map of the sampling sites at the eastern flank of Mt. Smolikas (inset). Red symbols refer to the climate stations used for interpolation of the closest CRU TS 3.24 precipitation grid (40.25°N/20.75°E). Large/small red diamonds indicate currently active/inactive climate stations. **b** Temporal coverage of instrumental station measurements. From top to bottom, lines refer to the climate stations in Skopje, Agrinion, Kozani, Petgorica-Grad, Tirana, Trikala, Igoumenitsa, Ioannina, Larissa, Thessaloniki, Patrai and Kerkyra.

3 – 2.2 Tree-ring measurement and chronology development

615 discs and core samples were prepared following standard dendrochronological techniques to produce finely polished surfaces for micrometre measurement. TRW was measured using Velmex and Lintab systems, TSAP-Win (Rinn 2003) and Cofecha programs (Holmes 1983). To emphasize varying frequencies in the TRW chronologies, age-related trends (Bräker 1981) were removed by applying two different detrending procedures to power transformed TRW series (Cook and Peters 1997). To remove age trends in the individual tree-ring series, and to preserve common frequency signals, a Regional Curve Standardization (RCS; Briffa *et al*. 1992; Cook and Peters 1997; Esper *et al*. 2003) was performed in order to produce a chronology retaining low frequency variance, and individual cubic smoothing spline (SPL) standardization, with a 50% frequency cut-off at 2/3 of the series length, was applied to preserve climatic information at annual-to-multidecadal scales (Cook and Peters 1997). Both chronologies were produced using the option configurations within the program ARSTAN (Cook *et al*. 2017). RCS allows climatic information to be preserved on time-scales longer than the individual segment length and long-term changes in environmental conditions are preserved (Cook *et al*. 1995). Ideally, RCS is applied to composite datasets integrating living and relict material with a heterogeneous age structure (Esper *et al*. 2003). The application of RCS to this dataset is limited, as samples from very old and slow-growing living trees are combined with relict samples that are heavily weathered and of shorter and mixed ages. Amongst all the individual TRW series, common variability over time was assessed using inter-series correlation (Rbar) and expressed population signal (EPS; Wigley *et al*. 1984) calculated over 30-year periods with 15 years of overlap. High inter-series correlation as well as common inter-site growth and climate response patterns (Klippel *et al*. 2017) permitted establishing a composite chronology including all samples. The composite chronology was formed by calculating the robust bi-weight mean of the RCS tree-ring indices of each calendar year, truncated at EPS > 0.85 (Cook 1985). Based on the number of samples and Rbar, variance stabilization was applied (Frank *et al*. 2007b). To investigate high-frequency changes, we used the (pre-whitened) residual version of the chronology, produced by removing common persistence by autoregressive modelling (Cook 1985).

3 – 2.3 Heteroscedasticity tests

The correct detection of extreme events requires that all preserved variance changes have a climatic origin and do not arise from biological and methodological artefacts (Fritts 1976). Any systematic trend in variance, in the individual series and/or chronology, could potentially bias the calculation of the tree-ring chronology. Raw ring width series are heteroscedastic by nature. Prior to detrending, the power transformation of the raw measurements minimizes age-dependent shifts in variance of non-climatic origin, by suspending the growth level versus spread relationship (Cook and Peters 1997). In the composite chronology, changes over time in the inter-series correlation and sample replication are another source of potential variance bias. According to Frank *et al*. (2007b), the process of variance

stabilization attempts to remove variance changes related to replication and inter-tree correlation, while it preserves variance related to climate. To assess these effects over the past millennium, variance changes in the SPL chronology were analysed by calculating 100-year moving window standard deviations (SD). We account for the effect of (i) sample replication and explore (ii) the age-structure of the dataset as potential drivers for non-climatic variance changes.

(i) Additional tests for remaining biases due to temporal variations of replication in the mean chronology were conducted by subsampling the residual SPL chronology to produce a suite of new residual chronologies with a time-invariant replication. In the first step, from the total of 615 residual series (Figure 3–S1a), 1000 subsample residual series, spanning the period 730- 2015, were generated by randomly new composition of the individual series (Figure 3–S1b). In the second step, 1000 times 80 of these series were randomly selected and averaged into a subset chronology with a balanced yearly sample size (Figure 3–S1c). The second step was repeated using only 15 series which is the minimum replication of the original chronology.

(ii) The age-dependency of variance was explored by analysing the spread of individual cambial age-aligned residual series. Tests for remaining bias due to a temporally changing age-structure were conducted by splitting the dataset into different age classes. Age-class chronologies range from 1-200 years, and 201-400 years. Additionally, an arithmetic mean chronology of the two age-class chronologies, 1-200 and 201-400, was created, balancing the age structure of the dataset through time.

Table 3–1 | Characteristics of the individual site and Mt. Smolikas regional (all) chronologies. EPS: expressed population signal, MSL: mean segment length, AGR: average growth rate [mm] of the first 300 years of growth, Lag-1: first-order autocorrelation, Rbar: interseries correlation.

Site	Elevation	Exposure	N Series	Start (EPS > 0.85)	End	MSL	AGR	Lag-1	Rbar
1	2141	NW	152	673 (980)	2015	394	0.82	0.77	0.31
2	2163	S	111	575 (1345)	2014	316	0.77	0.75	0.34
3	1951	N	98	720 (1555)	2015	320	0.79	0.76	0.32
4	2070	NE	99	685 (1500)	2014	308	0.78	0.77	0.42
5	2091	SE	60	1072 (1500)	2015	293	0.87	0.82	0.30
6	2209	S	43	1167 (1605)	2015	345	0.78	0.79	0.31
7	2103	SE	29	1172 (1630)	2015	359	1.08	0.82	0.40
8	2049	NW	23	1493 (1650)	2015	351	1.15	0.77	0.27
ALL	2097		615	575 (730)	2015	338	0.82	0.77	0.31

3 – 2.4 Instrumental data

Existing instrumental climate data, predominantly from distant low elevation sites, probably underestimate precipitation and overestimate temperature of the study area (Figure 3–1a). Due to the poor ability of local station data to capture climatic conditions at the upper tree line, we considered high-resolution 0.5° gridded CRU TS 3.24 climate data (Harris *et al*. 2014) to assess the temporal stability and spatial extent of the TRW climate signal. To exclude potential uncertainty in gridded data, calibration/verification tests were performed over the 1961-2015 period resulting from the limited number of reliable instrumental station records during the first half of the 20th century (Figure 3–1b). Using the interpolated CRU TS 3.24 precipitation data for each grid cell within 15-50°E and 34-50°N, we calculated the standardized precipitation index (SPI; McKee *et al*. 1993). SPI was chosen as the index because it has been identified as an effective metric for detecting dry and pluvial events in Mediterranean pine forests and is widely used to investigate meteorological drought on a range of time scales (Pasho *et al*. 20011; Levanic *et al*. 2012; Seftigen *et al*. 2013; Tejedor *et al*. 2016). Standardized precipitation is the deviation of rainfall totals over a defined time interval (in this study: 1-month and 2-months) from the average precipitation over the entire record divided by its standard deviation (McKee *et al*. 1993). The SPI value can be interpreted as the number of standard deviations by which the defined time interval deviates from the long-term mean. A normalized expression of precipitation enables cross-region comparisons of pluvial and drought conditions (McKee *et al*. 1993). The SPL residual, SPL standard and RCS chronologies were first calibrated against the 1-month and 2-month SPI, temperature and precipitation using the closest grid point at 20.5-21°E/40-40.5°N. To investigate the spatial extent of the signal with the strongest response, the procedure was repeated using all 0.5° grids within 15-50°E and 34-50°N. The average SPI of all grid points correlating at a p-value ≤ 0.001 during the most important season/month was considered for further calibration and verification tests.

3 – 2.5 SPI reconstruction and determination of extreme events

A linear model was established to explain the relationship between the regional SPL residual chronology and SPI. A split calibration/verification approach was used to estimate the reliability and predictive power of the transfer function over time. The explained variance (r^2), reduction of error statistic (RE; Briffa *et al*. 1988), coefficient of efficiency (CE; Cook *et al*. 1994) and the Durbin-Watson test (DW; Durbin and Watson 1951) were used to estimate the robustness of the final model. Positive RE and CE scores indicate reconstruction skill of the model (Cook *et al*. 1994). The DW statistic tests for autocorrelation in the model residuals. A DW value of 2 suggests little to no autocorrelation, whereas smaller (larger) values indicate positive (negative) autocorrelations, respectively. Two-tailed 95% confidence intervals were computed using a Monte Carlo approach to account for model uncertainty. In the first step, this procedure includes the random generation (n = 1000) of time series of the response variable SPI for the period 1961-2015 with an amount of variance equal to the residual standard error of the model. In the second step, we repeated the

procedure of linear modelling using the 1000 series to establish SPI estimates based on TRW. For the detection of extremely dry and pluvial events, we adopted the threshold of ±1 SD (McKee *et al*. 1993).

The final reconstruction was transferred using linear regression instead of a scaling to support the estimation of uncertainty due to unexplained instrumental SPI variance (Esper *et al*. 2005). All analysis was performed using the R software (R Core Team 2017).

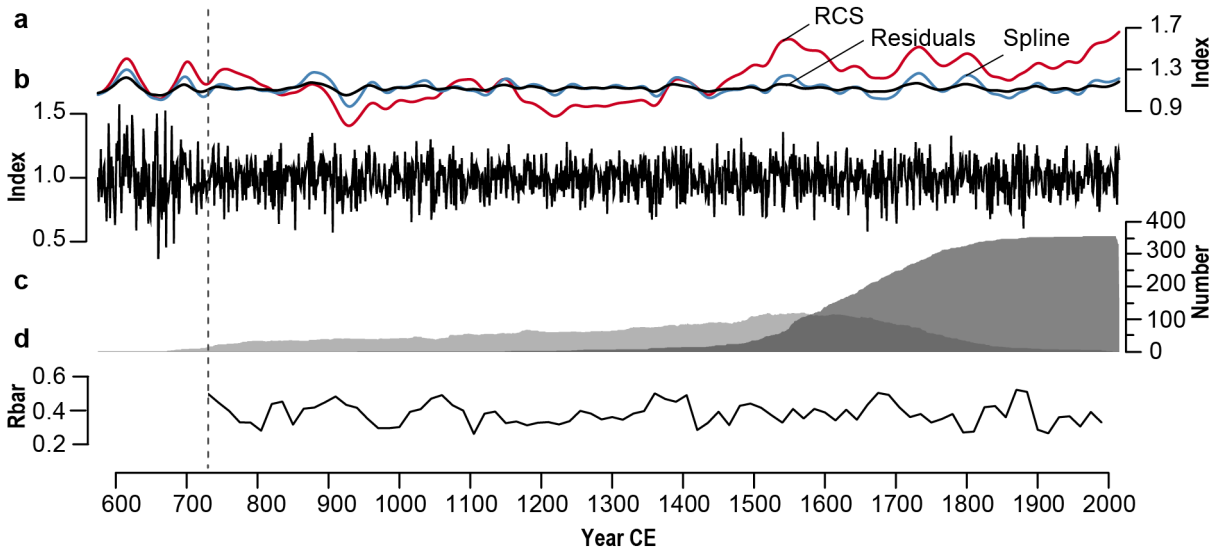

Figure 3–2 | Chronology characteristics **a** 50-year smoothed RCS (red), standard (blue) and SPL residual (black) chronologies. **b** Uncorrected SPL residual chronology. **c** Yearly sample size for relict and living material. **d** Rbar statistics of the standard chronology (calculated over 30 years lagged by 15 years). The vertical dashed line indicates 730 when the EPS passes the 0.85 threshold.

3 – 3 Results

3 – 3.1 Chronology characteristics and heteroscedasticity

By combining 615 living and dead wood series, we produced a chronology that covers the period 575-2015 (730-2015; EPS > 0.85) (Figure 3–2a, Figure 3–2b). The longest series from the living tree *Adonis* contains 1075 rings, and the longest relict series covering 873-1737 has 865 rings. Sample replication decreases from 329 series in 2014 to 146 series in 1500, 43 series in 1000, and 15 series in 730 (Figure 3–2c). Mean Rbar is 0.31 (Figure 3–2d) and first-order auto correlation is 0.77 (Table 3–1). Comparison of the SPL and RCS techniques clearly demonstrates that the RCS chronology captures longer-term variability, including multi-decadal and centennial scales, whereas variability of the SPL chronology is constrained to annual to decadal scales (Figure 3–2a). First-order autoregressive modelling removed all low-frequency information (Figure 3–2a, Figure 3–2b). Despite several statistical adjustments (power transformation, detrending, pre-whitening, variance adjustment) to account for sample size and inter-series correlation changes, the SPL residual chronology contains

changes in variance that might produce spurious periods with increased/reduced drought and pluvial events. The SPL residual chronology reveals periods of reduced variance from the 12th to 14th century, during the 18th and since the 20th century (Figure 3–3a).

To address the role of insufficient correction for heteroscedasticity as a potential driver of shifts in variance, we further examined the variance structure of 1000 residual chronologies with a constant yearly sample size of n = 80, and n = 15. The spread of the 100-year moving SD of these chronologies suggests that fluctuations in variance are persistent back in time and sample-size independent (Figure 3–3b). In the second experiment, cambial age-alignment of the residual series, the corresponding 100-year moving SD patterns demonstrate that despite spread-level adjustments, variance in the residual dataset is still a function of tree age (Figure 3–3c). Phases of high variability correspond to biologically younger states and phases of low variability correspond with older tree-ages, which demonstrate that despite power transformation (Cook and Peters 1997), an age-depended variance decline exists.

As the dataset includes many old and slow-growing living trees with several individuals of nearly millennial age, and age heterogeneous relict material, due to different stages of weathering, tree age increases towards the present (Figure 3–3d). With regard to age-effects in variance, age-class chronologies with homogenous age structures through the last millennium were created (Figure 3–3d). Considering only age-segments of 1-200 and 201-400 years, a comparison of moving window SD patterns of the original SPL residual chronology with age-class residual chronologies demonstrates that shifts in variance are partially a function of the age structure of the dataset (Figure 3–3e). For the entire dataset, in the 19th to 21st century, variance declines when tree age constantly increases and biologically old segments dominate. The age structure adjustment relying solely on age segments between 1-200 or the ones between 201-400, demonstrate that for the post-1800 period, a homogenous age structure increases variance (Figure 3–3e). To correct for this non-climatic artefact in variance, we used the arithmetic mean of the 1-200 and 201-400 SPL residual age-class chronologies for calibration and reconstruction (Figure 3–3f). Despite these variance adjustments, additional decadal-centennial variance changes remain in the chronology that may represent changes in long-term precipitation variability (Figure 3–3e).

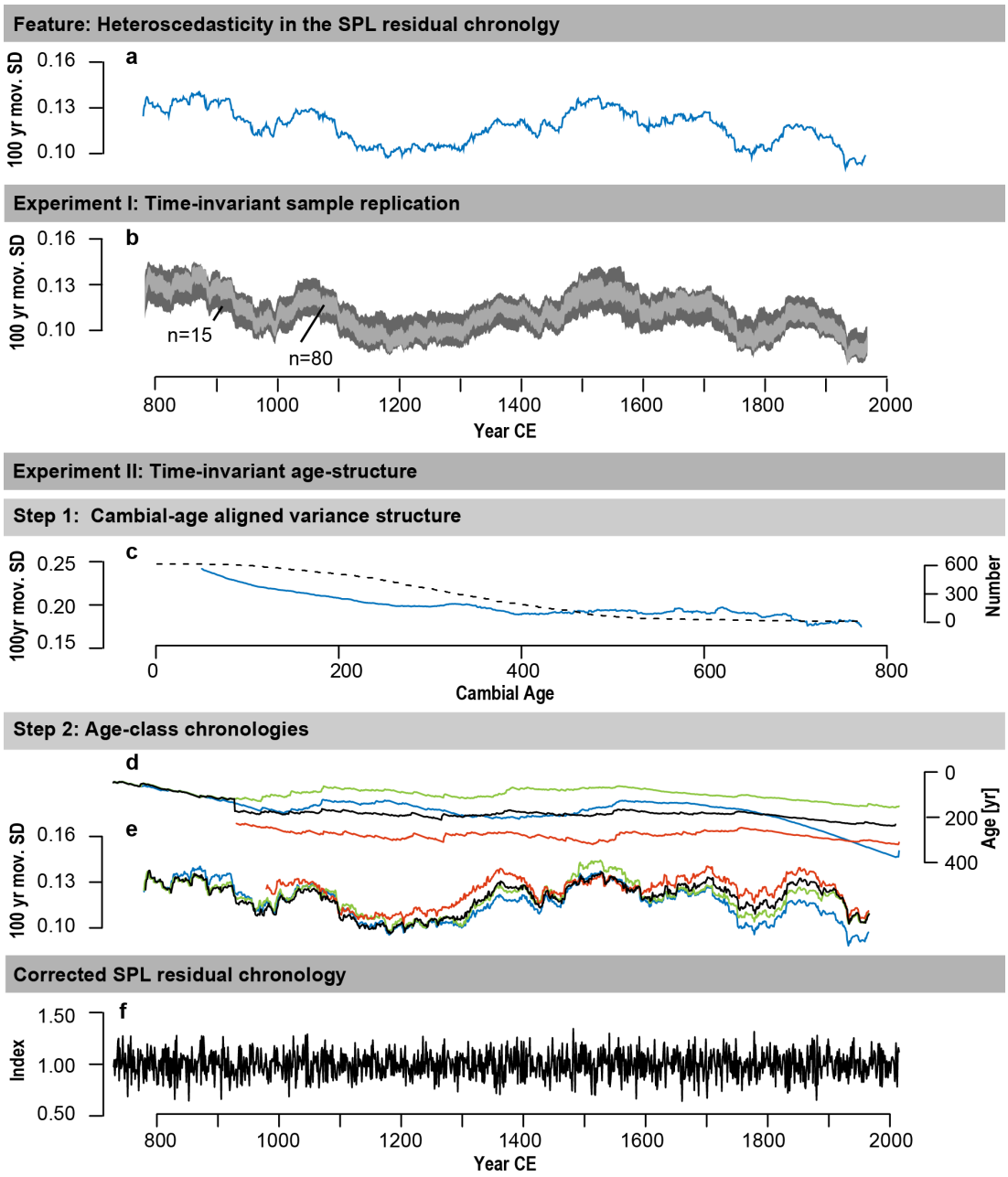

Figure 3–3 | Development of a variance-balanced chronology and analysis of sample size and tree age as potential biases **a** Heteroscedastic variance in the SPL residual chronology displayed as 100-year moving SD. **b** Bandwidth of 100-year moving SD of 1000 artificially generated residual SPL chronologies (see Figure 3–S1) with constant yearly sample sizes of 80 (light grey) and 15 series (dark grey). **c** 100-year moving SD of the mean of 615 cambial age aligned individual residual series (blue) and sample replication (dashed line). **d** Calendar year aligned mean tree ages of the initial SPL residual chronology (blue), the SPL residual age-class chronologies 1-200 (green), 201-400 (red) and their average (black). **e** Corresponding 100-year moving SD. **f** The age structure corrected SPL residual chronology used for calibration and reconstruction.

3 – 3.2 TRW climate signals

Correlation work on PIHE TRW revealed growth-climate relationships are not stable in the low-frequency domain (Seim *et al*. 2012; Klippel *et al*. 2017). Calibration tests support these findings as no significant relationship ($p < 0.01$) between temperature, precipitation, SPI and the RCS and SPL standard chronologies are identified (Figure 3–S2). Correlation analysis of the SPL residual chronology with SPI and precipitation data shows that the high-frequency TRW variations mirror moisture changes, with the highest coefficients being achieved using SPI as a calibration target. Therefore, we focused on high-frequency hydro-climatic changes, calibrating the SPL residual chronology against 1-month and 2-month SPI.

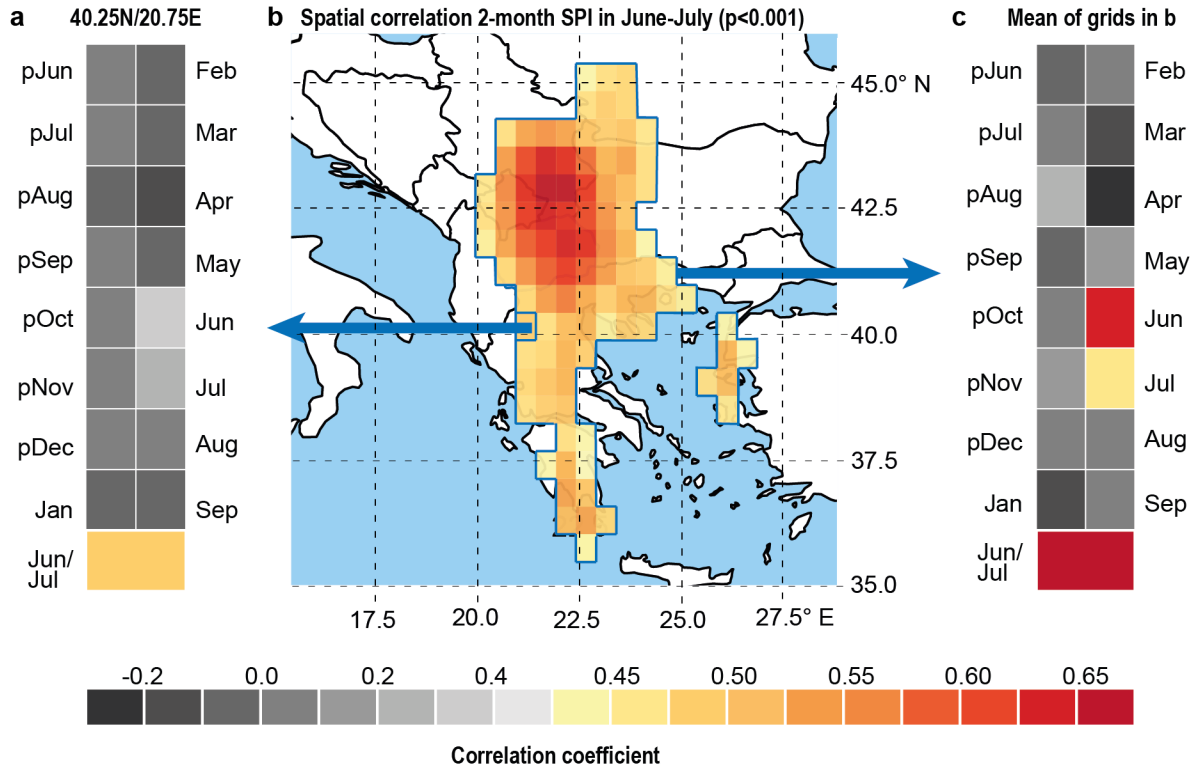

Figure 3–4 | Chronology calibration **a** SPL residual chronology correlated over the 1961-2015 period with 1-month SPI and 2-month SPI June-July based on precipitation data from the 0.5° grid 40.25°N/20.75°E. **b** Spatial extent of significant ($p \leq 0.001$) correlations of the SPL residual chronology and the 0.5° 2-month SPI June-July. **c** Same as Figure 3–4a but the 1-month SPI and 2-month SPI June-July are averages of all grids displayed in Figure 3–4b.

Using only data from the closest grid (20.5-21°E/40-40.5°N) over the common 1961-2015 proxy-target period ($r = 0.43$), the correlation with SPI is neither high nor temporally stable (Figure 3–4a, Figure 3–S3). However, a spatial analysis relying on gridded data reveals a robust correlation pattern with 2-month SPI in June-July with Pearson correlation ranging from 0.43 to 0.66. A strong

correlation is found north of the study region with grids over the central part of the Balkan Peninsula between 40-45°N and 20-25°E, including Albania, Bulgaria, Greece, Kosovo, Macedonia, Romania and Serbia (Figure 3–4b). With the exception of some correlations with grid-cells over the mountainous mainland of Greece, SPI data covering the peninsular coast have no significant influence (Figure 3–4b). Average SPI for all grids that show a significant correlation with the SPL residual chronology at $p < 0.001$ return a $r = 0.68$ (1961-2015) correlation in June-July (Figure 3–4c).

3 – 3.3 Calibration/verification tests

The SPL residual chronology explains 48% of the 2-month SPI June-July variance over the 1988-2015 calibration period (Figure 3–5a). RE and CE scores of the corresponding 1961-1988 verification period are 0.42 each, and DW-statistics indicate no autocorrelation in the model residuals. Transposing the periods and using 1961-1988 for calibration, the SPL residual chronology explains 47% of SPI variance, RE and CE scores of the corresponding 1988-2015 verification period are 0.46 and 0.45, respectively, and DW-statistics indicate no autocorrelation (Figure 3–5b). Calibration/verification procedures indicate a stable relationship; therefore, we used the entire 1961-2015 period to develop a linear model for the reconstruction:

2-month SPI June-July = 4.7 + (-4.7* $_{\text{residual}}$ SPL)

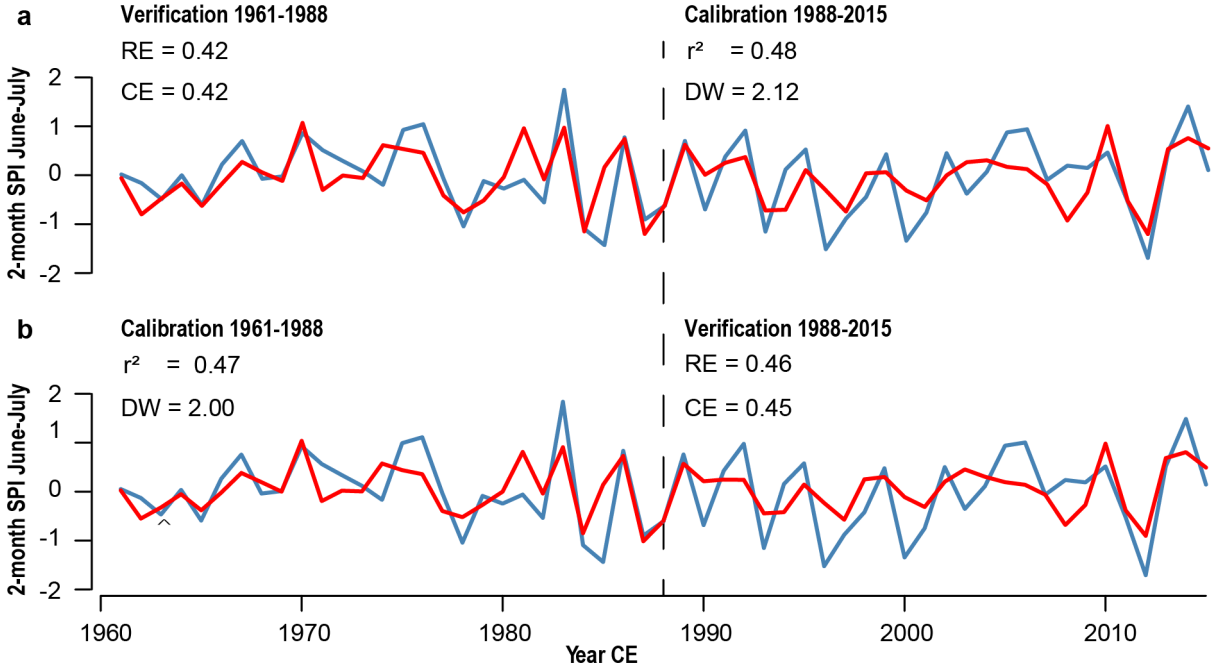

Figure 3–5 | Calibration and verification statistics for the grid-based 2-month SPI June-July reconstruction, blue lines indicate actual 2-month SPI June-July values and red lines the tree-ring derived estimates.

3 – 3.4 Identification of extreme years and variance changes

In total, the reconstruction contains 51 dry and 43 pluvial events exceeding the ±1 SD threshold since 730 (Figure 3–6). We identified a total of 72 new extreme events, 59 of which date prior to the 17th century. The driest and wettest years in the reconstruction are 1660 (-1.7 SD) and 1482 (+1.6 SD). Highest number of extremes were reconstructed during the 9th and 19th centuries, whereas the 12th century was characterized by few extremes. Extremes within the calibration period were the dry events of 1987 and 2012, and the pluvial event of 1970. Extreme dry and wet events of two-years duration occurred in 1517-1518, 1861-1862 and 737-738. Seemingly, extreme dry and pluvial events appear in decadal clusters, e.g. 822, 824, 830, 831, 833 and 1045, 1052, 1044, 1047 and 1880, 1873 and 1881, whereas we also find multiple decades without extreme events.

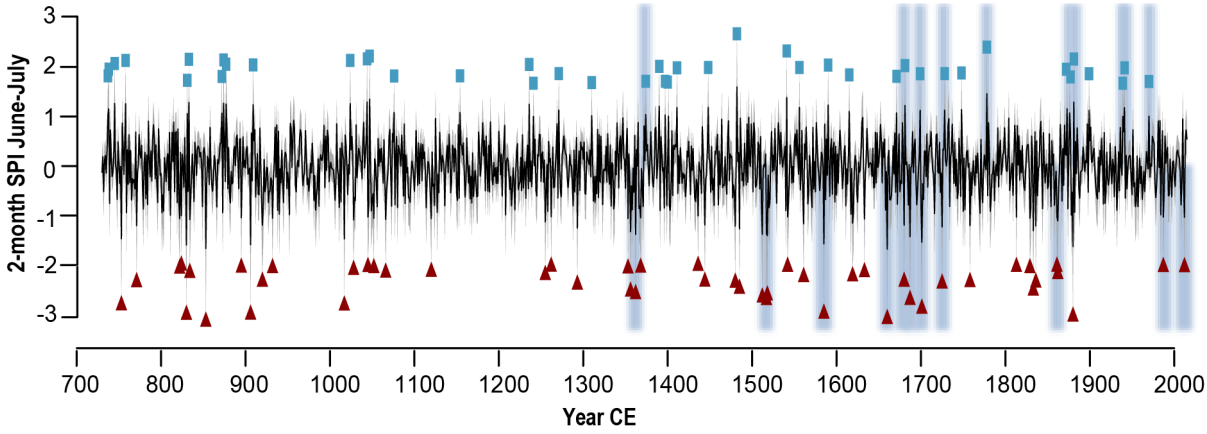

Figure 3–6 | 2-month SPI June-July reconstruction (black) and calibration uncertainty estimates (grey) since 730. Blue and red symbols indicate extreme events exceeding ±1 SD. Symbols were added at the tips of the uncertainty range. Shadings indicate extreme events verified by historical documents or previous hydroclimate reconstructions.

3 – 4 Discussion

We present the first PIHE-based reconstruction of hydro-climatic conditions for the Balkan Peninsula in the eastern Mediterranean from 730-2015. The reconstruction is based on a compilation of 615 TRW measurements reaching back to 575. The record's length makes it currently the longest PIHE TRW chronology.

3 – 4.1 Chronology characteristics and heteroscedasticity

The application of different standardization approaches demonstrates that PIHE TRW contains high-, medium- and low-frequency variance. RCS allows climatic information to be preserved on time-scales longer than the individual segments and long-term changes in environmental conditions are also preserved (Cook *et al.* 1995). When applying RCS to this dataset, one needs to be aware of the

contemporaneous old slow-growing trees as well as the relict material of mixed biological ages due to weathering. The significance of this combination on the low-frequency signal is not fully understood (Esper *et al*. 2003). However, RCS is used to evaluate potential low-frequency signals and to estimate the potential loss of low-frequency variance in the SPL residual chronology (Cook *et al*. 1995).

Our analysis has shown that despite the application of standardization procedures we still find a systematic relationship between tree-age and chronology variance, even after removing much of the low frequency variability in the SPL residual chronology (Carrer and Urbinati 2004; Esper *et al*. 2008; Linares *et al*. 2013; Konter *et al*. 2016). When using old slow-growing living trees only, mean segment length and tree age increase over time, resulting in a constant decrease in variance. We homogenised these age changes by creating two age-class chronologies that cover 1-200 years and 201-400 years, respectively, and by using the arithmetic mean chronology for reconstruction. This assessment underscored the importance of heterogeneous tree-ages for the calculation of unbiased tree-ring chronologies, as systematic tree-age changes add noise to the variance structure of a chronology (Frank *et al*. 2007a; Büntgen *et al*. 2015). These changes might affect the climate sensitivity of tree growth (Yu *et al*. 2008; Linares *et al*. 2013) and impact the magnitude and frequency of extreme events.

3 – 4.2 Hydro-climatic signal

The application of different detrending and filter techniques shows that the chronology mirrors high-frequency hydro-climatic changes more closely than low-frequency changes. Potential reasons for this discrepancy in the low-frequency domain include (i) a nonlinearity or decoupling of the growth/climate response on longer timescales (Fritts 1976); (ii) the more white precipitation spectrum compared to the red temperature spectrum (Ault and St. George 2010); (iii) potential biases in long-term trends inherent to instrumental data, e.g. caused by station relocations or changes in their operating system (Dienst *et al*. 2017), and (iv) the difficulty in preserving low-frequency variance in TRW (Esper *et al*. 2002). As also the reliable instrumental target extends only over 55 years back to 1961, the full spectrum of potential SPI variability, and particularly the low frequency end of that spectrum over longer timescales remains unaddressed.

In the high-frequency domain, tree growth is positively affected by moist summer conditions. This association is manifested by the high correlation between TRW and the 2-month SPI from June-July ($r > 0.43$; $p < 0.001$). We assume that cell production including enlargement in June-July is associated with stomatal responses to water availability that control water losses (Vieira *et al*. 2013). To avoid drought-induced hydraulic failure, stomata closure maintains a water potential above the threshold of xylem cavitation (Loustau *et al*. 1996) and metabolic processes like cell formation break down (Cherubini *et al*. 2003; McDowell *et al*. 2008; Hartl-Meier *et al*. 2015).

Spatial analysis reveals that the core region with highest 2-month SPI correlation from June-July ($r = 0.68$; $p < 0.001$) extends to a distance of 320 km from the study site, and that grids covering the

Pindus range and coast have minor or no significance. This is possibly due to the great spatial variability of precipitation caused by regional synoptic patterns and the orographic settings (Bolle 2003). During June and July, cool and dry Etesian winds blow from the Aegean Basin (Metaxas and Bartzokas 1994). These Etesian winds arise in conjunction with a low-pressure system located over the eastern Mediterranean and Near East, and a high-pressure system over the Balkan Peninsula (Repapis *et al*. 1978; Tritakis 1984). The frequency and force of these winds depends upon the strength of the pressure systems (Metaxas and Bartzokas 1994). We assume that the strength of the high-pressure cell situated over the central Balkan Peninsula modulates precipitation over the Pindus Mts., commonly in the form of thunderstorms (Marinaki *et al*. 2006). We assume a more pronounced warming and enhanced atmospheric instability in this region due to an increased continental climate, favouring the emergence of thunderstorms which penetrate into the Pindus Mts. from the North. Additionally, the remoteness of meteorological stations and the weighting of the data used for interpolation of the grid cells affects the spatial patterns. Grid cells differ by station data and weighting (Harris *et al*. 2014), causing differences in climate signal strength.

3 – 4.3 Drought history

We developed a 1286 year-long SPI reconstruction representative of a large area of the Balkan Peninsula (Figure 3–6). Since proxy data from the region are limited, we substantially improved our understanding about annually resolved hydro-climate prior to the LIA by producing a millennium length reconstruction. For the first time, regional evidence of past drought and pluvial events is extended back to 730. Multiple drought events, 59 (32) prior to the 17th (11th) century were detected, notably the exceptional 1482 pluvial.

TRW explains about 47% of the regional 2-month SPI June-July variance from 1961-2015. The explained variance lies within the range of previous SPI reconstructions developed in Romania (45%), Spain (40%), Sweden (45%; Seftigen *et al*. 2013) and Turkey (43%; Touchan *et al*. 2005). To assess patterns of past European precipitation variability, the new SPI estimates were compared with existing reconstructions from Spain (1694-2012; Tejedor *et al*. 2016) and Romania (1688-2010; Levanic *et al*. 2012) (in Figure 3–S4a, only Levanic *et al*.'s data are displayed). Whereas no significant correlation with the more remote reconstruction from Spain is found ($r = 0.002$; 1694-2012), the Romanian and our reconstructions correlate at $r = 0.31$ (1758-2015; Figure 3–S4b), suggesting a spatial coherence in drought variability over the Balkan Peninsula, probably driven by synoptic scale circulation (Xoplaki *et al*. 2003; Xoplaki *et al*. 2004). 31-year moving correlations between the Romanian and our record reveal an amplified coherency over time with increasing sample size in the Romanian record, and stable associations when EPS exceeds 0.85 (Figure 3–S2c) (Wigley *et al*. 1984).

Our reconstruction fills a spatial gap in a network of hydro-climatic records over the Balkan Peninsula and the eastern Mediterranean and refines our understanding of the spatial extent of hydro-climatic extremes. By comparing all regional hydro-climatic reconstructions (e.g. drought, sunshine,

precipitation) and historical records from Turkey (Purgstall 1983) and Spain (Alberola 1996) for the period of data overlap, we find a general correspondence between the strength of an event in our reconstruction and a number of historical/proxy pieces of evidence. The events in 1660 and 1725 are examples of severe droughts that extend over the entire Mediterranean. Over the Balkan Peninsula and eastern Mediterranean, the extremely dry summer of 1660 is captured in all tree-ring based climate reconstructions (D'Arrigo and Cullen 2001; Akkemik and Aras 2005; Akkemik *et al*. 2005; Touchan *et al*. 2005; Griggs *et al*. 2007; Akkemik *et al*. 2008; Köse *et al*. 2011), a finding that is consistent with historical documents reporting catastrophic fires and famines in Anatolia (Purgstall 1983). The dry summer of 1725 appears in drought reconstructions from Bosnia and Herzegovina, Greece, Romania, Spain and Turkey (Akkemik and Aras 2005; Akkemik *et al*. 2005; Köse *et al*. 2011; Levanic *et al*. 2012; Poljanšek *et al*. 2013; Klesse *et al*. 2015; Tejedor *et al*. 2016), and is verified in historical documents from Spain reporting a year without harvest (Alberola 1996).

The drought event in 1987 was spatially restricted to the Balkan Peninsula and does not appear in reconstructions from Turkey. The 1987 dry summer appeared as a narrow/negative pointer year in a PIHE chronology from Bulgaria when nearby climate stations recorded very dry conditions in June (Panayotov *et al*. 2010). In the same year, dry summer conditions were recorded in Romania (Levanic *et al*. 2012) and extremely dry June-August conditions were measured in Slovakia (Büntgen *et al*. 2009). Extremes with regional-scale influence include pluvial events in 1881 and 1970. The 1881 event is described as outstanding in Turkey (Akkemik *et al*. 2005; Akkemik *et al*. 2008; Köse *et al*. 2011) and Romania (Levanic *et al*. 2012). The wet summer of 1970 appears in multiple hydro-climatic reconstructions from Romania, Slovakia and Turkey (Akkemik *et al*. 2008; Büntgen *et al*. 2009; Levanic *et al*. 2012) and is also mentioned as a positive pointer year in Bulgaria (Panayotov *et al*. 2010). Although characterised by high proxy data availability, multiple extreme events in the post 17th century period e.g. 1633, 1748, 1829, 1873 and 1899, could not be linked with previous reconstructions or documentary evidence. As these extremes only slightly pass the threshold of ±1 SD, we assume they were caused by local environmental conditions.

3 – 4.4 Remaining uncertainties

We note that periods with extreme events in the reconstruction correspond to periods with high variance and periods without extreme events to periods with low variance. Despite statistical and age structure adjustments (described above), the final reconstruction reveals periods of increased drought and pluvial events and a decadal clustering of several extremes (Figure 3–6). The mechanisms of these long-term changes in extreme event occurrence remain unclear. We interpret phases with a lower/higher variance as stages of more balanced/variable climatic conditions, and assume no time dependent biases due to variance fluctuations that obscure the frequency of extreme events on decadal scales (Frank *et al*. 2007b). Across Spain, a linkage between summer warming and an increased frequency of extreme drought events during the 20th and 21st century has been identified (Tejedor *et*

al. 2016). However, at the high-elevation sites of Mt. Smolikas, the current aridification over the Mediterranean (Maheras and Anagnostopoulou 2003; García-Herra *et al*. 2007) does not impair tree growth as PIHE does not show any increased drought sensitivity in our study. We suggest that the current warming has increased the regional strength of orographic rainfall (Evans 2009; Black *et al*. 2010) and that PIHE now benefits from the addition, though these assumptions require further testing. Methodological considerations are unique to every proxy-climate reconstruction experiment, limiting inter-study comparisons of the frequency and magnitude of extremes. Ecological settings are heterogeneous, e.g. high-elevation vs. low-elevation (Griggs *et al*. 2007), and target parameters differ, e.g. SPI vs. precipitation (Klesse *et al*. 2015). In addition, extreme events are frequently defined differently: e.g., events that exceed ±1 SD (Touchan *et al*. 2005; Köse *et al*. 2011), ±1.76 SD (Türkes 1996; Akkemik and Aras 2005; Tejedor *et al*. 2016) and events that are ±2 SD (Köse *et al*. 2011) above or below the mean. These thresholds often correspond to percentiles of the observed data for the calibration period (Touchan *et al*. 2008) or are based on a fixed amount of extreme events, e.g. the 20 most positive/negative reconstructed values (Büntgen *et al*. 2009).

3 – 5 Conclusions

Based on a network of high-elevation sites on Mt. Smolikas in the Pindus Mts., Greece, regional summer drought variability was reconstructed for the first time back to 730. Summer drought was most severe in 1660 and climatic conditions most pluvial in 1482. Our reconstruction provides new insight on hydro-climatic variability in the north-eastern Mediterranean, especially prior to the Little Ice Age, and fills a temporal and spatial gap in a larger-scale drought reconstruction network (Griggs *et al*. 2007; Akkemik *et al*. 2008; Büntgen *et al*. 2009; Köse *et al*. 2011). We find that the frequency of extreme events has been variable, especially in the 20th century when the number of droughts considerably reduced. A set of tests, including power transformation (Cook and Peters 1997), variance stabilization (Frank *et al*. 2007b), pre-whitening, correction for age biases (Carrer and Urbinati 2004; Esper *et al*. 2008; Linares *et al*. 2013; Konter *et al*. 2016), and homogenising tree-age over time, showed that the variance change in the 20th century is not related to replication or inter-series correlation. We have successfully extended information on past hydro-climate variability into the first millennium and conclude that knowledge of the hydro-climatological history of the region has been markedly improved, especially prior to the LIA.

3 – 6 Acknowledgements

This study was supported by the German Research Foundation (DFG, ES 161/9-1) and National Science Foundation CAREER grant (NSF-CAREER #1349942). We thank Tilman Büttner, Markus Kochbeck, Oliver Konter, Amarita Krusic, Anna Krusic, Jonas Krusic, Fredrik C. Ljungqvist,

Matthew Meko, Valerie Trouet, and Sam Williams for valuable assistance in the field, and Tom Levanic and Ernesto Tejedor for providing SPI reconstructions and two reviewers for helpful suggestions. The authors declare no conflict of interest.

3 – 7 References

Akkemik U, Aras A. 2005. Reconstruction (1689-1994 AD) of April-August precipitation in the southern part of central Turkey. *Int. J. Climatol.* **25**: 537-548.

Akkemik U, D'Arrigo R, Cherubini P, Köse N, Jacoby GC. 2008. Tree-ring reconstructions of precipitation and streamflow for north-western Turkey. *Int. J. Climatol.* **28**: 173-183.

Akkemik U, Dagdeviren N, Aras A. 2005. A preliminary reconstruction (A.D. 1635-2000) of spring precipitation using oak tree rings in the western Black Sea region of Turkey. *Int. J.Biometeorol.* **49**: 297-302.

Alberola A. 1996. La percepción de la catástrofe: sequía e inundaciones en tierras valencianas durante la primera mitad del siglo XVIII. *Revista de Historia Moderna* **15**: 257-299.

Ault TR, St. George S. 2010. The magnitude of decadal and multidecadal variability in North American precipitation. *J. Clim.* **23**: 842-850.

Black E, Brayshaw DJ, Rambeau CM. 2010. Past, present and future precipitation in the Middle East: insights from models and observations. *Philos. Trans. A. Math. Phys. Eng. Sci.* **368**: 5173-5184.

Bolle HJ. 2003. *Mediterranean Climate*. Springer: Heidelberg, Germany.

Bräker OU. 1981. Der Alterstrend bei Jahrringdichten und Jahrringbreiten von Nadelhölzern und sein Ausgleich. *Mitt. Forstl. Bundes-Vers.anst. Wien* **142**: 75-102.

Brandes R. 2007. *Waldgrenzen griechischer Hochgebirge: Unter besonderer Berücksichtigung des Taygetos, Südpeloponnes*. Friedrich-Alexander-Universität Erlangen-Nürnberg: Erlangen, Germany.

Briffa KR, Jones PD, Pilcher JR, Hughes MK. 1988. Reconstructing summer temperatures in northern Fennoscandinavia back to A.D. 1700 using tree-ring data from Scots pine. *Arc. Alp. Res.* **20**: 385-394.

Briffa KR, Jones PD, Bartholin TS, Eckstein D, Schweingruber FH, Karlen W, Zetterberg P, Eronen M. 1992. Fennoscandian summers from AD 500 - temperature changes on short and long timescales. *Clim. Dyn.* **7**: 111-119.

Büntgen U, Brázdil R, Frank D, Esper J. 2009. Three centuries of Slovakian drought dynamics. *Clim. Dyn.* **35**: 315-329.

Büntgen U, Trnka M, Krusic PJ, Kyncl T, Kyncl J, Luterbacher J, Zorita E, Ljungqvist FC, Auer I, Konter O, Schneider L, Tegel W, Štěpánek P, Brönnimann S, Hellmann L, Nievergelt D, Esper J. 2015. Tree-ring amplification of the early nineteenth-century summer cooling in Central Europe. *J. Clim.* **28**: 5272-5288.

Carrer M, Urbinati C. 2004. Age-dependent tree-ring growth responses to climate in *Larix decidua* and *Pinus cembra*. *Ecology* **85**: 730-740.

Cherubini P, Gartner BL, Tognetti R, Bräker OU, Schoch W, Innes JL. 2003. Identification, measurement and interpretation of tree rings in woody species from mediterranean climates. *Biol. Rev. Cambridge Philosophical Society* **78**: 119-148.

Cook ER. 1985. *A time series analysis approach to tree ring standardization (PhD thesis)*. University of Arizona: Tucson, USA.

Cook ER, Briffa KR, Jones PD. 1994. Spatial regression methods in dendroclimatology: A review and comparison of two techniques. *Int. J. Clim.* **14**: 379-402.

Cook E, Briffa KR, Meko DM, Graybill D, Funkhouser G. 1995. The 'segment length curse' in long tree-ring chronology development for palaeoclimatic studies. *Holocene* **5**: 229-237.

Cook ER, Peters K. 1997. Calculating unbiased tree-ring indices for the study of climatic and environmental change. *Holocene* **7**: 361-370.

Cook E, Krusic PJ, Peters K, Holmes RL. 2017. Program ARSTAN version48d2, Autoregressive tree-ring standardization program. Tree-Ring Laboratory of Lamot-Doherty Earth Observatory. http://www.ldeo.columbia.edu/tree-ring-laboratory/resources/software.

Cufar K, De Luis M, Eckstein D, Kajfez-Bogataj L. 2008. Reconstructing dry and wet summers in SE Slovenia from oak tree-ring series. *Int. J. Biometeorol.* **52**: 607-615.

D'Arrigo R, Cullen HM. 2001. A 350-year (AD 1628-1980) reconstruction of Turkish precipitation. *Dendrochronologia* **19**: 169-177.

Dienst M, Linden J, Engstrom E, Esper J. 2017. Removing the relocation bias from the 155-year Haparanda temperature record in Northern Europe. *Int. J. Climatol.* **37**: 4015-4026.

Diffenbaugh NS, Giorgi F. 2012. Climate change hotspots in the CMIP5 global climate model ensemble. *Clim. Chang.* **114**: 813-822.

Dubrovský M, Hayes M, Duce P, Trnka M, Svoboda M, Zara, P. 2013. Multi-GCM projections of future drought and climate variability indicators for the Mediterranean region. *Reg. Environ. Chang.* **14**: 1907-1919.

Durbin J, Watson GS. 1951. Testing for serial correlation in least squares regression. *Biometrika* **38**: 159-178.

Esper J, Cook ER, Schweingruber FH. 2002. Low-frequency signals in long tree-ring chronologies for reconstructing past temperature variability. *Science* **295**: 2250-2253.

Esper J, Cook ER, Krusic PJ, Peters K, Schweingruber FH. 2003. Tests of the RCS method for preserving low-frequency variability in long tree-ring chronologies. *Tree-Ring Res.* **59**: 81-98.

Esper J, Frank D, Wilson R, Briffa KR. 2005. Effect of scaling and regression on reconstructed temperature amplitude for the past millennium. *Geophys. Res. Lett.* **32**: L07711, doi: 10.1029/2004GL021236.

Esper J, Frank D, Büntgen U, Verstege A, Luterbacher J. 2007. Long-term drought severity variations in Morocco. *Geophys. Res. Lett.* **34**: L17702, doi: 10.1029/2007GL030844.

Esper J, Niederer R, Bebi P, Frank D. 2008. Climate signal age effects–Evidence from young and old trees in the Swiss Engadin. *For. Ecolog. Manage.* **255**: 3783-3789.

Esper J, Krusic PJ, Ljungqvist FC, Luterbacher J, Carrer M, Cook E, Davi NK, Hartl-Meier C, Kirdyanov A, Konter O, Myglan V, Timonen M, Treydte K, Trouet V, Villalba R, Yang B, Büntgen U. 2016. Ranking of tree-ring based temperature reconstructions of the past millennium. *Quat. Sci. Rev.* **145**: 134-151.

Evans JP. 2009. Global warming impact on the dominant precipitation processes in the Middle East. *Theor. Appl. Climatol.* **99**: 389-402.

Fischer EM, Schar C. 2010. Consistent geographical patterns of changes in high-impact European heatwaves. *Nat. Geosci.* **3**: 398-403.

Fotiadi AK, Metaxas DA, Bartzokas A. 1999. A statistical study of precipitation in northwest Greece. *Int. J. Climatol.* **19**: 1221-1232.

Frank D, Büntgen U, Böhm R, Maugeri M, Esper J. 2007a. Warmer early instrumental measurements versus colder reconstructed temperatures: shooting at a moving target. *Quat. Sci. Rev.* **26**: 3298-3310.

Frank D, Esper J, Cook ER. 2007b. Adjustment for proxy number and coherence in a large-scale temperature reconstruction. *Geophys. Res. Lett.* **34**: L16709, doi: 10.1029/2007GL030571

Fritts HC. 1976. *Tree rings and climate*. Blackburn Press: Caldwell, USA.

Gao XJ, Giorgi F. 2008. Increased aridity in the Mediterranean region under greenhouse gas forcing estimated from high resolution simulations with a regional climate model. *Glob. Planet. Chang.* **62**: 195-209.

García-Herrera R, Hernández E, Barriopedro D, Paredes D, Trigo RM, Trigo IF, Mendes MA. 2007. The outstanding 2004/05 drought in the Iberian Peninsula: Associated atmospheric circulation. *J. Hydrometeorol.* **8**: 483-498.

Giorgi F, Lionello P. 2008. Climate change projections for the Mediterranean region. *Glob. Planet. Chang.* **63**: 90-104.

Griggs C, DeGaetano A, Kuniholm P, Newton M. 2007. A regional high-frequency reconstruction of May-June precipitation in the north Aegean from oak tree rings, AD 1089-1989. *Int. J. Clim.* **27**: 1075-1089.

Harris I, Jones PD, Osborn TJ, Lister DH. 2014. Updated high-resolution grids of monthly climatic observations - the CRU TS3.10. *Int. J. Clim.* **34**: 623-642.

Hartl-Meier C, Zang C, Büntgen U, Esper J, Rothe A, Gottlein A, Dirnbock T, Treydte K. 2015. Uniform climate sensitivity in tree-ring stable isotopes across species and sites in a mid-latitude temperate forest. *Tree Physiol.* **35**: 4-15.

Holmes RL. 1983. Computer-assisted quality control in tree-ring dating and measurement. *Tree-Ring Bulletin* **43**: 69-78.

Klesse S, Ziehmer M, Rousakis G, Trouet, Frank D. 2015. Synoptic drivers of 400 years of summer temperature and precipitation variability on Mt. Olympus, Greece. *Clim. Dyn.* **45**: 807-824.

Klippel L, Krusic PJ, Brandes R, Hartl-Meier C, Trouet V, Meko M, Esper J. 2017. High-elevation inter-site differences in Mount Smolikas tree-ring width data. *Dendrochronologia* **44**: 164-173.

Konter O, Büntgen U, Carrer M, Timonen M, Esper J. 2016. Climate signal age effects in boreal tree-rings: Lessons to be learned for paleoclimatic reconstructions. *Quat. Sci. Rev.* **142**: 164-172.

Konter O, Krusic PJ, Trouet V, Esper J. 2017. Meet Adonis, Europe's oldest dendrochronologically dated tree. *Dendrochronologia* ***42***: 12.

Köse N, Akkemik Ü, Dalfes HN, Özeren MS. 2011. Tree-ring reconstructions of May-June precipitation for western *Anatolia*. *Quat. Res.* **75**: 438-450.

Lange W, Janezic TS, Spanoudaki M. 1994. Cembratrienols and other components of white-bark pine (*Pinus heldreichii*) oleoresin. *Phytochemistry* **36**: 1277-1279.

Levanic T, Popa I, Poljansek S, Nechita C. 2012. A 323-year long reconstruction of drought for SW Romania based on black pine (*Pinus nigra*) tree-ring widths. *Int. J. Biometeorol.* **57**: 703-714.

Linares JC, Taïqui L, Sangüesa-Barreda G, Seco JI, Camarero JJ. 2013. Age-related drought sensitivity of Atlas cedar (*Cedrus atlantica*) in the Moroccan Middle Atlas forests. *Dendrochronologia* **31**: 88-96.

Ljungqvist FC, Krusic PJ, Sundqvist HS, Zorita E, Brattstrom G, Frank D. 2016. Northern Hemisphere hydroclimate variability over the past twelve centuries. *Nature* **532**: 94-98.

Loukas A, Vasiliades L, Dalezios NR. 2002. Hydroclimatic variability of regional droughts in Greece using the palmer moisture anomaly index. *Nord. Hydrol.* **33**: 425-442.

Loustau D, Breda N, Granier A. 1996. Transpiration of a 64-year-old maritime pine stand in Portugal. 1. Seasonal course of water flux through maritime pine. *Oecologia* **107**: 33-42.

Maheras P, Anagnostopoulou C. 2003. Circulation types and their influence on the interannual variability and precipitation changes in Greece. In *The climate of the Mediterranean region*: *From the past to the future*, Lionello P (ed). Elsevier, Amsterdam, pp. 215-239.

Marinaki A, Spiliotopoulos M, Michalopoulou H. 2006. Evaluation of atmospheric instability indices in Greece. *Adv. Geosci.* **7**: 131-135.

McDowell N, Pockman WT, Allen CD, Breshears DD, Cobb N, Kolb T, Plaut J, Sperry J, West A, Williams DG, Yepez EA. 2008. Mechanisms of plant survival and mortality during drought: why do some plants survive while others succumb to drought? *New Phytol.* **178**: 719-739.

McKee TB, Doesken NJ, Kleist J. 1993. The relationship of drought frequency and duration to time scales. *Conference Appl. Climatol.* **8**: 179-184.

Metaxas DA, Bartzokas A. 1994. Pressure covariability over the Atlantic, Europe and N Africa - application - centers of action for temperature, winter precipitation and summer winds in Athens, Greece. *Theor. Appl. Climatol.* **49**: 9-18.

Nastos PT, Kapsomenakis J. 2015. Regional climate model simulations of extreme air temperature in Greece. Abnormal or common records in the future climate? *Atmos. Res.* **152**: 43-60.

Panayotov M, Bebi P, Trouet V, Yurukov S. 2010. Climate signal in tree-ring chronologies of *Pinus peuce* and *Pinus heldreichii* from the Pirin Mountains in Bulgaria. *Trees* **24**: 479-490.

Pasho E, Camarero JJ, de Luis M, Vicente-Serrano SM. 2011. Impacts of drought at different time scales on forest growth across a wide climatic gradient in north-eastern Spain. *Agric. Forest Meteorol.* **151**: 1800-1811.

Poljanšek S, Ceglar A, Levanic T. 2013. Long-term summer sunshine/moisture stress reconstruction from tree-ring widths from Bosnia and Herzegovina. *Clim. Past* **9**: 27-40.

Purgstall B. 1983. *Ottoman state history. 1-7.* Üçdal Publishing: Istanbul, Turkey.

R Core Team 2017. R A language and environment for statistical computing, R Foundation for Statistical Computing, Vienna. URL https://www.r-project.org/.

Repapis C, Zerefos C, Tritakis B. 1978. On the Etesians over the Aegean. *Proceedings of the Academy of Athens* **52**: 572-606.

Rinn F. 2003. Time series analysis and presentation for dendrochronology and related applications, URL http://www.rimatech.com.

Schneider L, Smerdon JE, Büntgen U, Wilson RJS, Myglan VS, Kirdyanov AV, Esper J. 2015. Revising midlatitude summer temperatures back to A.D. 600 based on a wood density network. *Geophys. Res. Lett.* **42**: 4556-4562.

Seftigen K, Linderholm HW, Drobyshev I, Niklasson M. 2013. Reconstructed drought variability in southeastern Sweden since the 1650s. *Int. J. Climatol.* **33**, 2449-2458.

Seim A, Büntgen U, Fonti P, Haska H, Herzig F, Tegel W, Trouet V. Treydte K. 2012. Climate sensitivity of a millennium-long pine chronology from Albania. *Clim. Res.* **51**: 217-228.

Tejedor E, de Luis M, Cuadrat JM, Esper J, Saz MA. 2016. Tree-ring-based drought reconstruction in the Iberian Range (east of Spain) since 1694. *Int. J. Biometeorol.* **60**: 361-72.

Todaro L, Andreu L, D'Alessandro CM, Gutirrez E, Cherubinic P, Saracino A. 2007. Response of *Pinus leucodermis* to climate and anthropogenic activity in the National Park of Pollino (Basilicata, Southern Italy). *Biol. Conserv.* **137**: 507-519.

Touchan R, Funkhouser G, Hughes MK, Erkan N. 2005. Standardized precipitation index reconstructed from Turkish tree-ring widths. *Clim. Chang.* **72**: 339-353.

Touchan R, Meko DM, Aloui A. 2008. Precipitation reconstruction for Northwestern Tunisia from tree rings. *J. Arid Environ.* **72**: 1887-1896.

Tritakis VP. 1984. Possible solar signature on a well-established weather phenomenon. *J. Geophys. Res.* **89**: 2609-2615.

Trouet V, Panayotov MP, Ivanova A, Frank D. 2012. A pan-European summer teleconnection mode recorded by a new temperature reconstruction from the northeastern Mediterranean (AD 1768-2008). *Holocene* **22**: 887-898.

Türkes M. 1996. Meteorological drought in Turkey: A historical perspective, 1930-93. *Drought Netw. News* **8**: 17-21.

Vieira J, Rossi S, Campelo F, Freitas H, Nabais C. 2013. Seasonal and daily cycles of stem radial variation of *Pinus pinaster* in a drought-prone environment. *Agric. Forest Meteorol.* **180**: 173-181.

Wigley T, Briffa KR, Jones PD. 1984. On the average of correlated time series, with applications in dendroclimatology and hydrometeorology. *J. Clim. Appl. Meteorol.* **23**: 201-213.

Wilson R, Anchukaitis K, Briffa KR, Büntgen U, Cook E, D'Arrigo R, Davi N, Esper J, Frank D, Gunnarson B, Hegerl G, Helama S, Klesse S, Krusic PJ, Linderholm HW, Myglan V, Osborn TJ, Rydval M, Schneider L, Schurer A, Wiles G, Zhang P, Zorita E. 2016. Last millennium northern hemisphere summer temperatures from tree rings: Part I: The long term context. *Quat. Sci. Rev.* **134**: 1-18.

Xoplaki E, Luterbacher J, González-Rouco JF, Wanner H. 2003. Mediterranean summer air temperature variability and its connection to the large-scale atmospheric circulation and SSTs. *Clim. Dyn.* **20**: 723-739.

Xoplaki E, Gonzalez-Rouco JF, Luterbacher J, Wanner H. 2004. Wet season Mediterranean precipitation variability: influence of large-scale dynamics and trends. *Clim. Dyn.* **23**: 63-78.

Yu G, Liu Y, Wang X, Ma K. 2008. Age-dependent tree-ring growth responses to climate in Qilian juniper (Sabina przewalskii Kom.). *Trees* **22**: 197-204.

3 – 8 Supplement

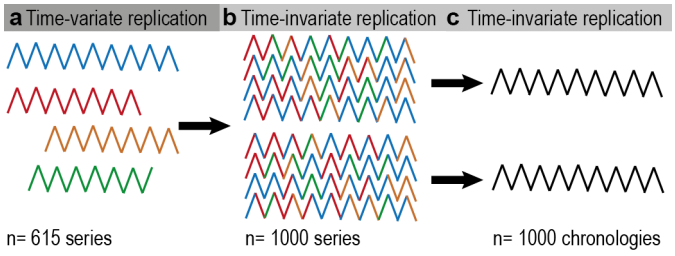

Figure 3–S1 | Calendar year specific series decomposition and generation of homogenous time series. **a** From 615 residual series. **b** 1000 artificial residual series spanning the period 730-2015 were generated by a new random composition of calendar year specific values. **c** 1000 mean chronologies, of which 80 (15) were randomly selected to create subset residual chronologies.

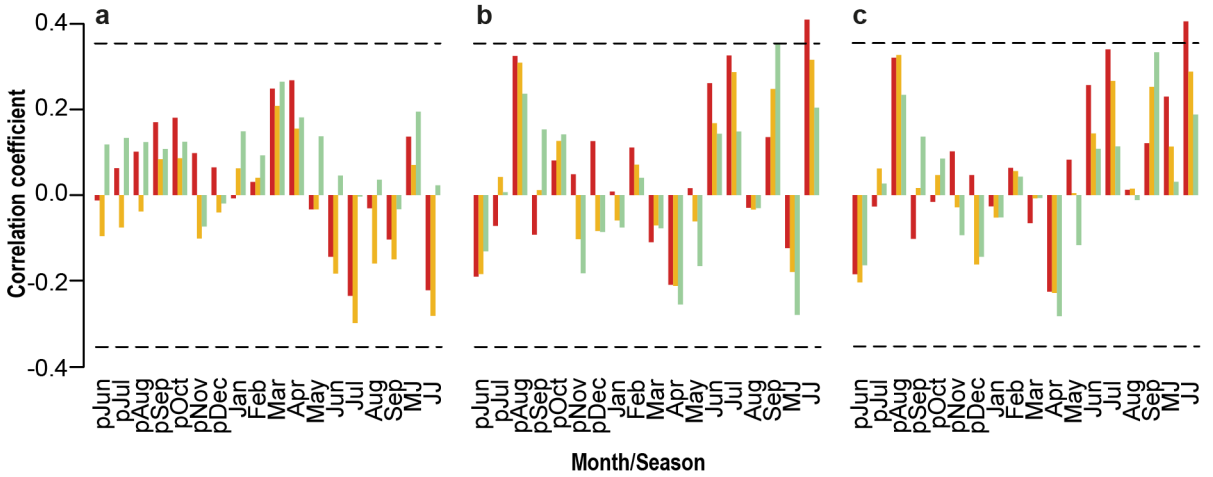

Figure 3–S2 | Correlation coefficients of the SPL residual (red), SPL standard (yellow), and RCS (green) chronologies with 1-month and 2-month **a** temperature, **b** precipitation, and **c** SPI data derived from the 20.5-21°E/40-40.5°N grid cell for the period 1961-2015. Dashed lines indicate $p < 0.01$ threshold.

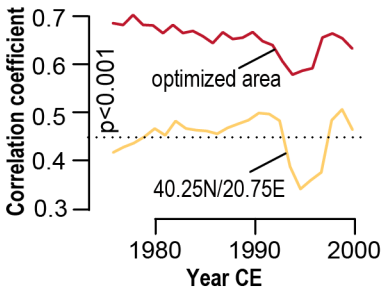

Figure 3–S3 | 31-year moving window correlations between the SPL residual chronology and 2-month SPI for June-July derived from the 20.5-21°E/40-40.5°N grid cell (yellow) and all grids displayed in Figure 3–4b (red).

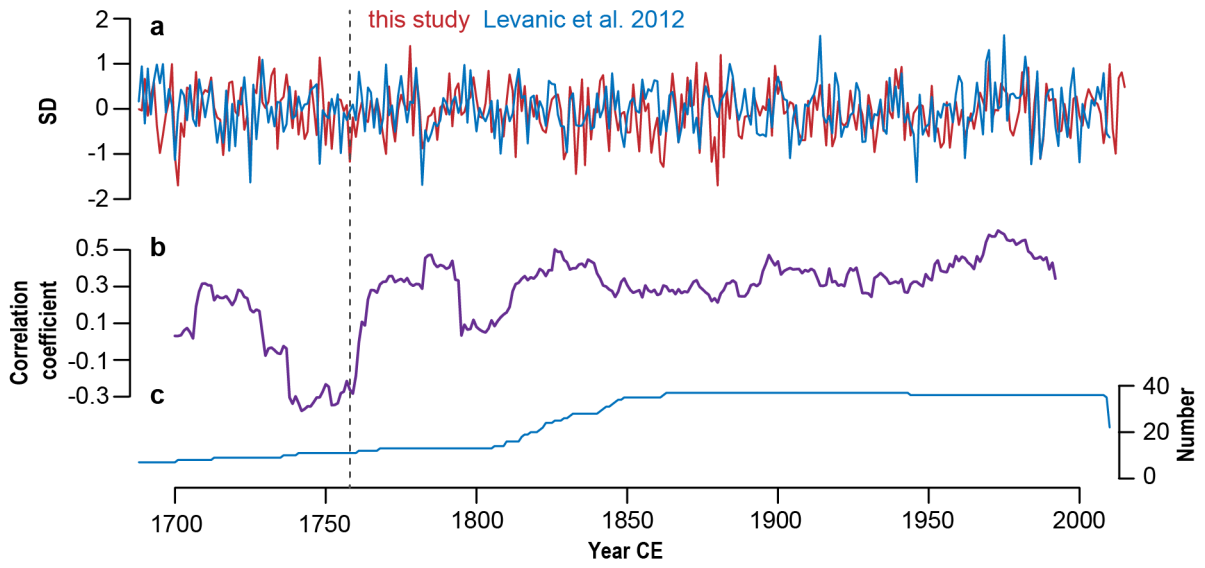

Figure 3–S4 | Inter-study comparison. **a** The Mt. Smolikas 2-month SPI June-July reconstruction (this study) shown together with a 3-month SPI June-August reconstruction from SW-Romania (Levanic *et al*. 2012). **b** Corresponding 31-year moving window correlations (1688-2010). **c** Number of *Pinus nigra* samples. The vertical dashed line indicates 1758 when EPS passes the 0.85 threshold in the Romanian record.

4 | A 1200+ year reconstruction of temperature extremes for the northeastern Mediterranean region

Lara Klippel[1], Paul J. Krusic[2,3,4], Oliver Konter[1], Scott St. George[5], Valerie Trouet[6], Jan Esper[1,4]

[1]*Department of Geography, Johannes Gutenberg University, 55099 Mainz, Germany*

[2]*Department of Geography, University of Cambridge, Cambridge CB2 3EN, United Kingdom*

[3]*Department of Physical Geography, Stockholm University, Stockholm, Sweden, SE106-91*

[4]*Navarino Environmental Observatory, Messinia, Greece*

[5]*Department of Geography, Environment and Society, University of Minnesota, Minneapolis, Minnesota, United States of America*

[6]*Laboratory of Tree-Ring Research, University of Arizona, Tucson, AZ 85721, United States of America*

International Journal of Climatology, 2018, published

4 – 1 Introduction

In the Mediterranean region, an overall warming trend (Xoplaki *et al*. 2003a; Alexandrov *et al*. 2004; Philandras *et al*. 2008; Toreti *et al*. 2009) has prevailed in the 20th century, with increasing frequency of hot summer temperature extremes (Kostopoulou and Jones 2005; Diffenbaugh *et al*. 2007). The intensity, length, and number of heat waves along the western Balkans and southern Black Sea coast have risen since the 1960s (Kuglitsch *et al*. 2010). Climate models agree on a persistent summer temperature increase in coming decades (Li *et al*. 2012), accompanied by extremely hot summers, which occurred only rarely during the past decades, but are projected to become common in the second half of the 21st century (Lelieveld *et al*. 2013). Additionally, risks of summer drought extremes are increasing in west-central Mediterranean regions (Alpert 2002; Sousa *et al*. 2011; Hoerling *et al*. 2012; Vicente-Serrano *et al*. 2014; Spinoni *et al*. 2015) affecting the overall fire risk (Moriondo *et al*. 2006). Meteorological records reveal a precipitation decrease in the eastern Mediterranean (García-Herrera *et al*. 2007) and extreme drought episodes have become more frequent and persistent (Xoplaki *et al*. 2004). In a centennial-to-millennial scale context, proxy-based climate reconstructions are needed to evaluate current climatic trends and changes in the frequency and magnitude of extremes, and to assess the full range of projected forcing impacts (Ljungqvist *et al*. 2016). Proxy archives also provide the background to study the impact of climate on societies and economies (Büntgen *et al*. 2011; Xoplaki *et al*. 2016) and support the differentiation between naturally and anthropogenically forced variations.

Tree growth at high-elevation sites in the Mediterranean region is typically influenced by a combination of temperature and precipitation (Seim *et al*. 2012; Trouet *et al*. 2012) limiting the use of tree-ring width (TRW) as a temperature proxy (Esper *et al*. 2016). Multiple TRW records and reconstructions have been produced in the region with hydroclimate as the dominant climatic signal (Akkemik and Aras 2005; Touchan *et al*. 2005; Griggs *et al*. 2007; Akkemik *et al*. 2008; Köse *et al*. 2011; Levanic *et al*. 2012; Seim *et al*. 2012; Esper *et al*. 2014b; Klesse *et al*. 2015; Tejedor *et al*. 2016; Klippel *et al*. 2017; Klippel *et al*. 2018). Progress has also been made in the assessment of long-term temperature dynamics based on indices from documentary sources (Camuffo *et al*. 2010; Kiss *et al*. 2011). In dendroclimatology, maximum latewood density (MXD) from *P. heldreichii* (PIHE) in central-eastern Mediterranean treeline forests was shown to contain a robust July-September temperature signal ($r > 0.6$; Trouet *et al*. 2012; Klesse *et al*. 2015). PIHE MXD derived temperature reconstructions have been developed for the Mt. Olympus region in Greece (1521-2010; Klesse *et al*. 2015), the Pirin Mountains in Bulgaria (1768-2008; Trouet *et al*. 2012), multiple sites in the northeastern Mediterranean basin (1675-1980; Trouet 2014), and Italy (1650-1980; Leonelli *et al*. 2017). However, millennium-length MXD chronologies have not yet been developed for the region, which limits our understanding of the occurrence, magnitude, and possible causes of naturally forced temperature extremes. Prior to 1550 (Klesse *et al*. 2015), regional temperature information is available

solely from low resolution (decadal to multi-decadal) proxy archives (Grauel *et al*. 2013; Gogou *et al*. 2016; Izdebski *et al*. 2016).

Millennium-length MXD based temperature reconstructions have been produced in locations where tree growth is temperature limited and wood material has been preserved for several hundreds of years (Esper *et al*. 2016). In Europe, MXD chronologies spanning the past millennium have been developed at the northern tree line in Scandinavia (Esper *et al*. 2012; Melvin *et al*. 2013; Esper *et al*. 2014a; Linderholm *et al*. 2014) and at the elevational tree line in the Pyrenees (Büntgen *et al*. 2008; Dorado Liñán *et al*. 2012; Büntgen *et al*. 2017b) and Alps (Schweingruber *et al*. 1988; Büntgen *et al*. 2006). Especially in the Mediterranean region, an improved spatial distribution of high-resolution proxy archives is required to refine our knowledge about pre-instrumental climate variability patterns and their association with natural forcings at regional to continental scales (PAGES 2k PMIP3 group 2015).

Here, we address these topics by (1) introducing a new MXD tree-ring chronology from 132 density profiles of living and relict high-elevation pine trees in the Pindus Mountains of Greece, that covers the period 738-2014 and reflects August-September temperature variability; (2) identifying past temperature extremes at annual-to-decadal scales, as well as detecting their spatial extent and association with atmospheric patterns and climatic forcings.

4 – 2 Data and methods

4 – 2.1 Geographical settings and sampling design

Between 2011 and 2016, 47 cores and 85 discs were collected at four *P. heldreichii* sites, with different exposures within the tree line ecotone at 2100m a.s.l on Mt. Smolikas (SMO) (Figure 4–1a to c; subset of Klippel *et al*. 2017). MXD measurements are produced using the high-precision DENDRO2003 X-ray radio densitometer from Walesch Electronic. Samples were prepared according to standard dendrochronological techniques for X-ray exposure (Lenz *et al*. 1976; Schweingruber *et al*. 1978). Cores and wedges are treated for 34 hours with alcohol in a Soxhlet to extract resins and other compounds. Each sample was split into three cm long sections to avoid biases from internal changes in stem-fibre direction. Two mm thick laths from these sections are cut perpendicular to the tracheid's longitudinal axis using a twin blade saw. The laths and a five-step cellulose calibration wedge are placed on X-ray films and exposed for 14 minutes. Depth levels of the calibration wedge returned reference values that are used to transform the X-ray film grey-scales into estimates of wood density.

We produced two versions of the Smolikas density record considering two detrending methods to remove biological age trends (Bräker 1981) from the MXD series: (i) ratios from cubic splines with a 50% frequency-response cut-off at 100 years to emphasize inter-annual to multi-decadal scale

variability (100SP), and (ii) ratios from a spline with a 50% frequency-response cut-off at 10 years to emphasize inter-annual variability (10SP; Cook and Peters 1981; Cook *et al*. 2017). These detrendings are specifically designed to preserve high-frequency variance and remove long-term fluctuations. Trends in variance, which mainly originate from changes in sample replication and inter-series correlation (Frank *et al*. 2007), are corrected by fitting 30-year splines to the mirrored chronologies and calculating ratios (Cook and Peters 1997). The two (100SP and 10SP) chronologies are truncated at n < 10 series. The inter-series correlation (Rbar) is calculated using 30-year segments lagged by 15 years to evaluate temporal coherence changes among the MXD series (Wigley *et al*. 1984). Variance changes are analysed by calculating 100-year moving window standard deviations (SD). In addition, the spline chronologies and absolute density values (g/cm^3) are compared with PIHE MXD data from the nearby Katarapass (KAT) and Mt. Olympus (OLY) in Greece (Klesse *et al*. 2015), Bulgaria (VIH; Trouet *et al*. 2012), and Italy (ITP; Schweingruber and Briffa 1996) (Table 4–1). Some of these chronologies are available on the ITRDB (https://www.ncdc.noaa.gov/paleo-search/; Grissino-Mayer and Fritts 1997), while others were provided to us by the authors.

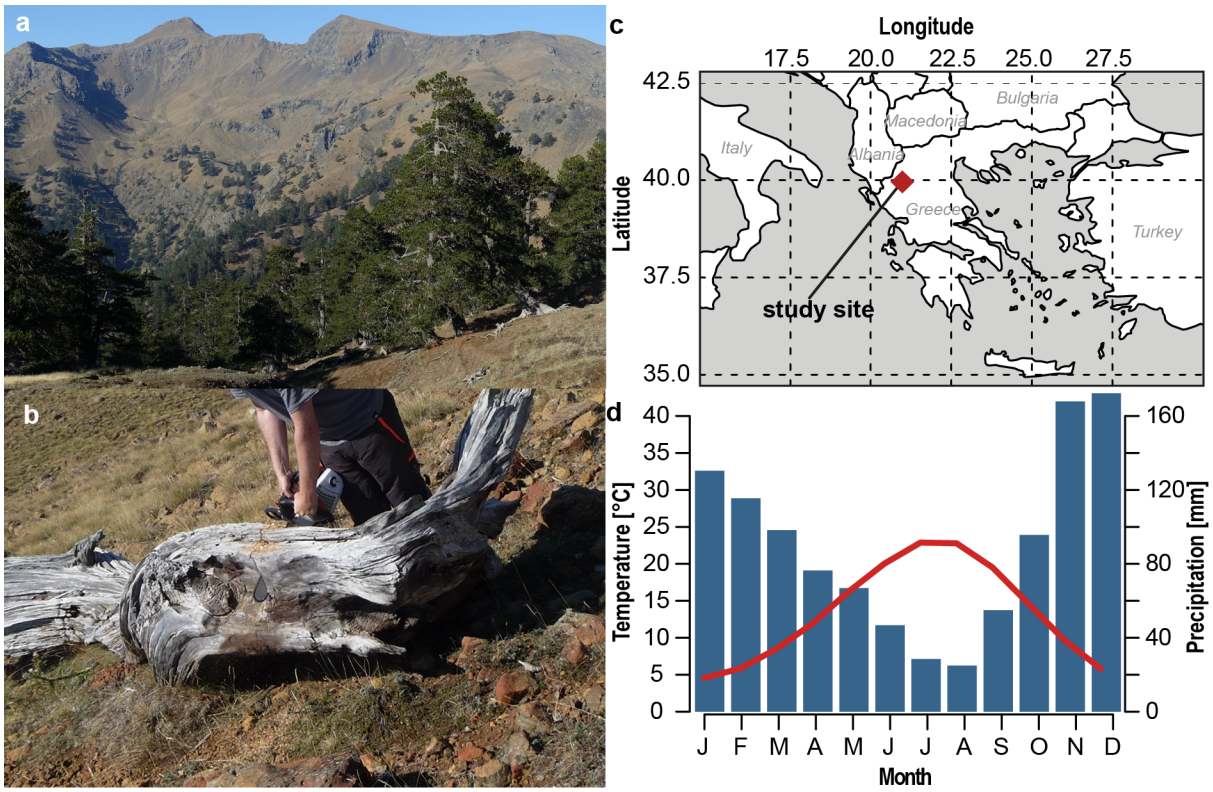

Figure 4–1 | Site characteristics. **a** Typical shape of the oro-mediterranean ecotone (2000-2200m a.s.l.) at the eastern foothills of Mt. Smolikas in northwestern Greece with open stands of *Pinus heldreichii* forming the tree-line and **b** sampling of relict material. **c** Map of the of the study region and **d** climate diagram of the meteorological station in Ioannina (39.70°N/20.80°E, 488m a.s.l.) for the period 1961-1990.

4 – 2.2 Climate data and signal detection

The study region is characterized by a Mediterranean climate with warm to hot summers, droughts during June-September, and humid winters (Figure 4–1d). The distinct intra-annual precipitation differences are caused by seasonal alternations in the occurrence of cyclonic storms in winter and subtropical high-pressure cells in summer (Bolle 2003). Climate at the elevation of the study site is characterized by cold, snowy winters with snow melt occurring in late spring, and summer dryness is limited to June-August (Fotiadi *et al*. 1999; Loukas *et al*. 2002).

The 0.5° gridded EOBS v.15 climate data of the 20.75°E/40.25°N grid point are used for the analysis of growth-climate responses (Haylock *et al*. 2008). The use of station data (Ioannina Figure 4–1d, Thessaloniki) and other gridded products (CRU TS 3.24 climate data; Harris *et al*. 2014) yielded no significant differences in calibration results. As with the MXD data, the temperature data are high-pass filtered by calculating residuals from 100-year and 10-year smoothing splines to emphasize inter-annual to decadal scale variance. Growth-climate relationships are assessed by the Pearson correlation coefficients between the chronologies and high-pass filtered temperature and precipitation data for the period 1950-2014, on a monthly basis and using seasonal windows ranging from previous-year August to current-year October. The pre-1950 instrumental data have previously been shown to be insufficiently reliable for grid interpolations over the mountainous terrain of northern Greece (Klippel *et al*. 2017; Klippel *et al*. 2018). Spatial correlation maps were produced using the KNMI Climate Explorer (https://climexp.knmi.nl/; Trouet and van Oldenborgh 2013).

We used a partial correlation approach to distinguish the competing but inter-related influences of precipitation and temperature on MXD formation (Meko *et al*. 2011). In a first step, simple Pearson correlations between 1-month and 2-month windows of temperature or precipitation and the MXD chronologies were calculated. In the second step, a partial correlation was applied removing the effect of the inter-correlation between temperature and precipitation, thereby accentuating the pure temperature or precipitation signal. The stability of the growth-climate relationship for the most important season was tested by modifying sample replication to assess the significance of earlier, less replicated periods of the record (Esper *et al*. 2012). Correlation coefficients were derived from calibrating a total of 2000 subsamples of the spline chronologies against August-September temperatures. The replicate tree-ring chronologies were developed using 5 to 35 MXD series randomly drawn 2000 times from the population of 43 series that cover the entire calibration period.

4 – 2.3 Reconstruction of temperature extremes

A scaling approach is used for calibration where both the mean and standard deviation of the spline-detrended chronologies are adjusted to their corresponding values of the (spline-detrended) instrumental temperature data to retain the spectrum of instrumental variance in the reconstructions (Esper *et al*. 2005). Uncertainties in the reconstruction increase back in time due to the decreasing number of series (chronology error), and are estimated in ARSTAN software (Cook *et al*. 2017) by

bootstrapping (Briffa *et al*. 1992), and transferred into temperature estimates via scaling (Esper *et al*. 2007; Trouet 2014). The reduction of error statistic (RE; Briffa *et al*. 1988) and coefficient of efficiency (CE; Cook *et al*. 1994) are used to estimate the strength of the relationship between reconstructed and observed temperatures. Positive RE and CE scores indicate reconstruction skill of the model (Cook 1994). For the detection of extremely cold and warm summers, the ± 1.5 SD threshold is used. Thresholds and detection method are thus unique to every proxy-climate reconstruction experiment and their value affects inter-study comparisons of extremes (Akkemik *et al*. 2005; Köse *et al*. 2011; Tejedor *et al*. 2016). Temporal changes in the frequency of extremes are analysed by counting the numbers of cold and warm events using running 100-year windows.

Superposed Epoch Analysis (SEA) is performed to quantify post-volcanic cooling over the past millennium (Panofsky and Brier 1958). We extracted the dates of the 11 largest sulphur peaks in the composite Greenland and Antarctic ice core records (excluding 1458; Sigl *et al*. 2015), which are thought to be caused by large extratropical eruptions as well as the 1835 Cosiguina, 1883 Krakatau (Esper *et al*. 2013b) and 1452 Kuwae (Esper *et al*. 2017) eruptions to set the timing of the impulse spike. All SEA results are displayed as temperature anomalies with respect to five years prior to the eruptions. Temporal mismatches of two years between known and unknown eruptions and reconstructed cooling arise due to dating uncertainties in the ice core sulphur record (Baillie and McAneney 2015; Schneider *et al*. 2017).

4 – 2.4 Spatial patterns of temperature extremes

A European-wide comparison of summer temperatures is performed to examine the spatial extent of reconstructed extremes. We compiled a collection of ten MXD datasets from various locations across Europe including five sites within a 1000 km radius from the Pindus Mts. (Table 4–1). All datasets are described as having a clear summer temperature signal, and we accessed the data via the ITRDB or from the original authors. In addition to the four *P. heldreichii* chronologies (KAT, OLY, VIH, ITP) detailed above, we added an *Abies alba* (ITA) chronology from Italy (Schweingruber and Briffa 1996), a *Larix decidua* chronology from the High Tatras in Slovakia (TAT; Büntgen *et al*. 2007), a *Larix decidua* chronology from the Swiss Alps (ALP; Büntgen *et al*. 2006), a *Pinus uncinata* chronology from the Pyrenees in Spain (PYR; Büntgen *et al*. 2017b), a *Pinus sylvestris* regional chronology from 11 sites across British Isles (BRI; Schweingruber and Briffa 1996; Trouet *et al*. 2018), and a *Pinus sylvestris* chronology from north Scandinavia (SCA; Esper *et al*. 2012).

Before comparing the temperature history in our reconstruction with that of the ten European MXD collections, the raw data in each of the latter are re-standardized and re-calibrated to produce a similar ratio of high-to-low frequency temperature variability in all datasets (Franke *et al*. 2013; Esper *et al*. 2016). Each collection's raw data is standardized according to the methods applied to the SMO dataset (see above). A re-calibration is performed using temperature data from the 0.5° EOBS v.15 dataset (Haylock *et al*. 2008). The spatial extent of the datasets varies, thus the EOBS temperature grid-size is

adjusted to the size of the respective study region described by the chronologies' authors and provided in Table 4–1. For those datasets previously used for climate reconstruction, seasonal grid-cell means with the highest temperature response is used. For example, the SCA record is calibrated against the mean JJA grid-cell temperatures over the region 67-70°N and 20-28°E. All reconstructions are rescaled and extremes are defined as values exceeding ±1.5 SD.

Table 4–1 | Description and temperature signals of ten tree-ring maximum latewood density chronologies from Europe used for inter-site comparison of temperature extremes.

Code	Site	Country	Species	Length n > 10	Seasonal target	r = 100 / 10 SPL	EOBS grid N / E	Distance km
SCA	NScan	Finland	PISY	-4-2006	JJA	0.75/0.75	67 - 70N 20 - 28E	3200
BRI	Scotland	UK	PISY	1720-1978	JJA	0.75/0.69	47 - 57N 10W - 2E	2600
PYR	Pyrenees	Spain	PIUN	1229-2014	MJAS	0.65/0.68	42 - 42.5N 0.5 - 1E	1800
ALP	Lötschental	Switzerl.	LADE	783-2004	JJAS	0.72/0.73	45 - 47N 6 - 9E	1350
TAT	Tatra	Slovakia	LADE	1707-2004	MJJ	0.67/0.74	49 - 49.5N 20 - 20.5E	1000
ITA	Bosque di Ceppo	Italy	ABAL	1741-1980	AS	0.66/0.74	42.5 - 43N 13 - 13.5E	700
ITP	Sierra di Cripo	Italy	PIHE	1683-1980	JAS	0.54/0.66	39.5 - 40N 16 - 16.5E	400
VIH	Vihren	Bulgaria	PIHE	1769-2008	A	0.67/0.73	41.5 - 42N 23 - 23.5E	300
OLY	Olymp	Greece	PIHE	1530-2010	JAS	0.54/0.60	40 - 40.5N 22 - 22.5E	40
KAT	Katarapass	Greece	PIHE	1759-1981	AS	0.37/0.65	39.5 - 40N 21 - 21.5E	10

*Correlation coefficients derived from re-calibration against EOBS v.15 gridded temperature data since 1950. ABAL = *Abies alba*, Lade = *Larix decidua*, PIHE = *Pinus heldreichii*, PISY = *Pinus sylvestris*, PIUN = *Pinus uncinata*

The analysis of synchronous temperature extremes is performed over the common period between the other individual European reconstructions and SMO, as well as the common period 1769-1978 between all reconstructions. Given all the reconstructions differ in their lengths and absolute number of extreme events, the percent overlap is calculated as a mean to enable inter-site comparisons. This analysis is repeated using August temperatures from the EOBS network to explore potential differences between instrumental and tree-ring derived temperature extremes. The analysis is restricted to the month of August to set a comparable time span among different station data. Due to the limited length of instrumental data, and in lieu of the 1.5 SD threshold, the five coldest and five warmest instrumental temperature anomalies from each of the ten calibration time series are compared to the average temperature of the calibration grid-cell (Haylock *et al*. 2008).

The significance of the number of common events is tested using a bootstrap approach. All reconstructions and instrumental time series were randomized 1000 times to ensure that extreme events appear by chance over time. This degree of repetition quantifies the range of possible overlaps in extremes that occur in a random time series. A larger number of common extreme years between the unperturbed reconstructions, compared to the randomized series, indicates common (climatic) forcing.

4 – 3 Results

4 – 3.1 Chronology characteristics

After truncation at a minimum sample replication of n < 10 series, the new SMO MXD chronology includes 1277 years and spans the period 738-2014. The number of series changes through time with a minimum of 11 series in 738 and a maximum of 44 series in the beginning of the 18th century (Figure 4–2c). The two detrendings reveal consistent results in the high-frequency domain, but mid-frequency variability only appears in the 100SP chronology (Figure 4–2a and Figure 4–2b). Mean tree age is balanced prior to 1700 and increases towards the present due to the integration of several near millennium-length series (Figure 4–2d). Coherency among the individual measurement series, expressed by the inter-series correlation (Rbar), is moderate with mean Rbar values of 0.30 and 0.38 for the 100SP and 10SP chronologies, respectively (Figure 4–2e). The Rbar values indicate the potential to provide high-resolution reconstructions of climate back to the first millennium. The moving SDs indicate that variance is stable through time with a general higher SD in the 100SP chronology compared to the 10SP chronology resulting from the additionally retained decadal scale variability (Figure 4–2f). The spline chronologies correlate significantly at high and mid frequencies with PIHE MXD chronologies from the northeastern Mediterranean. Correlation coefficients range from r = 0.55 to 0.82 (Figure 4–S1a and Figure 4–S1b). Absolute density values largely overlap, only the values from the OLY-2010 dataset are significantly lower (Figure 4–S1c). For the first 200 years of growth, the average MXD per sample is 0.71 g/cm^3 and 0.70 g/cm^3 during the last 200 years of

growth. From the relict material, the values are 0.71 g/cm^3 and 0.69 g/cm^3, respectively, indicating the material is not significantly affected by weathering processes. Inter-site differences in absolute density values are not significant (Figure 4–S2).

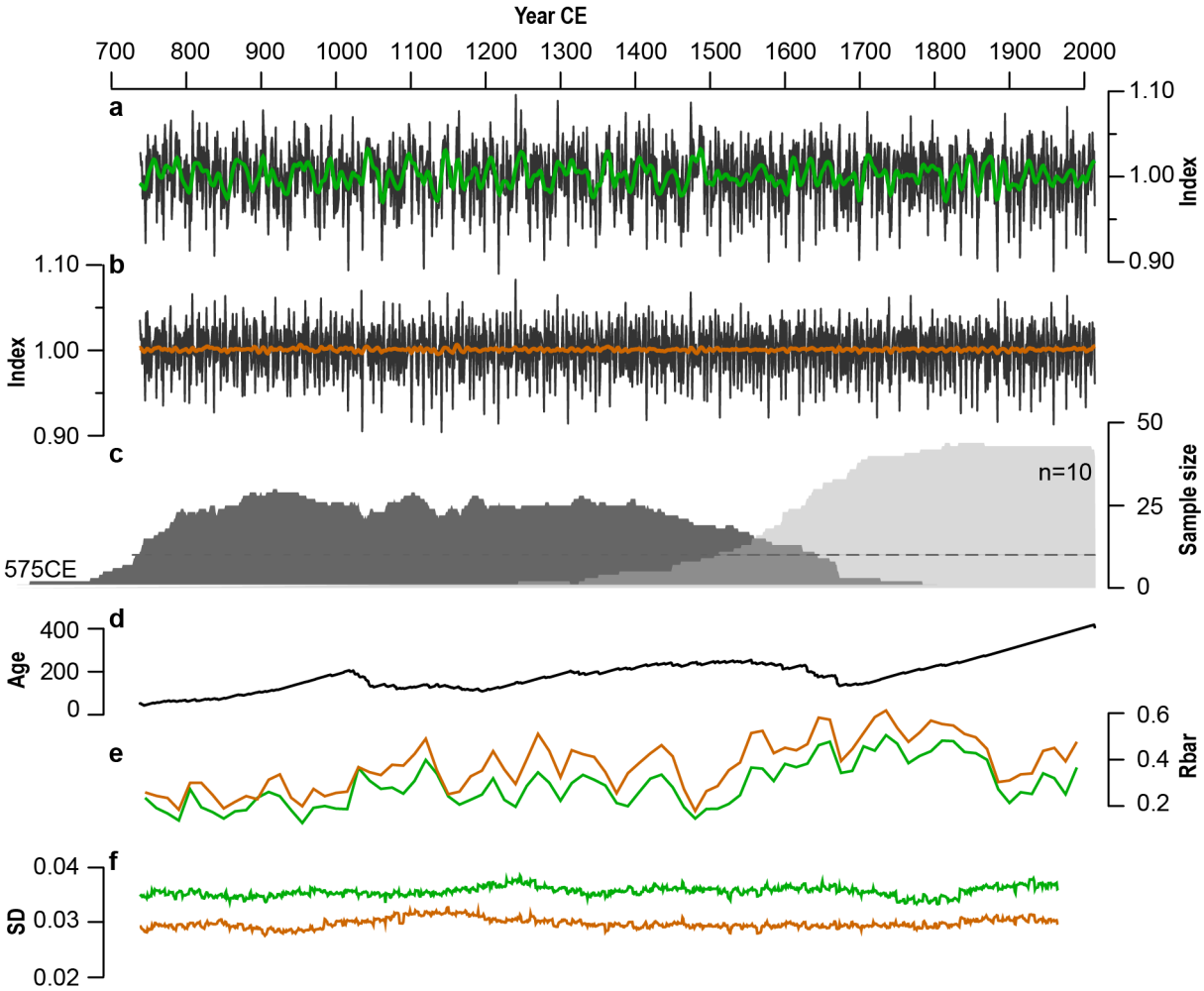

Figure 4–2 | Chronology characteristics. **a** 100SP chronology (black) and 15-year smoothed version (green). **b** 10SP chronology (black) and 15-year smoothed version (orange). **c** Yearly sample size for relict (dark grey) and living (light grey) material. **d** Annual mean tree age. **e** Rbar statistics (calculated over 30 years lagged by 15 years) and **f** 100-year moving standard deviations (SD) for the 100SP chronology (green) and 10SP chronology (orange).

4 – 3.2 Climate signals

The SMO record is significantly correlated to temperatures from July to September, with the strongest seasonal response to the August-September mean using the 10SP detrended proxy and instrumental data ($r = 0.71$; $p < 0.01$; 1950-2014). The correlations are (insignificantly) smaller for the 100SP detrended data ($r = 0.63$), indicating a stronger proxy/temperature coherency at inter-annual time scales. Partial correlation analyses reveal that SMO MXD data display a pure temperature signal

during the summer months, without artefacts derived from an intercorrelation between temperature and precipitation (Figure 4–S3). The recalculation of subsets of 2000, 100SP and 10SP chronologies, and their correlation with August-September temperature, shows that the signal is robust down to a replication of 10 series. The lowest correlation coefficient with a random subset of ten 100SP detrended series is $r = 0.27$ ($p < 0.05$) and $r = 0.45$ ($p < 0.001$) for a random subset of ten 10SP series. The lowest replication in the chronology is 11 series, indicating that the less-replicated parts in the early section of the reconstruction likely still contain a statistically significant association with temperature (Figure 4–3b). Spatial correlations between the spline chronologies and gridded August-September temperatures are also robust, with the highest degree of variance explained by those grid cells closest to the study site (Figure 4–4). Positive, significant correlation coefficients between MXD indices and August-September temperatures extend from central Italy to western Turkey. Correlations over Austria, Slovenia and Romania are weaker, but still significant. Significantly negative correlation coefficients are found over the British Isles and Scandinavia.

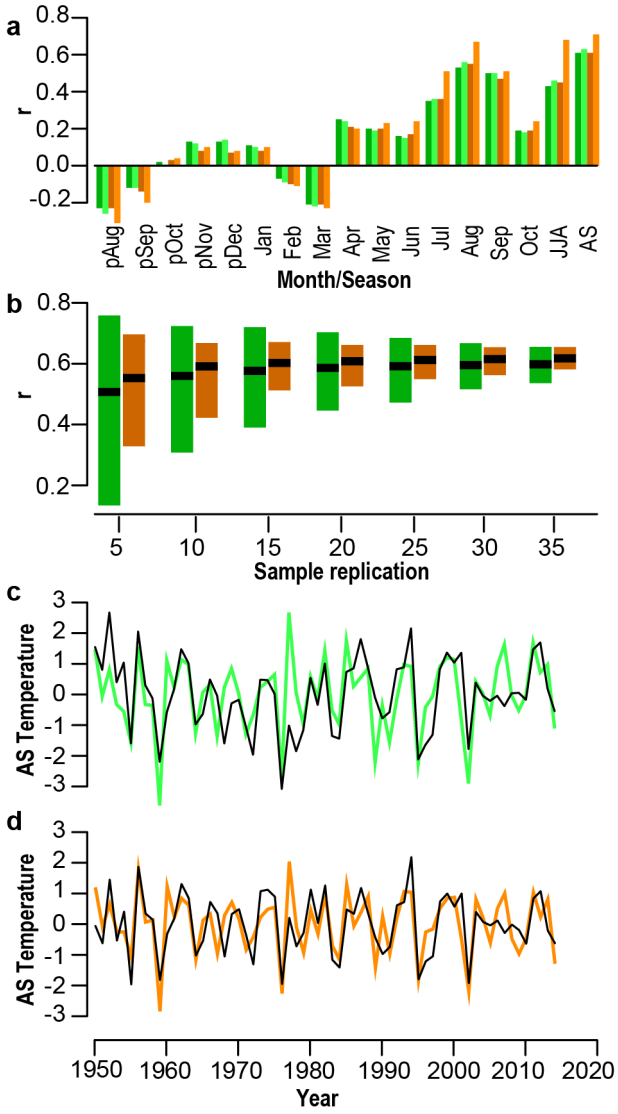

Figure 4–3 | Calibration tests. **a** Pearson correlation of the 100SP (dark green), and 10SP (dark orange) chronology with temperature data from the EOBS v.15 grid 40.25°N and 20.75°E for the period 1950-2014 and respective high-pass filtered versions (light green and light orange). **b** Multiple correlation coefficients returned from calibrating a total of 2000 100SP (dark green) and 10SP (dark orange) chronologies against August-September temperatures for the period 1950-2014. The 100SP and 10SP chronologies were established randomly selecting from 5 to 35 MXD series from a population of 43 living tree-ring series that span the full calibration period, **c** instrumental 100-year high-pass filtered August-September temperatures (black) and 100SP reconstructed temperatures (light green) and **d** instrumental 10-year high-pass filtered August-September temperatures (black) and 10SP reconstructed temperatures (light orange).

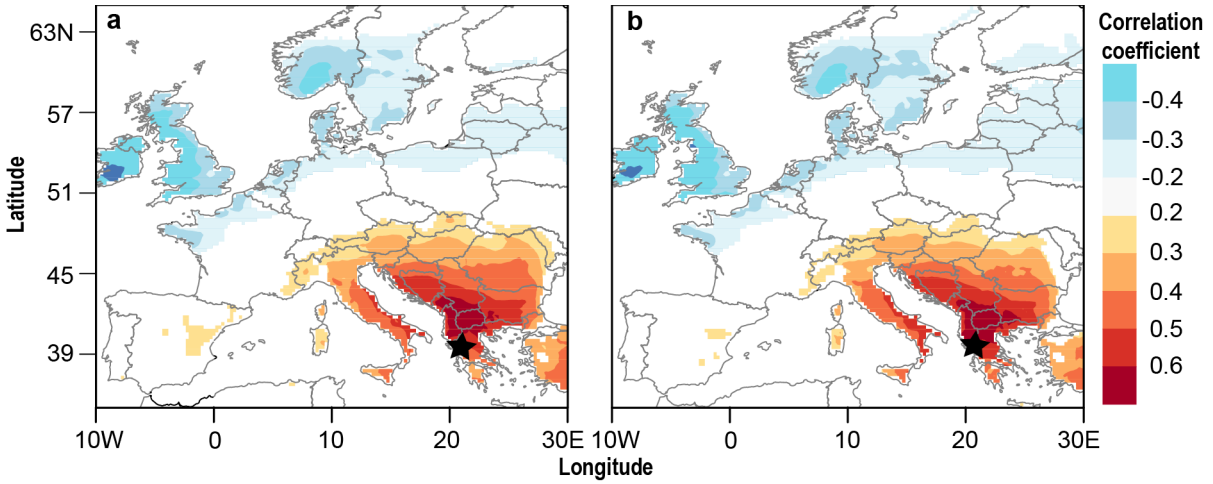

Figure 4–4 | Spatial correlation maps ($p < 0.05$) between gridded EOBS v.15 0.25° August-September temperatures and **a** 100SP and **b** 10SP chronologies. Stars refer to the location of the study site.

4 – 3.3 Temperature extremes

Results from the calibration/verification exercises indicate a stable growth-climate relationship permitting the use of the entire 1950-2014 climate record to develop a scaling model for reconstruction. The spline chronologies explain 43% and 51% of the August-September temperature variance over the 1983-2014 calibration period. RE and CE scores for the corresponding 1950-1982 verification period are 0.28 and 0.25 for the 100SP and 0.40 and 0.39 for the 10SP chronology. Transposing the periods, using 1950-1982 for calibration, the 100-year and 10SP chronologies explain 38% and 49% of the August-September temperature variance, RE and CE scores of the corresponding 1983-2014 verification are 0.25 and 0.22 for the 100SP both 0.44 for the 10SP chronology, respectively. Comparison of the August-September temperature trends in both the reconstruction and instrumental data reveals similar inter-annual to decadal scale variance (Figure 4–3c and Figure 4–3d). The three coldest years in the 100SP reconstruction and the four coldest years in the 10SP reconstruction agree with the five coldest measured years, suggesting that both reconstructions contain some skill in capturing temperature extremes.

In total, 110 cold and 48 warm extremes appear in the 100SP reconstruction, and 105 cold and 57 warm extremes in the 10SP reconstruction (Figure 4–5 and Table 4–S1). The year 1240 was the warmest summer, with reconstructed anomalies of +3.13 °C and +2.64 °C in the 100SP and 10SP reconstructions, respectively. The two coldest summers in the 100SP reconstruction are 1217 and 1884 with anomalies of -3.71 °C and -3.61 °C, respectively. The two coldest summers in the 10SP reconstruction occurred in different years, 1035 and 1117, with anomalies of -3.11 °C and -3.14 °C, respectively. The third coldest summer in the 100SP and fourth coldest summer in the 10SP reconstructions, is 1959, which is the second coldest year in the instrumental EOBS v.15 record. The coldest decade is 1811-1820 (-0.73 °C) and the warmest decade 1481-1490 (+0.88 °C; calculated only

for 100SP reconstruction). The elimination of decadal trends in the 10SP reconstruction causes events to appear more evenly distributed. However, over the past 450 years the occurrence of warm temperature extremes is substantially less frequent compared to preceding centuries. In contrast, the number of cold extremes moderately increased between 800-1700, rapidly decreased from 1700-1800, and increased again to the present (Figure 4–5).

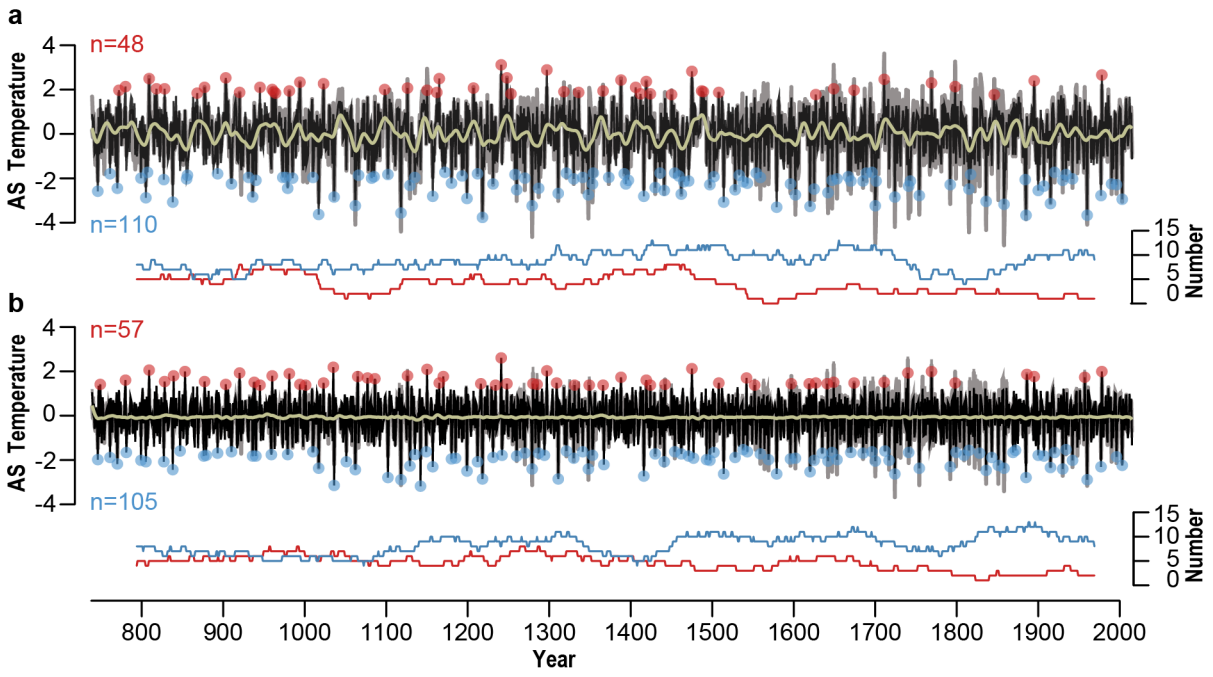

Figure 4–5 | Northeastern Mediterranean annually resolved August-September temperatures back to 738 and cold (blue) and warm (red) temperature extremes that exceed the threshold of ±1.5 SD and corresponding number of extremes in running 100-year windows (lower panels). Panel **a** shows an August-September temperature reconstruction and extremes derived from a 100SP standardized chronology (black), the 15-year smoothed version (yellow) and uncertainty estimates based on the sample bootstrap error (grey) and **b** same for a 10SP chronology.

The SEA results suggest that volcanic eruptions are a strong driver of temperature minima (Figure 4–S4). In 10 out of 11 cases, a low temperature anomaly occurred in the year of, or one year after, the sulphur peaks in the ice-core record. Years with a significant post-volcanic cooling are 939, 1108, 1171, 1230, 1257, 1453, 1601, 1641, 1695, 1783, 1815, 1835 and 1883. The average temperature response in the first post-volcanic August-September, is -1.72 °C to -1.34 °C ($p < 0.01$).

4 – 3.4 Spatial patterns of temperature extremes

Comparison of the temperature extremes in the re-standardized and re-calibrated European records (Figure 4–S5) with the SMO MXD reconstructions reveals two main patterns: (i) for distant sites (≥ 1000 km), the synchronous occurrence of extremes is rare for cold and warm events, and (ii) for

nearby sites (< 1000 km), the synchronicity is high for cold extremes but moderate to weak for warm extremes (Figure 4–6). Between the SCA, BRI, PYR, ALP, TAT reconstructions and SMO, the percentage of overlap is 0-14% for cold and 0-6% for warm extremes. Over Britain and Scandinavia (BRI and SCA), we find an inverse relationship. The majority of extreme SMO cold temperature anomalies appears as warm summers in these records. However, the pattern is less distinct for warm extremes (Figure 4–6a). The common extremes between the ITA, ITP, VIH, OLY, KAT, and SMO reconstructions, over their individual common periods, range between 43-56% for cold and 0-27% for warm extremes. Using a bootstrap approach to assess the significance of common inter-series extremes, we find that only the ITP and OLY, and the ITA, VIH and KAT cold extremes occur non-randomly (Figure 4–6b). Constraining the analysis to the common period 1769-1978 produces similar results (Figure 4–6c).

Divergence in the spatial scale of warm and cold extremes, which is only visible in tree-ring derived temperature anomalies with cold extremes showing wider synchronicity than warm extremes, is lacking in the instrumental data. Comparison of the synchronicity of the coldest and warmest instrumental temperature anomalies across Europe indicates no differences between cold and warm extremes, and with decreasing site distance, the general overlap increases (Figure 4–6d).

4 – 4 Discussion

Here, we present the longest, annually resolved temperature reconstruction for the Mediterranean region, covering the period 738-2014. Due to the outstanding length, the regional climate history of temperature extremes is extended by roughly 700 years compared to previous temperature reconstructions.

4 – 4.1 Chronology characteristics

At the high-to-mid-frequency range, a strong correlation is found between the SMO spline chronologies and other PIHE records from the central-eastern Mediterranean region, and absolute density levels are in line with previous measurements. Similar values of absolute density between living and relict material (Tegel *et al*. 2010; Boswijk *et al*. 2014), and habitat homogeneity (Esper *et al*. 2016) allows combining the material to extend the SMO chronology back in time. Moderate Rbar values point to potential micro-site effects (Düthorn *et al*. 2013) or tree-specific density variations as a consequence of four differently exposed sites (Figure 4–1c; Klippel *et al*. 2017). However, absolute values in the range of previous studies from lower altitudes pine trees (Büntgen *et al*. 2008; Klesse *et al*. 2015).

4 – 4.2 Climate signals

Partial correlation analysis (Meko *et al*. 2011) has shown that MXD displays a pure temperature signal that is not affected by the interrelation between temperature and precipitation (Büntgen *et al*. 2009).

Maximum temperature sensitivity is detected towards the end of the growing season in August and September, which is consistent with the physiological response of cell wall thickening and lignification processes (Fritts 1976). This response causes cell lumen area to shrink to its minimum and cell wall thickness to increase to its maximum with associated highest MXD values (Cherubini *et al*. 2004). Similar patterns in climate signal strength in the 100SP and 10SP chronologies suggest that MXD variability is clearly associated with temperature at the mid- and high-frequency.

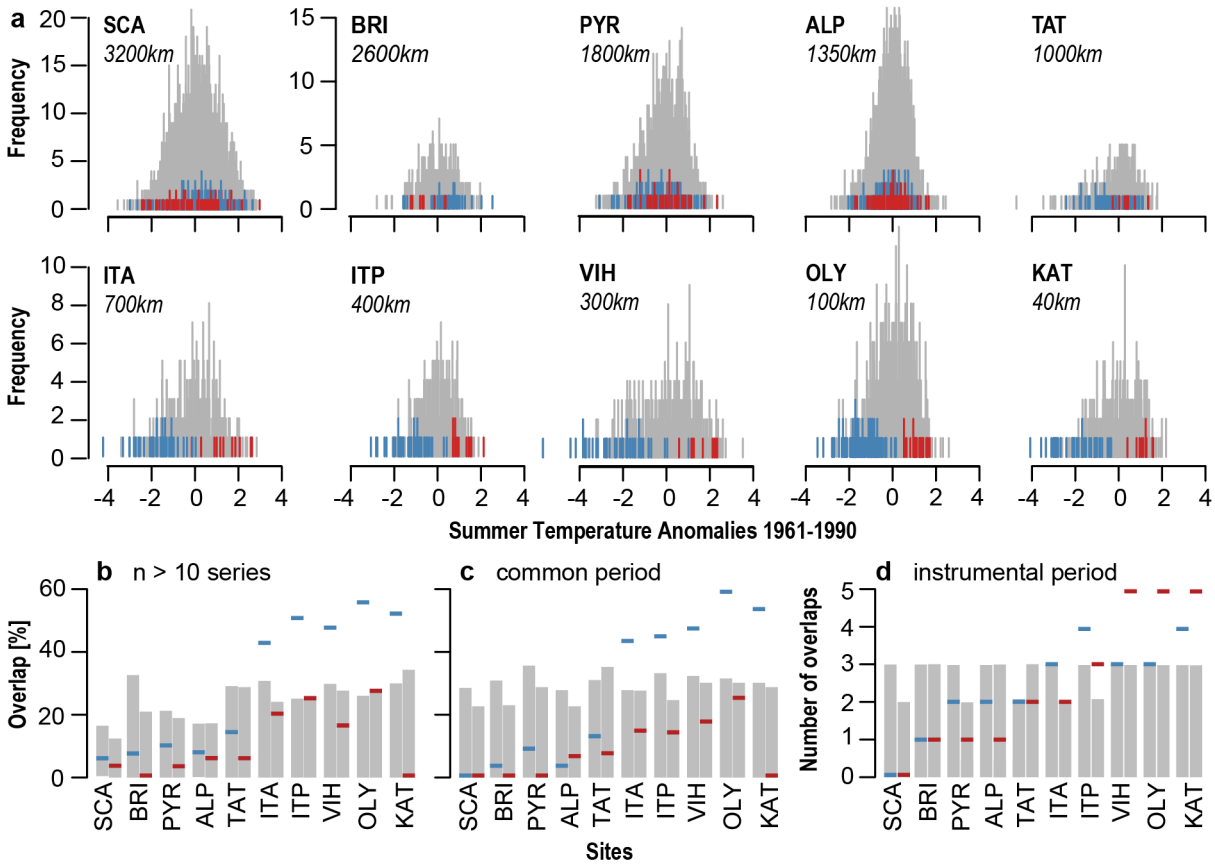

Figure 4–6 | Comparison of temperature anomalies and extremes (± 1.5 SD) across Europe. **a** MXD based 100SP and 10SP temperature reconstructions from Scandinavia (SCA), United Kingdom (BRI), Spain (PYR), Switzerland (ALP), Slovakia (TAT), Italy (ITA and ITP), Bulgaria (VIH), and Greece (OLY and KAT) displayed as histograms (grey). Blue and red ticks indicate cold or warm extremes in the SMO 100SP and 10SP reconstructions and **b** percent of common cold (blue) and (warm) temperature extremes between SMO and the reconstructions displayed in Figure 4–6a over the individual period of overlap (n > series) and **c** the common period 1769-1978. Values refer to the mean overlap from the 100SP and 10SP reconstruction. Grey bars display uncertainty estimates derived from a Monte Carlo simulation with 1000 randomized reconstructions. **d** Analysis was repeated comparing the overlap of the 5 coldest and 5 warmest instrumental 10-year high pass filtered August temperatures from the EOBS v.15 grids that were used for calibration over the period 1950-2014.

4 – 4.3 Temperature extremes

In contrast to the multiple climate stations along the Mediterranean that report a general warming in recent decades (Xoplaki *et al*. 2003a; Alexandrov *et al*. 2004; Philandras *et al*. 2008; Toreti *et al*. 2009), an analysis of instrumental temperatures for the period 1955-2013 shows that in northwestern Greece, statistically significant trends in summer temperature are absent (Feidas 2016). The cooling trend from 1950-1976, previously reported throughout the Mediterranean basin, was followed by an, so far, insignificant warming (Piervitali *et al*. 1997; del Río *et al*. 2011). Our reconstruction mirrors this absence of a clear positive trend at decadal scale. Differences in the frequency and magnitude of extreme events between the 100SP and 10SP reconstruction appear because only 76% of the cold, and 65% of the warm events overlap between the two chronology versions. Hence, methods of frequency preservation add uncertainty to the strength of extreme events (Battipaglia *et al*. 2010). This finding demonstrates how the standardization method employed substantially influences the expression of extremes, thus emphasizes the difficulty in comparing extremes across studies composed of tree-ring data from different sites and, perhaps even, different tree species (Fritts 1976).

The second coldest decade from 1061-1070 also falls into a period of grand solar minima - the Oort minimum (Guiot *et al*. 2010). The coldest decade 1811-1820 falls into the periods of the Dalton minimum (Usoskin *et al*. 2002) and Little Ice Age (Grove 1988), which coincides with the unknown eruption in 1809 (Guevara-Murua *et al*. 2014) and the eruption of Tambora in 1815 (Stothers 1984) causing the 'year without summer' 1816 (Oppenheimer 2003). Cool summers during this decade are also recorded throughout central Europe, parts of Asia and North America by proxy evidence inferred from glacier advances (Luckman 2000; Zumbühl and Nussbaumer 2017) and tree-ring data (D'Arrigo *et al*. 2003; Büntgen *et al*. 2006; D'Arrigo *et al*. 2013; Bräuning 2016), and in long instrumental station data (Böhm *et al*. 2009). The SEA results demonstrate that several cold summers correspond to volcanic eruptions and changes in radiative forcing (Robock 2000; Esper *et al*. 2013a; Esper *et al*. 2013b). Typical of MXD-based temperature reconstructions (Schneider *et al*. 2015), the cooling in the first post-volcanic year is followed by a rapid recovery in the second post-volcanic year (Esper *et al*. 2015). The eruption of Krakatau in 1883 (Sigl *et al*. 2015) is captured with anomalies of -2.02 °C in the 100SP and -0.88 °C in the 10SP chronology. Also, the 1257 Samalas (-1.79 °C, -1.10 °C), 1452 Kuwae (-1.72 °C, -1.59 °C), 1601 Huaynaputina (-2.70 °C, -1.88 °C), 1641 Parker (-2.60 °C, -2.01 °C), 1783 Laki (-0.62 °C, -1.27 °C), 1835 Cosiguina (-2.99 °C, -2.43 °C), and the 1991 Pinatubo (-1.56 °C, -0.98 °C) eruptions are related to temperature minima. The 822-823 Katla eruption (Büntgen *et al*. 2017a) and the unknown eruption in 1809 (Guevara-Murua *et al*. 2014), did not cause extreme MXD minima at Mt. Smolikas. The cold summer temperatures in 1699, 1914, and 1857 corroborate reports of previously reported regional climatic extremes (Trouet *et al*. 2012; Klesse *et al*. 2015; Leonelli *et al*. 2017). Instrumental station data in the Mediterranean region (Xoplai *et al*. 2003b) confirm the cold summer of 1959 when extremely cool air masses appeared at Mt. Olympus and in Bulgaria. The cold extreme in 1347 (-2.70 °C, -2.37 °C) coincides to severe plague (*Yersinia pestis*)

outbreaks on the Mediterranean islands Sicily, Corsica, and Sardinia as well as well as in the cities Split and Dubrovnik, though a causal link between low temperatures and *Yersinia pestis* seems unlikely (Büntgen *et al*. 2012).

4 – 4.4 Spatial patterns of temperature extremes

Volcanic eruptions are pulse-like disturbance events capable of causing distinct cooling over Europe (Sigl *et al*. 2015; Schneide*r et al*. 2017). Despite the Hadley circulation and stable warm high pressure cells that bring predominantly high temperatures and summer droughts to the Mediterranean (Bolle 2003; Alfaro-Sanchez *et al*. 2018), the expression of temperature extremes differs between the northeastern (Pindus Mts.) and western Mediterranean (Pyrenees) basin (Seim *et al*. 2015). In the western Mediterranean, previous studies report a stronger influence of the East Atlantic Jetstream (Dünkeloh and Jacobeit 2003; Xoplaki *et al*. 2003b) and West African Monsoon (Fontaine *et al*. 2010). By contrast, in the northeastern Mediterranean we find an association with the latitudinal position of the NAJ (Mahlstein *et al*. 2012; Belmecheri *et al*. 2017; Trouet *et al*. 2018) that causes temperature extremes and synoptic timing of events in Bulgaria, Italy, and Greece as well as anti-phase associations with temperature anomalies over Scandinavia and the British Isles (Hughes *et al*. 2001; Oikonomou *et al*. 2010; Trouet *et al*. 2012; Trouet 2014; Klesse *et al*. 2015). When the NAJ is in anomalously northerly position, it generates anticyclonic conditions in northwestern Europe associated with warm and dry conditions but also heat waves and droughts (Chronis *et al*. 2011), and extreme cold temperatures in the northeastern Mediterranean. A southerly NAJ increases the blocking frequency over the northeastern Mediterranean and promotes hot summers, droughts, and wildfires in southeastern Europe (Mahlstein *et al*. 2012; Trouet *et al*. 2018). To evaluate these associations, the SMO reconstruction is compared to a reconstruction of the latitudinal position of the NAJ (NAJ_T; 1725-1978) developed from tree-ring data from the northeastern Mediterranean (NEMED) and the British Isles (BRIT; Trouet *et al*. 2018). We used the 100SP SMO reconstruction due to similar spectral properties of the records (Figure 4–7). Correlation between the SMO August-September temperature reconstruction and reconstructed NAJ_T anomalies is $r = -0.66$ ($p < 0.001$).

For validation, we tested the suitability of our SMO dataset for NAJ reconstruction. We repeated the reconstruction NAJ_T procedure outlined in Trouet *et al*. (2018) using our SMO reconstruction in lieu of the NEMED dataset (herein NAJ_K reconstruction). The sole difference involves the use of EOBS v.15 gridded temperature data as a target for reconstruction of August temperatures. The original NEMED MXD chronology and the SMO chronology are significantly correlated with NAJ position ($r = -0.57$ and $r = -0.54$, respectively, $p < 0.001$; 1920-1978). Also, the original BRIT-NEMED and BRIT-SMO composites reflect changes in the latitudinal position of the NAJ ($r = 0.63$ and $r = 0.59$, respectively, $p < 0.001$; 1920-1978). Reasons that could cause slightly weaker coefficients for SMO include differences in the temperature dataset, reduced sample replication (Esper *et al*. 2016), and limited spatial representation, as compared to the NEMED data. However, the NAJ_T and NAJ_K

reconstructions correlate at r = 0.9 ($p < 0.001$) over their common period 1725-2014 (Figure 4–7c). This highlights the potential for extending NAJ variability back to the first millennium and forward to the 21st century by including the SMO dataset in future analyses of the temperature seesaw between the British Isles and the northeastern Mediterranean.

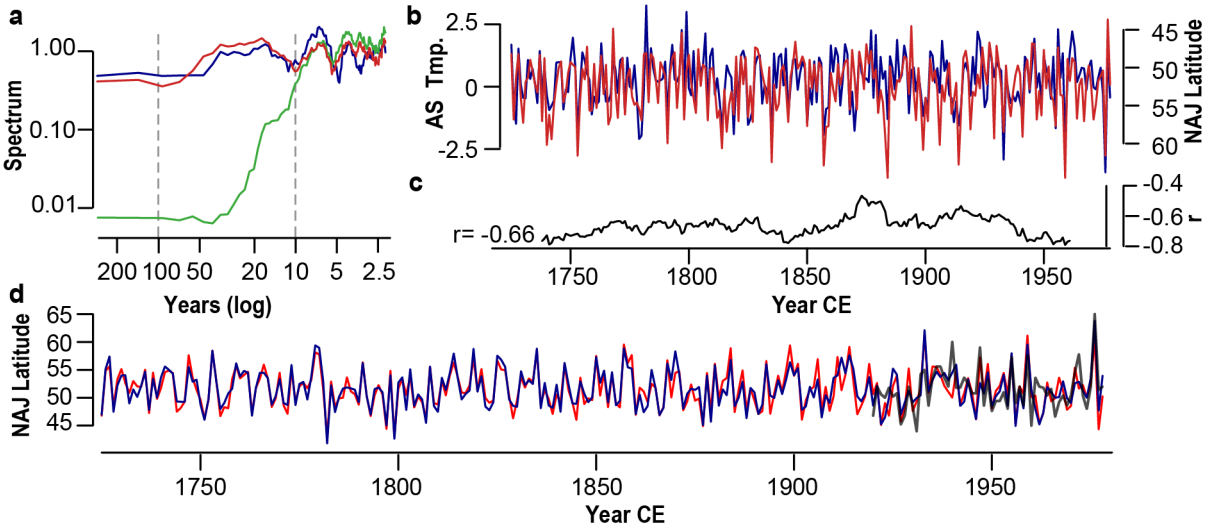

Figure 4–7 | a Frequency analysis of the SMO 100SP (red), 10SP (green) spline August-September temperature reconstruction and reconstruction of the position of the summer North Atlantic jet (NAJ_T; Trouet *et al*. 2018) (blue) over the common period 1725-1978. **b** Reconstructed 100SP August-September temperature anomalies (red), summer NAJ_T reconstruction (blue) and **c** corresponding 31 year moving window correlations (black). **d** NAJ_T (blue) and NAJ_K (red), a reanalysis of the latitudinal jet stream position using the SMO tree-ring data instead of the original NEMED compilation and instrumental August NAJ position (black).

4 – 4.5 Differences between warm and cold extremes

Reconstructed warm temperatures are spatially heterogeneous, which we would not expect from the inspection of instrumental data (Figure 4–6c). We suggest potential weaknesses in MXD to track warm events, due to a decoupling between summer temperature and MXD formation. Except for Scotland, revision of the calibration tests demonstrates that the coldest instrumental temperature anomalies match the lowest density values to a higher degree than the five warmest instrumental temperature anomalies and the highest density values (Figure 4–S6). This weakness to track warm extremes by the same degree as cold extremes causes the warm extremes to be less synchronized on a regional scale.

We suggest that in a cold summer, temperature is the limiting factor affecting regional growth (Cherubini *et al*. 2004), whereas in hot summers, this relationship is more complex with a stronger contribution of endogenous factors affecting cell wall thickening and lignification, causing substantial inter-tree and inter-site differences (Plomion *et al*. 2001). In addition, slope exposure might influence

the rate of warming, which in turn causes a site-specific growth cessation and spatial heterogeneity of warm temperature extremes (Holland and Steyn 1975; Klippel *et al*. 2017). Further research is necessary to disentangle the impact of slope exposure and changes in insolation on MXD formation.

4 – 5 Conclusions

Based on a network of high-elevation sites on Mt. Smolikas in the Pindus Mts. of Greece, regional August-September temperature variability is reconstructed back to 738. Our reconstruction provides new insight in extreme temperatures in the northeastern Mediterranean prior to the second millennium, and fills a temporal and spatial gap in larger-scale reconstruction efforts. Analysis of temperature extremes shows that cool summers were most severe in 1035, 1117, 1217, 1884 and 1959. The dominant mode that drives annual-decadal temperature variability along the northeastern Mediterranean are atmospheric conditions associated with the position of the NAJ that in the anomalous northward position generates extremely cold summer temperatures in the region, and in an anomalous southward position brings extremely warm summer temperatures. Our new millennium-long MXD chronology bears the potential to reconstruct the dynamics of the NAJ over longer timescales. Further research is needed (1) to explore low-frequency trends including transitions between cold and warm phases, and (2) to update existing regional-scale composite chronologies in order to fill the spatial and temporal gap in the northeastern Mediterranean region in larger-scale temperature reconstructions.

4 – 6 Acknowledgements

This research was supported by the German Research Foundation [projects: Inst 247/665-1 FUGG and ES 161/9-1], the National Science Foundation [AGS-1349942], the Alexander von Humboldt Foundation, and the Swedish Society for Anthropology and Geography. We thank Markus Kochbeck, Eileen Kuhl and Philipp Römer for producing MXD measurements, and Claudia Hartl and Robert Brandes for discussion and helpful comments.

4 – 7 References

Akkemik U, Aras A. 2005. Reconstruction (1689-1994 AD) of April-August precipitation in the southern part of central Turkey. *Int. J. Clim.* **25**: 537-548.

Akkemik U, Dagdeviren N, Aras A. 2005. A preliminary reconstruction (A.D. 1635-2000) of spring precipitation using oak tree rings in the western Black Sea region of Turkey. *Int. J. Biometeorol.* **49**: 297-302.

Akkemik U, D'Arrigo R, Cherubini P, Köse N, Jacoby GC. 2008. Tree-ring reconstructions of precipitation and streamflow for north-western Turkey. *Int. J. Clim.* **28**: 173-183.

Alexandrov V, Schneider M, Koleva E, Moisselin JM. 2004. Climate variability and change in Bulgaria during the 20th century. *Theor. Appl. Climatol.* **79**: 33-149.

Alfaro-Sánchez R, Nguyen H, Klesse S, Hudson A, Belmecheri S, Köse N, Diaz HF, Monson RK, Villalba R, Trouet V. 2018. Natural drivers of spring northern tropical belt movements over the past 800 years. *Nat. Geosci.* **11**: 933-938.

Alpert P. 2002. The paradoxical increase of Mediterranean extreme daily rainfall in spite of decrease in total values. *Geophys. Res. Lett.* **29**: 1536, doi: https://doi.org/10.1029/2001GL013554.

Baillie MGL, McAneney J. 2015. Tree ring effects and ice core acidities clarify the volcanic record of the first millennium. *Clim. Past* **11**: 105-114.

Battipaglia G, Frank D, Büntgen U, Dobrovolný P, Brázdil R, Pfister C, Esper J. 2010. Five centuries of Central European temperature extremes reconstructed from tree-ring density and documentary evidence. *Glob. Planet. Chang.* **72**: 182-191.

Belmecheri S, Babst F, Hudson AR, Betancourt J, Trouet V. 2017. Northern hemisphere jet stream position indices as diagnostic tools for climate and ecosystem dynamics. *Earth Interactions* **21**: 1-23.

Böhm R, Jones PD, Hiebl J, Frank D, Brunetti M, Maugeri M. 2009. The early instrumental warm-bias: a solution for long central European temperature series 1760-2007. *Clim. Chang.* **101**: 41-67.

Bolle HJ. 2003. *Mediterranean Climate*. Springer: Heidelberg, Germany.

Boswijk G, Fowler AM, Palmer JG, Fenwick P, Hogg A, Lorrey A, Wunder J. 2014. The late Holocene kauri chronology: assessing the potential of a 4500-year record for palaeoclimate reconstruction. *Quat. Sci. Rev.* **90**: 128-142.

Bräker OU. 1981. Der Alterstrend bei Jahrringdichten und Jahrringbreiten von Nadelhölzern und sein Ausgleich. *Mitt. Forstl. Bundes-Versanst. Wien* **142**: 75-102.

Bräuning A. 2016. Tree-ring evidence of 'Little Ice Age' glacier advances in southern Tibet. *Holocene* **16**: 369-380.

Briffa KR, Jones PD, Pilcher JR, Hughes MK. 1988. Reconstructing summer temperatures in northern Fennoscandinavia back to AD 1700 using tree-ring data from Scots pine. *Arct., Antarc., Alp. Res.* **20**: 385-394.

Briffa KR, Jones PD, Bartholin TS, Eckstein D, Schweingruber FH, Karlen W, Zetterberg P, Eronen M. 1992. Fennoscandian summers from AD 500 - temperature changes on short and long timescales. *Clim. Dyn.* **7**: 111-119.

Büntgen U, Frank DC, Nievergelt D, Esper J. 2006. Summer temperature variations in the European Alps, AD 755-2004. *J. Clim.* **19**: 5606-5623.

Büntgen U, Frank DC, Kaczka RJ, Verstege A, Zwijacz-Kozica T, Esper J. 2007. Growth responses to climate in a multi-species tree-ring network in the Western Carpathian Tatra Mountains, Poland and Slovakia. *Tree Physiol*. **27**: 689-702.

Büntgen U, Frank D, Grudd H, Esper J. 2008. Long-term summer temperature variations in the Pyrenees. *Clim. Dyn*. **31**: 615-631.

Büntgen U, Frank D, Trouet V, Esper J. 2009. Diverse climate sensitivity of Mediterranean tree-ring width and density. *Trees* **24**: 261-273.

Büntgen U, Tegel W, Nicolussi K, McCormick M, Frank D, Trouet V, Kaplan JO, Herzig F, Heussner KU, Wanner H, Luterbacher J, Esper J. 2011. 2500 years of European climate variability and human susceptibility. *Science* **331**: 578-82.

Büntgen U, Ginzler C, Esper J, Tegel W, McMichael AJ. 2012. Digitizing historical plague. *Clin. Infect. Dis*. **55**: 1586-1588.

Büntgen U, Eggertsson O, Wacker L, Sigl M, Ljungqvist FC, Di Cosmo N, Plunkett G, Krusic PJ, Newfield TP, Esper J, Lane C, Reinig F, Oppenheimer C. 2017a. Multi-proxy dating of Iceland's major pre-settlement Katla eruption to 822-823 CE. *Geology* **45**: 783-786.

Büntgen U, Krusic PJ, Verstege A, Sangüesa-Barreda G, Wagner S, Camarero JJ, Ljungqvist FC, Zorita E, Oppenheimer C, Konter O, Tegel W, Gärtner H, Cherubini P, Reinig F, Esper J. 2017b. New tree-ring evidence from the Pyrenees reveals western Mediterranean climate variability since medieval times. *J. Clim*. **30**: 5295-5318.

Camuffo D, Bertolin C, Barriendos M, Dominguez-Castro F, Cocheo C, Enzi S, Sghedoni M, della Valle A, Garnier E, Alcoforado MJ, Xoplaki E, Luterbacher J, Diodato N, Maugeri M, Nunes MF, Rodriguez R. 2010. 500-year temperature reconstruction in the Mediterranean Basin by means of documentary data and instrumental observations. *Clim. Change* **101**: 169-199.

Cherubini P, Gärtner H, Esper J, Dobbertin MK, Kaiser KF, Rigling A, Treydte K, Zimmermann NE, Bräker OU. 2004. Jahrringe als Archive für interdisziplinäre Umweltforschung | Annual rings as an archive for interdisciplinary environmental research. *Schweiz. Z. Forstwes*. **155**: 162-168.

Chronis T, Raitsos DE, Kassis D, Sarantopoulos A. 2011. The summer North Atlantic Oscillation influence on the eastern Mediterranean. *J. Clim*. **24**: 5584-5596.

Cook ER, Peters K. 1981. The smoothing spline: a new approach to standardizing forest interior tree-ring width series for dendroclimatic studies. *Tree-Ring Bulletin* **41**: 45-53.

Cook ER, Briffa KR, Jones PD. 1994. Spatial regression methods in dendroclimatology: A review and comparison of two techniques. *Int. J. Clim*. **14**: 379-402.

Cook E, Peters K. 1997. Calculating unbiased tree-ring indices for the study of climatic and environmental change. *Holocene* **7**: 361-370.

Cook E, Krusic PJ, Peters K, Holmes RL. 2017. Program ARSTAN version48d2, Autoregressive tree-ring standardization program. Tree-Ring Laboratory of Lamot-Doherty Earth Observatory. http://www.ldeo.columbia.edu/tree-ring-laboratory/resources/software.

D'Arrigo R, Buckley B, Kaplan S, Woollett J. 2003. Interannual to multidecadal modes of Labrador climate variability inferred from tree rings. *Clim. Dyn.* **20**: 219-228.

D'Arrigo R, Wilson R, Anchukaitis KJ. 2013. Volcanic cooling signal in tree ring temperature records for the past millennium. *J. Geophys. Res. Atmos.* **118**: 9000-9010.

del Río S, Herrero L, Pinto-Gomes C, Penas A. 2011. Spatial analysis of mean temperature trends in Spain over the period 1961-2006. *Glob. Planet. Chang.* **78**: 65-75.

Diffenbaugh NS, Pal JS, Giorgi F, Gao XJ. 2007. Heat stress intensification in the Mediterranean climate change hotspot. *Geophys. Res. Lett.* **34:** L11706, doi: 10.1029/2007GL030000.

Dorado Liñán I, Büntgen U, González-Rouco F, Zorita E, Montávez JP, Gómez-Navarro JJ, Brunet M, Heinrich I, Helle G, Gutiérrez E. 2012. Estimating 750 years of temperature variations and uncertainties in the Pyrenees by tree-ring reconstructions and climate simulations. *Clim. Past* **8**: 919-933.

Dünkeloh A, Jacobeit J. 2003. Circulation dynamics of Mediterranean precipitation variability 1948-98. *Int. J. Clim.* **23**: 1843-1866.

Düthorn E, Holzkämper S, Timonen M, Esper J. 2013. Influence of micro-site conditions on tree-ring climate signals and trends in central and northern Sweden. *Trees* **27**: 1395-1404.

Esper J, Frank D, Wilson R, Briffa KR. 2005. Effect of scaling and regression on reconstructed temperature amplitude for the past millennium. *Geophys. Res. Lett.* **32**: L07711, doi: 10.1029/2004GL021236.

Esper J, Frank D, Büntgen U, Verstege A, Luterbacher J. 2007. Long-term drought severity variations in Morocco. *Geophys. Res. Lett.* **34**: L17702, doi: 10.1029/2007GL030844.

Esper J, Büntgen U, Timonen M, Frank DC. 2012. Variability and extremes of northern Scandinavian summer temperatures over the past two millennia. *Glob. Planet. Chang.* **88-89**: 1-9.

Esper J, Büntgen U, Luterbacher J, Krusic PJ. 2013a. Testing the hypothesis of post-volcanic missing rings in temperature sensitive dendrochronological data. *Dendrochronologia* **31**: 216-222.

Esper J, Schneider L, Krusic PJ, Luterbacher J, Büntgen U, Timonen M, Sirocko F, Zorita E. 2013b. European summer temperature response to annually dated volcanic eruptions over the past nine centuries. *Bull. Volcanol.* **75**: 736.

Esper J, Düthorn E, Krusic PJ, Timonen M, Büntgen U. 2014a. Northern European summer temperature variations over the Common Era from integrated tree-ring density records. *J. Quat. Sci.* **29**: 487-494.

Esper J, Großjean J, Camarero JJ, García-Cervigón AI, Olano JM, González-Rouco JF, Domínguez-Castro F, Büntgen U. 2014b. Atlantic and Mediterranean synoptic drivers of central Spanish juniper growth. *Theor. Appl. Climatol.* **121**: 571-579.

Esper J, Schneider L, Smerdon JE, Schöne BR, Büntgen U. 2015. Signals and memory in tree-ring width and density data. *Dendrochronologia* **35**: 62-70.

Esper J, Krusic PJ, Ljungqvist FC, Luterbacher J, Carrer M, Cook E, Davi NK, Hartl-Meier C, Kirdyanov A, Konter O, Myglan V, Timonen M, Treydte K, Trouet V, Villalba R, Yang B, Büntgen U. 2016.

Ranking of tree-ring based temperature reconstructions of the past millennium. *Quat. Sci. Rev.* **145**: 134-151.

Esper J, Büntgen U, Hartl-Meier C, Oppenheimer C, Schneider L. 2017. Northern Hemisphere temperature anomalies during the 1450s period of ambiguous volcanic forcing. *Bull. Volcanol.* **79**: 41.

Feidas H. 2016. Trend analysis of air temperature time series in Greece and their relationship with circulation using surface and satellite data: recent trends and an update to 2013. *Theor. Appl. Climatol.* **129**: 1383-1406.

Fontaine B, Garcia-Serrano J, Roucou P, Rodriguez-Fonseca B, Losada T, Chauvin F, Gervois S, Sijikumar S, Ruti P, Janicot S. 2010. Impacts of warm and cold situations in the Mediterranean basins on the West African monsoon: observed connection patterns (1979-2006) and climate simulations. *Clim. Dyn.* **35**: 95-114.

Fotiadi AK, Metaxas DA, Bartzokas A. 1999. A statistical study of precipitation in northwest Greece. *Int. J. Clim.* **19**: 1221-1232.

Frank D, Esper J, Cook ER. 2007. Adjustment for proxy number and coherence in a large-scale temperature reconstruction. *Geophys. Res. Lett.* **34**: L16709, doi: 10.1029/2007GL030571.

Franke J, Frank D, Raible CC, Esper J, Bronnimann S. 2013. Spectral biases in tree-ring climate proxies. *Nat. Clim. Chang.* **3**: 360-364.

Fritts HC. 1976. *Tree Rings and Climate*. Blackburn Press: Caldwell, USA.

García-Herrera R, Hernández E, Barriopedro D, Paredes D, Trigo RM, Trigo IF, Mendes MA. 2007. The outstanding 2004/05 drought in the Iberian Peninsula: Associated atmospheric circulation. *J. Hydrometeorol.* **8**: 483-498.

Gogou A, Triantaphyllou M, Xoplaki E, Izdebski A, Parinos C, Dimiza M, Bouloubassi I, Luterbacher J, Kouli K, Martrat B, Toreti A, Fleitmann D, Rousakis G, Kaberi H, Athanasiou M, Lykousis V. 2016. Climate variability and socio-environmental changes in the northern Aegean (NE Mediterranean) during the last 1500 years. *Quat. Sci. Rev.* **136**: 209-228.

Grauel AL, Leider A, Goudeau MLS, Müller IA, Bernasconi SM, Hinrichs KU, de Lange GJ, Zonneveld KAF, Versteegh GJM. 2013. What do SST proxies really tell us? A high-resolution multiproxy (UK′37, TEXH86 and foraminifera δ18O) study in the Gulf of Taranto, central Mediterranean Sea. *Quat. Sci. Rev.* **73**: 115-131.

Griggs C, DeGaetano A, Kuniholm P, Newton M. 2007. A regional high-frequency reconstruction of May-June precipitation in the north Aegean from oak tree rings, AD 1089-1989. *Int. J. Clim.* **27**: 1075-1089.

Grissino-Mayer HD, Fritts HC. 1997. The International Tree-Ring Data Bank: An enhanced global database serving the global scientific community. *Holocene* **7**: 235-238.

Grove JM. 1988. *The little ice age*. Methuen & Co: New York, USA.

Guevara-Murua A, Williams CA, Hendy EJ, Rust AC, Cashman KV. 2014. Observations of a stratospheric aerosol veil from a tropical volcanic eruption in December 1808: is this the unknown ~ 1809 eruption? *Clim. Past* **10**, 1707-1722.

Guiot J, Corona C, ESCARSEL members. 2010. Growing season temperatures in Europe and climate forcings over the past 1400 years. *PLoS One* **5**: e9972, doi:10.1371/journal.pone.0009972.

Harris I, Jones PD, Osborn TJ, Lister DH. 2014. Updated high-resolution grids of monthly climatic observations - the CRU TS3.10. *Int. J. Clim.* **34**: 623-642.

Haylock MR, Hofstra N, Tank A, Klok EJ, Jones PD, New M. 2008. A European daily high-resolution gridded data set of surface temperature and precipitation for 1950-2006. *J. Geophys. Res.* **113**: D20119, 10.1029/2008JD010201.

Hoerling M, Eischeid J, Perlwitz J, Quan X, Zhang T, Pegion P. 2012. On the increased frequency of Mediterranean drought. *J. Clim.* **25**: 2146-2161.

Holland PG, Steyn DG. 1975. Vegetational responses to latitudinal variations in slope angle and aspect. *J. Biogeogr.* **2**: 179-183.

Hughes MK, Kuniholm PI, Eischeid JK, Garfin G, Griggs CB, Latini C. 2001. Aegean tree-ring signature years explained. *Tree-Ring Res.* **57**: 67-73.

Izdebski A, Koloch G, Słoczyński T. 2016. Exploring Byzantine and Ottoman economic history with the use of palynological data: a quantitative approach. *Jahrb. d. östr. Byzantinistik* **1**: 67-110.

Kiss A, Wilson R, Bariska I. 2011. An experimental 392-year documentary-based multi-proxy (vine and grain) reconstruction of May-July temperatures for Koszeg, West-Hungary. *Int. J. Biometeorol.* **55**: 595-611.

Klesse S, Ziehmer M, Rousakis G, Trouet V, Frank D. 2015. Synoptic drivers of 400 years of summer temperature and precipitation variability on Mt. Olympus, Greece. *Clim. Dyn.* **45**: 807-824.

Klippel L, Krusic PJ, Brandes R, Hartl-Meier C, Trouet V, Meko M, Esper J. 2017. High-elevation inter-site differences in Mount Smolikas tree-ring width data. *Dendrochronologia* **44**: 164-173.

Klippel L, Krusic PJ, Brandes R, Hartl C, Belmecheri S, Dienst M, Esper J. 2018. A 1286-year hydro-climate reconstruction for the Balkan Peninsula. *Boreas* (Online Version before inclusion in an issue), doi: 10.1111/bor.12320.

Köse N, Akkemik Ü, Dalfes HN, Özeren MS. 2011. Tree-ring reconstructions of May-June precipitation for western Anatolia. *Quat. Res.* **75**: 438-450.

Kostopoulou E, Jones PD. 2005. Assessment of climate extremes in the Eastern Mediterranean. *Meteorol. Atmos. Phys.* **89**: 69-85.

Kuglitsch FG, Toreti A, Xoplaki E, Della-Marta PM, Zerefos CS, Turkes M, Luterbacher J. 2010. Heat wave changes in the eastern Mediterranean since 1960. *Geophys. Res. Lett.* **37**: L04802, doi: 10.1029/2009GL041841.

Lelieveld J, Hadjinicolaou P, Kostopoulou E, Giannakopoulos C, Pozzer A, Tanarhte M, Tyrlis E. 2013. Model projected heat extremes and air pollution in the eastern Mediterranean and Middle East in the twenty-first century. *Reg. Environ. Chang.* **14**: 1937-1949.

Lenz O, Schär E, Schweingruber FH. 1976. Methodische Probleme bei der radiographisch-densitometrischen Bestimmung der Dichte und der Jahrringbreiten von Holz. *Holzforschung* **30**: 114-123.

Leonelli G, Coppola A, Salvatore MC, Baroni C, Battipaglia G, Gentilesca T, Ripullone F, Borghetti M, Conte E, Tognetti R, Marchetti M, Lombardi F, Brunetti M, Maugeri M, Pelfini M, Cherubini P, Provenzale A, Maggi V. 2017. Climate signals in a multispecies tree-ring network from central and southern Italy and reconstruction of the late summer temperatures since the early 1700s. *Clim. Past* **13**: 1451-1471.

Levanic T, Popa I, Poljansek S, Nechita C. 2012. A 323-year long reconstruction of drought for SW Romania based on black pine (*Pinus nigra*) tree-ring widths. *Int. J. Biometeorol.* **57**: 703-714.

Li L, Casado A, Congedi L, Dell'Aquila A, Dubois C, Elizalde A, L'Hévéder B, Lionello P, Sevault F, Somot S, Ruti P, Zampieri M. 2012. Modeling of the Mediterranean Climate System. In *The Climate of the Mediterranean Region from the past to the future,* Lionello P (ed). Elsevier: Lecce, Italy, 419-448.

Linderholm HW, Björklund J, Seftigen K, Gunnarson BE, Fuentes M. 2014. Fennoscandia revisited: a spatially improved tree-ring reconstruction of summer temperatures for the last 900 years. *Clim. Dyn.* **45**: 933-947.

Ljungqvist FC, Krusic PJ, Sundqvist HS, Zorita E, Brattstrom G, Frank D. 2016. Northern Hemisphere hydroclimate variability over the past twelve centuries. *Nature* **532**: 94-98.

Loukas A, Vasiliades L, Dalezios NR. 2002. Hydroclimatic variability of regional droughts in Greece using the palmer moisture anomaly index. *Nord. Hydrol.* **33**, 425-442.

Luckman BH. 2000. The Little Ice Age in the Canadian Rockies. *Geomorphology* **32**: 357-384.

Mahlstein I, Martius O, Chevalier C, Ginsbourger D. 2012. Changes in the odds of extreme events in the Atlantic basin depending on the position of the extratropical jet. *Geophys. Res. Lett.* **39**: L22805, doi: 10.1029/2012GL053993.

Meko DM, Touchan R, Anchukaitis KJ. 2011. Seascorr: A MATLAB program for identifying the seasonal climate signal in an annual tree-ring time series. *Com. & Geosci.* **37**: 1234-1241.

Melvin TM, Grudd H, Briffa KR. 2013. Potential bias in 'updating' tree-ring chronologies using regional curve standardisation: Re-processing 1500 years of Torneträsk density and ring-width data. *Holocene* **23**: 364-373.

Moriondo M, Good P, Durao R, Bindi M, Giannakopoulos C, Corte-Real J. 2006. Potential impact of climate change on fire risk in the Mediterranean area. *Clim. Res.* **31**: 85-95.

Oikonomou C, Flocas HA, Hatzaki M, Nisantzi A, Asimakopoulos DN. 2010. Relationship of extreme dry spells in Eastern Mediterranean with large-scale circulation. *Theor. Appl. Climatol.* **100**: 137-151.

Oppenheimer C. 2003. Climatic, environmental and human consequences of the largest known historic eruption: Tambora volcano (Indonesia) 1815. *Prog. Phys. Geogr.* **27**: 230-259.

PAGES 2k PMIP3 group. 2015. Continental-scale temperature variability in PMIP3 simulations and PAGES 2k regional temperature reconstructions over the past millennium. *Geophys. Res. Lett.* **11**: 1673-1699.

Panofsky HA, Brier GW. 1958. *Some applications of statistics to meteorology*. College of Earth and Mineral Sciences University Park: Pennsylvania, USA.

Philandras CM, Nastos PT, Repapis CC. 2008. Air temperature variability and trends over Greece. *Global NEST J.* **10**: 273-285.

Piervitali E, Colacino M, Conte M. 1997. Signals of climatic change in the Central-Western Mediterranean basin. *Theor. Appl. Climatol.* **58**: 211-219.

Plomion C, Leprovost G, Stokes A. 2001. Wood formation in trees. *Plant Physiol.* **127**: 1513-1523.

Robock A. 2000. Volcanic eruptions and climate. *Rev. Geophys.* **38**: 191-219.

Schneider L, Smerdon JE, Büntgen U, Wilson R, Myglan VS, Kirdyanov AV, Esper J. 2015. Revising midlatitude summer temperatures back to AD 600 based on a wood density network. *Geophys. Res. Lett.* **42**: 4556-4562.

Schneider L, Smerdon JE, Pretis F, Hartl-Meier C, Esper J. 2017. A new archive of large volcanic events over the past millennium derived from reconstructed summer temperatures. *Environ. Res. Lett.* **12**: 119501, doi: https://doi.org/10.1088/1748-9326/aa9426.

Schweingruber FH, Fritts HC, Bräker OU, Drew LG, Schär E. 1978. The X-Ray technique as applied to Dendroclimatology. *Tree-Ring Bulletin* **38**: 61-91.

Schweingruber FH, Bartholin T, Schaur E, Briffa KR. 1988. Radiodensitometric-dendroclimatological conifer chronologies from Lapland (Scandinavia) and the Alps (Switzerland). *Boreas* **17**: 559-566.

Schweingruber FH, Briffa KR. 1996. Tree-ring density networks for climate reconstruction. In *Climatic variations and forcing mechanisms of the last 2000 years*, Jones PD, Bradley RS, Jouzel J (eds). Springer: Heidelberg, Germany, 43-66.

Seim A, Büntgen U, Fonti P, Haska H, Herzig F, Tegel W, Trouet V, Treydte K. 2012. Climate sensitivity of a millennium-long pine chronology from Albania. *Clim. Res.* **51**: 217-228.

Seim A, Treydte K, Trouet V, Frank D, Fonti P, Tegel W, Panayotov M, Fernandez-Donado L, Krusic P, Büntgen U. 2015. Climate sensitivity of Mediterranean pine growth reveals distinct east-west dipole. *Int. J. Clim.* **35**, 2503-2513.

Sigl M, Winstrup M, McConnell JR, Welten KC, Plunkett G, Ludlow F, Büntgen U, Caffee M, Chellman N, Dahl-Jensen D, Fischer H, Kipfstuhl S, Kostick C, Maselli OJ, Mekhaldi F, Mulvaney R, Muscheler R, Pasteris DR, Pilcher JR, Salzer M, Schupbach S, Steffensen JP, Vinther BM, Woodruff TE. 2015. Timing and climate forcing of volcanic eruptions for the past 2,500 years. *Nature* **523**: 543-549.

Sousa PM, Trigo RM, Aizpurua P, Nieto R, Gimeno L, Garcia-Herrera R. 2011. Trends and extremes of drought indices throughout the 20th century in the Mediterranean. *Nat. Hazards Earth Syst. Sci.* **11**, 33-51.

Spinoni J, Naumann G, Vogt J, Barbosa P. 2015. European drought climatologies and trends based on a multi-indicator approach. *Glob. Planet. Chang.* **127**: 50-57.

Stothers RB. 1984. The great tambora eruption in 1815 and its aftermath. *Science* **224**: 1191-1198.

Tegel W, Vanmoerkerke J, Büntgen U. 2010. Updating historical tree-ring records for climate reconstruction. *Quat. Sci. Rev.* **29**: 1957-1959.

Tejedor E, de Luis M, Cuadrat JM, Esper J, Saz MA. 2016. Tree-ring-based drought reconstruction in the Iberian Range (east of Spain) since 1694. *Int. J. Biometeorol.* **60**: 361-72.

Toreti A, Desiato F, Fioravanti G, Perconti W. 2009. Seasonal temperatures over Italy and their relationship with low-frequency atmospheric circulation patterns. *Clim. Chang.* **99**: 211-227.

Touchan R, Funkhouser G, Hughes MK, Erkan N. 2005. Standardized precipitation index reconstructed from Turkish tree-ring widths. *Clim. Chang.* **72**: 339-353.

Trouet V, Panayotov MP, Ivanova A, Frank D. 2012. A pan-European summer teleconnection mode recorded by a new temperature reconstruction from the northeastern Mediterranean (AD 1768-2008). *Holocene* **22**: 887-898.

Trouet V, van Oldenborgh GJ. 2013. KNMI Climate Explorer: A web-based research tool for high-resolution paleoclimatology. *Tree-Ring Res.* **69**: 3-13.

Trouet V. 2014. A tree-ring based late summer temperature reconstruction (AD 1675-1980) for the northeastern Mediterranean. *Radiocarbon* **56**: 69-78.

Trouet V, Babst F, Meko M. 2018. Recent enhanced high-summer North Atlantic Jet variability emerges from three-century context. *Nat. Commun.* **9**, 180-189.

Usoskin IG, Mursula K, Kovaltsov GA. 2002. Lost sunspot cycle in the beginning of Dalton minimum: New evidence and consequences. *Geophys. Res. Lett.* **29**: 2183, doi: 10.1029/2002GL015640.

Vicente-Serrano SM, Lopez-Moreno JI, Beguería S, Lorenzo-Lacruz J, Sanchez-Lorenzo A, García-Ruiz JM, Azorin-Molina C, Morán-Tejeda E, Revuelto J, Trigo R, Coelho F, Espejo F. 2014. Evidence of increasing drought severity caused by temperature rise in southern Europe. *Environ. Res. Lett.* **9**: Art. No. 044001, doi: 10.1088/1748-9326/9/4/044001.

Wigley T, Briffa KR, Jones PD. 1984. On the average of correlated time series, with applications in dendroclimatology and hydrometeorology. *J. Clim. Appl. Meteorol.* **23**: 201-213.

Xoplaki E, Gonzalez-Rouco JF, Gyalistras D, Luterbacher J, Rickli R, Wanner H. 2003a. Interannual summer air temperature variability over Greece and its connection to the large-scale atmospheric circulation and Mediterranean SSTs 1950-1999. *Clim. Dyn.* **20**: 537-554.

Xoplaki E, Luterbacher J, González-Rouco JF, Wanner H. 2003b. Mediterranean summer air temperature variability and its connection to the large-scale atmospheric circulation and SSTs. *Clim. Dyn.* **20**: 723-739.

Xoplaki E, Gonzalez-Rouco JF, Luterbacher J, Wanner H. 2004. Wet season Mediterranean precipitation variability: influence of large-scale dynamics and trends. *Clim. Dyn.* **23**: 63-78.

Xoplaki E, Fleitmann D, Luterbacher J, Wagner S, Haldon JF, Zorita E, Telelis I, Toreti A, Izdebski A. 2016. The Medieval Climate Anomaly and Byzantium: A review of the evidence on climatic fluctuations, economic performance and societal change. *Quat. Sci. Rev.* **136**: 229-252.

Zumbühl HJ, Nussbaumer SU. 2017. Little Ice Age glacier history of the Central and Western Alps from pictorial documents. *Cuadernos de Investigación Geográfica* **44**: 115.

4 – 8 Supplement

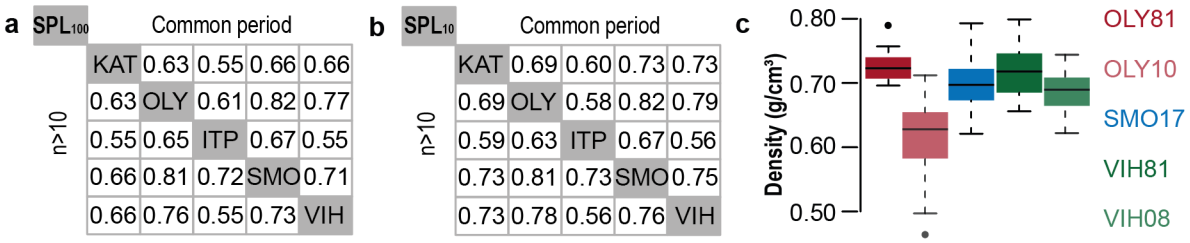

Figure 4–S1 | Coherence among **a** 100SP and **b** 10SP *Pinus heldreichii* MXD chronologies from the Katarapass (KAT), Mt Olympus (OLY), Mt. Smolikas (SMO) in Greece, Sierra de Crispo (ITP) in Italy and the Vihren peak (VIH) in Bulgaria. Pairwise correlations were established for the individual common period with n > 10 series and over the common period 1769-1980. **c** Growth rates for the first 200 years (only living material considered) for the sites OLY, SMO and VIH. Material was split according to the measuring dates in 1981, 2008, 2010 and 2017.

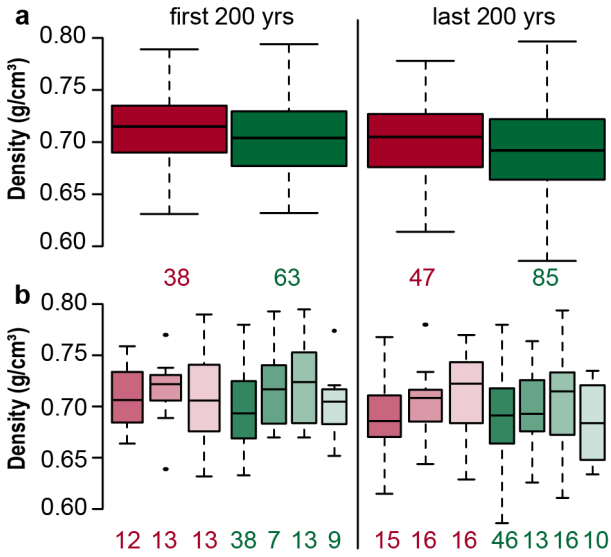

Figure 4–S2 | Density comparison between **a** living (red) and relict (green) material for the first and last 200 years of growth and **b** same as in a but additional data split by site. Living material origins from three sites (red shadings) and relict material from four sites (green shadings). Numbers indicate the sample replication.

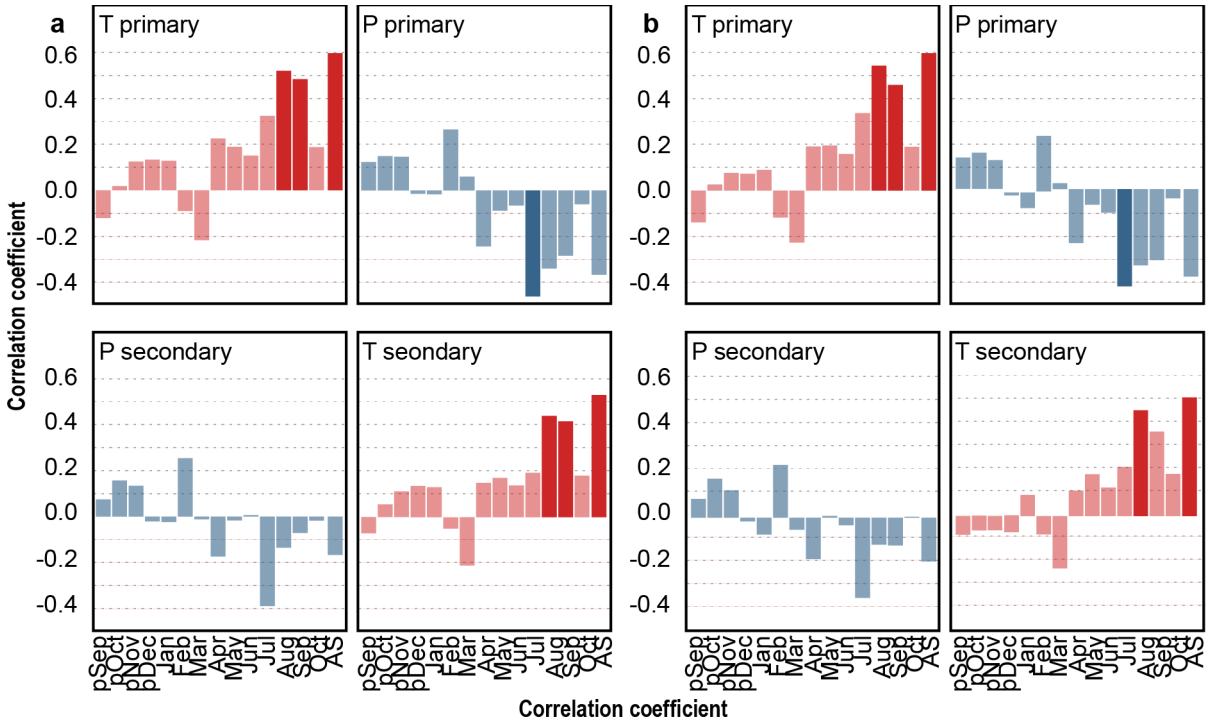

Figure 4–S3 | Correlations and partial correlations of the **a** 100SP and **b** 10SP chronology with climate data from the EOBS v. 15 grid 40.25°N and 20.75°E over the period 1950-2014. Simple Pearson correlations were performed with the primary climate variable (upper panels). For a partial correlation, the effect of the inter-correlation between primary and secondary climate variable was removed (lower panels).

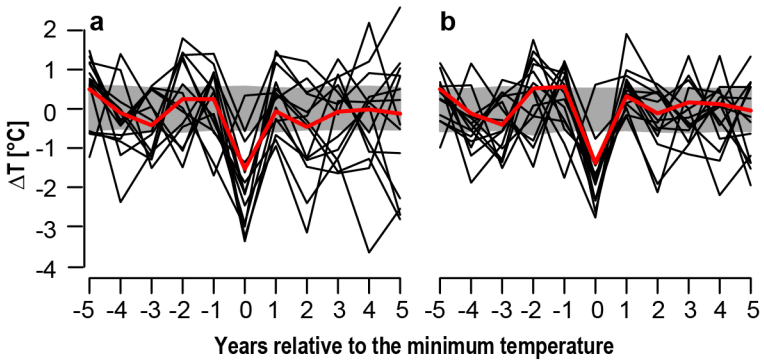

Figure 4–S4 | Super epoch analysis. **a** 100SP reconstructed temperature anomalies with respect to five years prior to the assumed NH forcing dates of the eruptions Eldgja 939, Unknown Eruption (UE) 1108, UE 1171, UE 1230, Samalas 1257, Kuwae 1452, Huaynaputina 1601, Parker 1641, UE 1695, Laki 1783, UE 1809, Tambora 1815, 1835 Cosiguina and 1883 Krakatau (black) and its mean (red). Grey shadings indicate 99% confidence intervals, and **b** same for 10SP reconstruction.

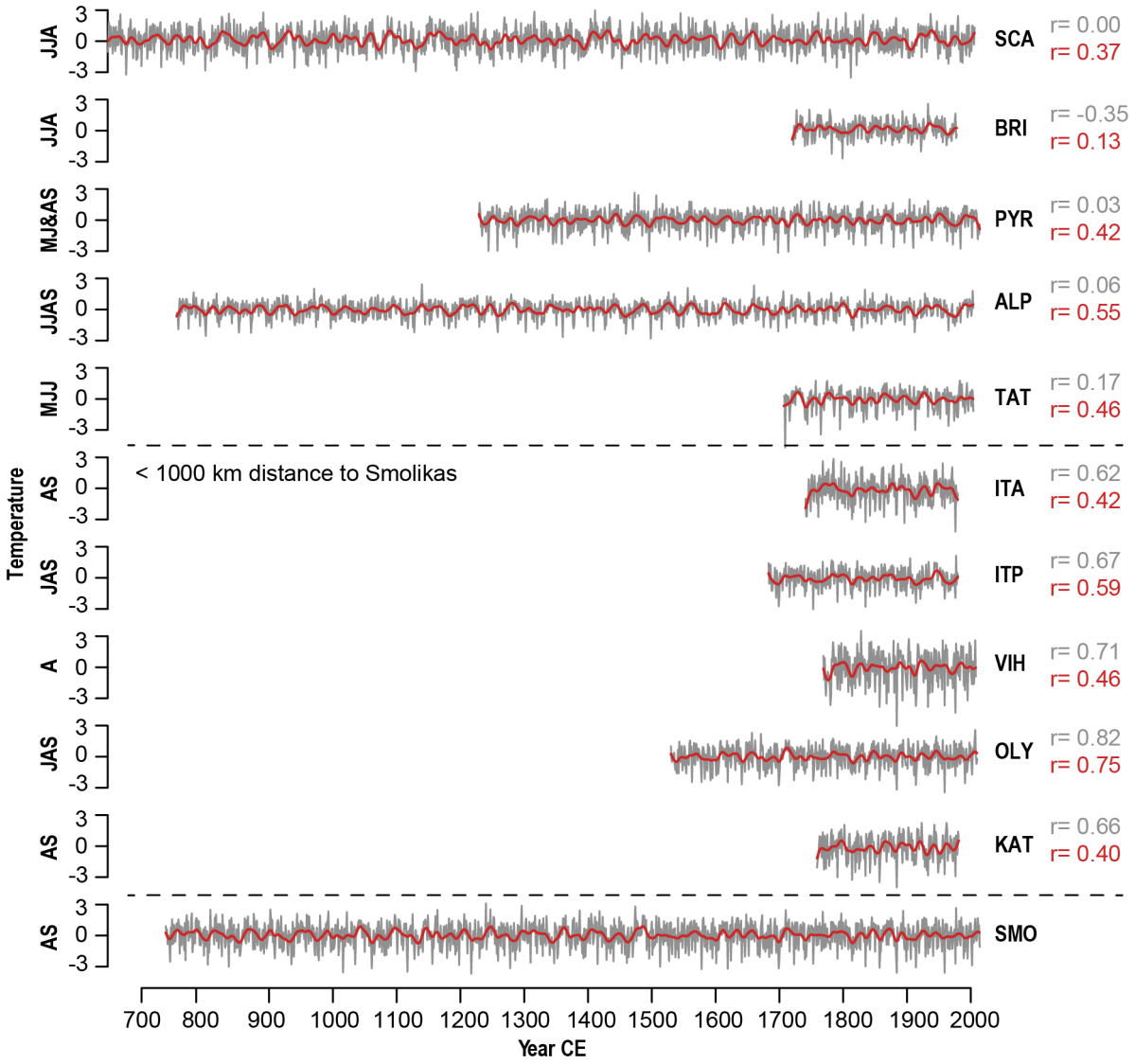

Figure 4–S5 | 100SP SMO reconstruction and re-standardized and re-calibrated temperature reconstructions for 10 tree-ring sites (listed in Table 4–1) across Europe (grey), corresponding 20-year smoothed values (red) and their respective correlation coefficients with the SMO reconstruction over the common period 1769-1978.

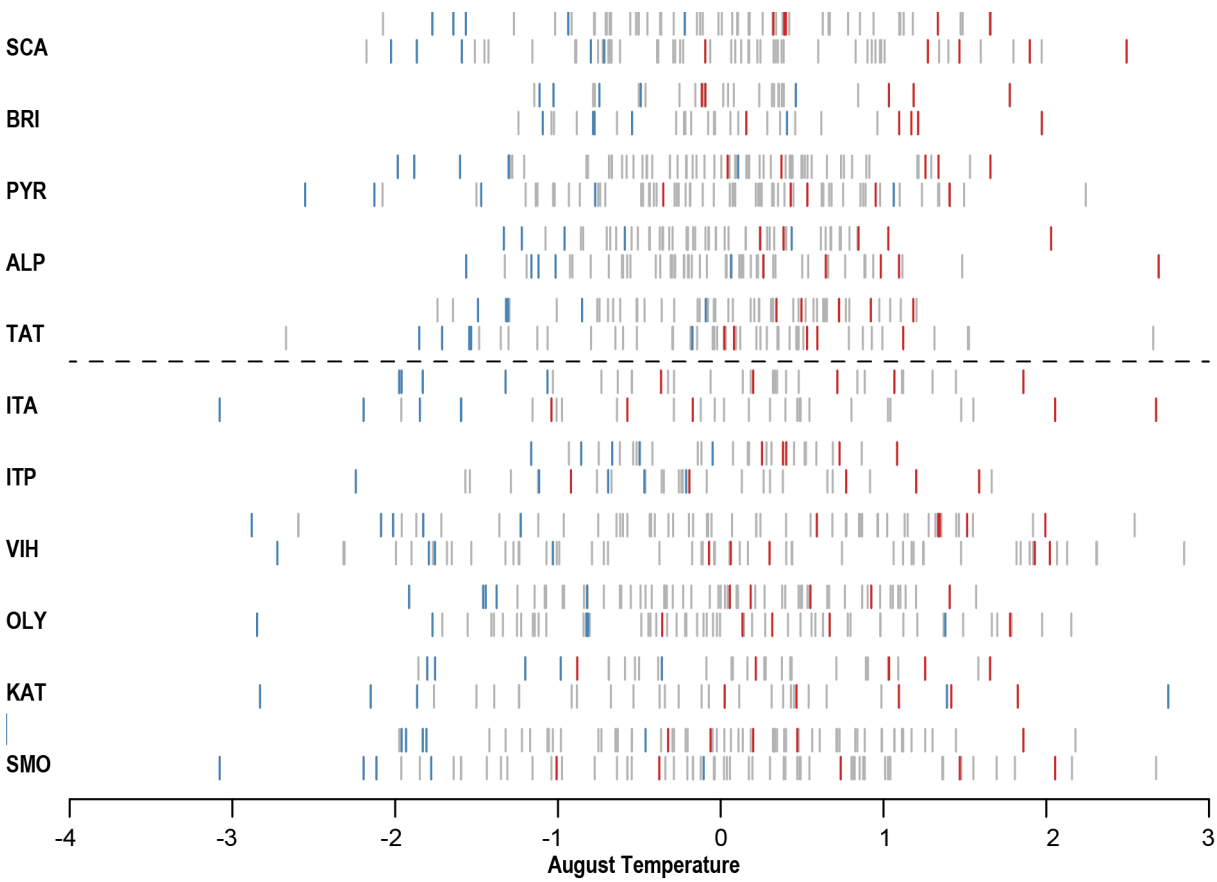

Figure 4–S6 | Temperature sequence of instrumental data used for calibration (grey) and position of the five coldest (blue) and five warmest (red) reconstructed temperatures (lower panel 100SP and upper panel 10SP) for the SMO reconstruction and all records listed in Table 4–1.

Table 4–S1. Twenty coldest and warmest reconstructed August-September summer temperatures since 738 that appear at mid (100SP) to high (10SP) frequencies.

Cold Extremes					Warm Extremes				
Year	**100SP**	**10SP**	**Rank 100**	**Rank 10**	**Year**	**100SP**	**10SP**	**Rank 100**	**Rank 10**
804	-2.83	-2.04	18	33	779	2.15	1.64	16	25
837	-3.03	-2.40	13	16	808	2.51	2.09	7	5
935	-2.80	-1.78	19	61	838	1.50	1.84	99	14
1016	-3.58	-2.33	4	21	852	1.11	2.03	224	7
1035	-2.80	-3.11	20	2	876	2.12	1.58	18	28
1061	-3.19	-2.40	8	17	902	2.54	1.45	5	46
1101	-1.79	-2.75	93	7	919	1.89	1.97	37	10
1117	-3.51	-2.85	5	3	944	2.12	1.42	19	50
1141	-1.59	-3.14	118	1	959	2.02	1.84	26	15

1198	-2.86	-2.46	17	14
1217	-3.71	-2.82	1	5
1278	-3.19	-2.37	9	18
1310	-2.63	-2.82	29	6
1347	-2.70	-2.37	26	19
1415	-2.77	-2.69	23	9
1513	-3.03	-2.59	14	10
1578	-3.25	-2.59	6	11
1619	-3.22	-2.49	7	13
1699	-3.19	-2.01	10	39
1723	-2.80	-2.59	21	12
1835	-2.99	-2.43	15	15
1857	-3.12	-2.44	11	23
1884	-3.61	-2.75	2	8
1914	-3.09	-2.30	12	24
1929	-2.05	-2.37	66	20
1959	-3.61	-2.85	3	4
2002	-2.90	-2.20	16	30

980	1.95	1.93	31	12
993	2.35	1.45	13	47
1022	2.28	1.51	15	32
1034	0.91	2.22	300	2
1064	0.52	1.80	493	17
1125	2.08	1.84	21	16
1149	1.99	2.13	29	4
1164	2.51	1.51	8	33
1169	0.98	1.80	271	18
1240	3.13	2.64	1	1
1247	2.54	1.48	6	40
1296	2.90	2.06	2	6
1387	244	1.77	10	20
1405	2.12	1.19	20	106
1418	2.38	1.64	12	26
1474	2.83	2.16	3	3
1710	2.48	1.55	9	31
1739	1.14	1.97	217	11
1768	2.31	2.03	14	8
1797	2.15	1.51	17	38
1885	0.82	1.90	359	13
1894	2.41	1.80	11	19
1977	2.67	2.03	4	9

5 | Differing pre-industrial cooling trends between tree-rings and lower-resolution temperature proxies

Lara Klippel[1], Scott St. George[2], Ulf Büntgen[3,4,5], Paul J. Krusic[3,6,7], Jan Esper[1,7]

[1]*Department of Geography, Johannes Gutenberg University, Mainz, Germany*

[2]*Department of Geography, Environment and Society, University of Minnesota, Minneapolis, Minnesota, USA*

[3]*Department of Geography, University of Cambridge, Cambridge, United Kingdom*

[4]*Swiss Federal Research Institute for Forest, Snow, and Landscape (WSL), Birmensdorf, Switzerland*

[5]*Global Change Research Centre (Czech Globe) and Department of Geography, Masaryk University, Brno, Czech Republic*

[6]*Department of Physical Geography, Stockholm University, Stockholm, Sweden*

[7]*Navarino Environmental Observatory, Messinia, Greece*

Climate of the Past, 2019, submitted

5 – 1 Introduction

Apart from documentary archives (Pfister *et al*. 1999), our perception of climate variability prior to the systematic collection of instrumental measurements in the mid nineteenth century relies on climate sensitive proxy data (Frank *et al*. 2010). Paleotemperature information can be extracted from natural archives such as ice cores (Steig *et al*. 2013), speleothems (Martín-Chivelet *et al*. 2011), tree-rings (Esper *et al*. 2014), lake and marine sediments (Nieto-Moreno *et al*. 2013), and glacier fluctuations (Solomina *et al*. 2016), among others (Wanner *et al*. 2008; Jones *et al*. 2009). Today, a number of multiproxy (Jones *et al*. 1998; Hegerl *et al*. 2007; Mann *et al*. 2008; Christiansen and Ljungqvist 2011; Ljungqvist *et al*. 2012; Shi *et al*. 2013), and solely tree-ring based reconstructions (Briffa 2000; Esper *et al*. 2002; D'Arrigo *et al*. 2006; Schneider *et al*. 2015; Stoffel *et al*. 2015; Wilson *et al*. 2016) of Northern Hemisphere (NH) and global temperatures have been established. These reconstructions provide an opportunity to study pre-instrumental, naturally forced climate variability at annual to millennial timescales (Christiansen and Ljungqvist 2017), and are essential for placing Anthropogenic warming in a long-term context. Proxy data themselves provide valuable climate information needed to test and verify paleoclimate model simulations (Braconnot *et al*. 2012; Fernández-Donado *et al*. 2013; Hartl-Meier *et al*. 2017).

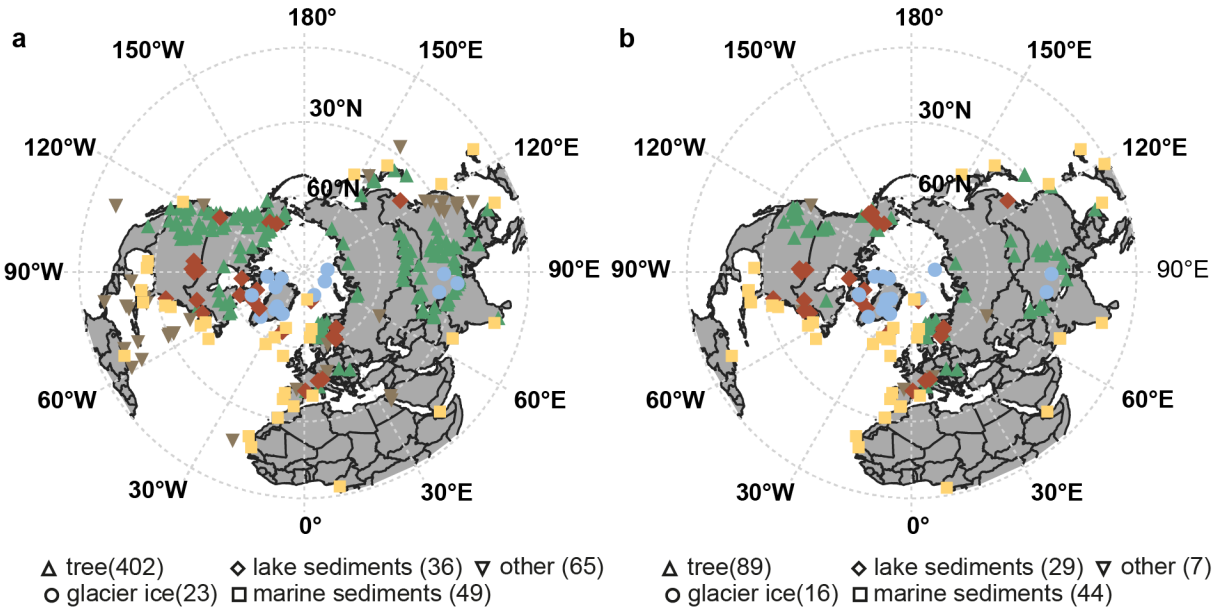

Figure 5–1 | a Map showing the spatial distribution of Northern Hemisphere proxy records from the PAGES 2k 2.0.0 database including primary tree-ring (green), glacier ice (blue), marine (orange) and lake (red) sediment records as well as a smaller number of records from bivalves, boreholes, corals, documents, hybrids, sclerosponges, and speleothems (brown). **b** same as Figure 5–1a but only records longer than 800 years.

The PAGES 2k database represents a unique community effort organized by PAGES (http://pastglobalchanges.org), to amass the world's largest collection of proxy records covering the

Common Era (CE) (PAGES 2k Consortium, 2017). The PAGES 2k database 2.0.0 contains 692 temperature-sensitive proxy records from trees (415), ice cores (49), lake (42) and marine sediments (58), corals (96), documentary evidence (15), sclerosponges (8), speleothems (4), boreholes (3), bivalves (1) and a hybrid tree/borehole (1), and represents 648 locations from all continents and major oceans (Figure 5–1). Unlike previously published multiproxy compilations (Mann *et al*. 2008; PAGES 2k Consortium 2013), the PAGES 2k database includes substantially more evidence from sources other than tree-rings and many more records that cover the first millennium, thereby expanding the spatial and temporal coverage over oceanic and polar regions (PAGES 2k Consortium 2017). The number, spatial distribution, and diversity of the PAGES 2k dataset provides an unprecedented opportunity to analyse regional to large-scale temperature patterns over the Common Era.

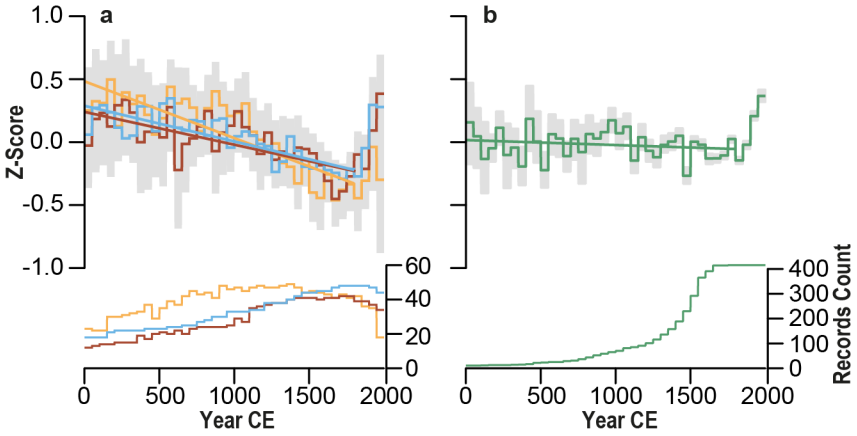

Figure 5–2 | Compilation of temperature-sensitive proxy records from the PAGES 2k initiative. **a** 50-year binned composites from 58 marine sediment (orange), 42 lake sediment (red) and 49 glacier ice (blue) records expressed in standard deviation units. Straight lines highlight the pre-industrial temperature trends (1-1800 CE) and lower panels show the corresponding temporal distribution of the records. Grey shadings indicate 95% bootstrap confidence intervals with 500 replicates. **b** same as in Figure 5–2a for 415 tree-ring records.

The PAGES 2k Consortium (2017) produced a collection of global mean composites from each of the major proxy types in its dataset. The average summer temperature of all marine sediments, lake sediments, and glacial ice cores (Figure 5–2a) exhibit strong negative trends that are consistent with the gradual pre-1800 cooling reported previously by other major syntheses of Holocene proxies (cited previously). By contrast, the global composite derived from just the tree-ring records (Figure 5–2b) shows the rapid post-1800 increase was preceded by an essentially flat trend from 1-1800 CE. A pre-industrial cooling can be attributed to gradual changes in orbital forcing, shown to be an important driver of Holocene long-term climate oscillations (Milanković 1941; Wanner *et al*. 2015). Changes in solar insolation (Huybers and Curry 2006) are caused by variations in the Earth's tilt (obliquity), orbit (eccentricity) and rotation axis (precession). Over the Common Era, precession triggers a shift of the

Perihelion (the closest point between sun and Earth) from December to January (Berger 1978; Berger and Loutre 1991). The collective effects of eccentricity, precession and obliquity cause a decrease of incoming solar radiation of ~9 W/m^2 at 90°N, 5.5 W/m^2 at 60°N, and 3.4 W/m^2 at 30°N in June-August over the NH, and a corresponding warm season increase of ~3.8 W/m^2 at 90°S, 4.1 W/m^2 at 60°S, and 5° W/m^2 at 30°S in December-February over the Southern Hemisphere (Laskar *et al*. 2004) (Figure 5–3). These long-term changes in orbital forcing, from a theoretical perspective, affect regional temperatures differentially (Masson-Delmotte *et al*. 2013).

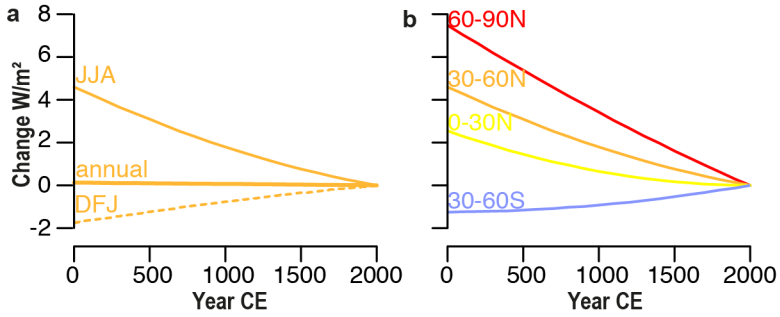

Figure 5–3 | a June-August, December-February, and annual insolation changes at 30-60°N relative to 2000 CE and **b** June-August insolation changes at different latitudinal bands (Laskar *et al*. 2004).

The lack of a long-term negative trend in the average global tree-ring record stands in stark contrast to the cooling detected in the well-replicated maximum latewood density (MXD) record from northern Scandinavia (Esper *et al*. 2012). Esper *et al*. (2012) argues that, unlike long MXD records, tree-ring width (TRW) records are incapable of capturing orbital trends. If this is the case, then including TRW records in past global temperature assessments might result in an underestimate of pre-instrumental warmth, e.g. during Medieval and Roman Times (Esper *et al*. 2004; Frank *et al*. 2010; Wang *et al*. 2014). Combining proxies that systematically vary in their low-frequency trends seemingly contributes to the development of temperature reconstructions of differing temperature amplitudes over the pre-industrial era (Jones *et al*. 1998; Mann *et al*. 1999; D'Arrigo *et al*. 2006; Juckes *et al*. 2007; Mann *et al*. 2008; Christiansen and Ljungqvist 2011; Christiansen and Ljungqvist 2012; Ljungqvist *et al*. 2012; Schneider *et al*. 2015; Wilson *et al*. 2016). Here, we analyse the PAGES 2k collection of temperature-sensitive proxy records to understand why the mean tree-ring record lacks a pre-industrial millennial-scale cooling trend that is otherwise preserved in ice core, lake and marine sediment data. We hypothesize that the absence of this long-term negative trend in tree-ring chronologies may be a consequence of the climate sensitivity of the trees used, their detrending, and spatial distribution of the datasets. To test these potential explanations, here we explore the effect of three significant attributes of just the tree-ring component that may have bearing on the long-term temperature trend reported in the PAGES 2k initiative.

(1) Based on the spatial and seasonally varying effect of orbital forcing over the Common Era, we expect a millennial-scale cooling trend prior to the industrial period, particularly in summer-sensitive, high northern latitude proxies, compared to annually-sensitive proxies (Kaufman *et al*. 2009; Esper *et al*. 2012). Therefore, the absence of a distinct pre-industrial cooling in the PAGES 2k tree-ring network could be a by-product of the spatial distribution of tree-ring proxies in the network. If the network were not biased by northern, mid-latitude tree-ring sites it should capture the millennial-length cooling trend in summer, as we expect proxy records from high northern latitudes to contain a stronger summer cooling trend than their mid-latitude counterparts.

(2) All tree-ring parameters, with the possible exception of $\delta^{18}O$ (Young *et al*. 2011; Esper *et al*. 2015; Helama *et al*. 2015), include age-related, non-climatic signals that need to be removed prior to chronology development and reconstruction (Douglass 1919; Fritts 1976; Bräker 1981; Cook 1990). The selection of a suitable tree-ring detrending method is one of the fundamental challenges in the field of dendroclimatology (Briffa *et al*. 1992; Cook *et al*. 1995; Esper *et al*. 2004; Melvin *et al*. 2013). However, tree-ring detrending methods vary in their approach to model tree growth and if applied indiscriminately can remove long-term cooling trends related to orbital forcing, either intentionally or inadvertently, interpreted as biological noise (Cook *et al*. 1995; Esper *et al*. 2004). Given that the PAGES 2k database contains no information regarding the detrending method used to produce the tree-ring chronologies in its collection, we assume all were produced using different detrending methods, and that those methods are applied to differently structured tree-ring datasets (i.e. the temporal distributions of short and long tree-ring measurements series, indicative of young and old trees, over the past 2k years are not the same). If this is the case, such disparities will affect the database chronologies' low frequency variance, causing the tree-ring mean to lack millennial scale trends (Briffa *et al*. 2013; Linderholm *et al*. 2014; Büntgen *et al*. 2017).

(3) The inclusion of chronologies having a mixed climate sensitivity (Seim *et al*. 2012) and their potential introduction of non-temperature related noise (Baltensweiler *et al*. 2008) might weaken a reconstruction. The establishment of large-scale (continental or hemispheric) temperature reconstructions relies on the assumption that all proxy records used to produce the reconstruction have a substantial temperature signal, and that the signal is temporally stable over the entire record length (Esper *et al*. 2016). We assume the inclusion of tree-ring chronologies with a mixed sensitivity, including other climate parameters besides temperature (Baltensweiler *et al*. 2008; Seim *et al*. 2012), weakens a reconstruction, and that reconstructions composed of weakly calibrating chronologies contain less or no orbitally forced trends.

Here we first describe the varying ability of the proxies used in the PAGES 2k network to preserve orbitally forced, millennial-scale, temperature trends. Then we evaluate and discuss how a more critical proxy selection could improve our understanding of past climate variability over the Common Era.

5 – 2 Data and methods

5 – 2.1 Data preparation

The PAGES 2k database (Figure 5–1) was accessed via the website of the NCEI-Paleo/World Data Service for Paleoclimatology (https://www.ncdc.noaa.gov/paleo/study/21171). All 692 records were normalized over their individual record lengths by subtracting the time series mean (μ) from each single proxy value, then dividing the difference by the series' standard deviation (σ). Normalization is a necessary step to eliminate differences in measuring scale, as the database includes a variety of measured parameters, including $\delta^{18}O$ (Horiuchi *et al*. 2008), TRW (Luckman and Wilson 2005), MXD (Klippel *et al*. 2018), blue intensity (Björklund *et al*. 2014), varve thickness (Moore *et al*. 2001) or Sr/Ca (Rosenheim 2005). We realize that the choice of normalization period, from which we calculate μ and σ, has an influence on the expression of low-frequency trends as seen in the tree-ring data (Figure 5–4). Using μ and σ of all the tree-ring chronologies' common period (1758-1972) leads to a slightly different millennial-scale trend compared to the PAGES 2k procedure of using the individual records' total lengths. Large trend discrepancies arise from using μ and σ of even shorter periods (e.g., 1800-50, 1850-1900 and 1900-50; Figure 5–4). A $\mu_{\text{sub period}}$ and $\sigma_{\text{sub period}}$ smaller, or a $\mu_{\text{sub period}}$ and $\sigma_{\text{sub period}}$ larger, than the entire time series μ and σ produces records with increased or decreased temperature levels and trends, respectively (Figure 5–S2). By normalizing all the proxies in the same manner, we minimize the influence of the normalization method on the preservation of low-frequency trends in tree-rings.

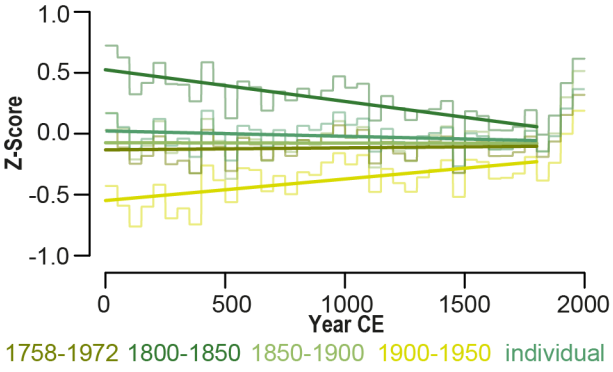

Figure 5–4 | Effect of tree-ring normalization on low-frequency temperature trends. Composite tree-ring records from 415 records normalized using the means and standard deviations over different time spans.

All proxy records having a negative correlation with instrumental temperature were inverted (multiplied by -1) to ensure that high proxy values represent warm temperatures and low proxy value cold temperatures. To account for the varying temporal resolution among the proxies, from sub-annual to multi-decadal, all normalized records are averaged and set to the same resolution consisting of 50-year bins (e.g. 1901-1950; 1951-2000; Figure 5–4). The Southern Hemisphere was excluded from this

analysis due to having too few samples (111 records in total, with 13 tree-ring records) and the suggestion of ambiguous links between the hemispheres on orbital timescales (Petit *et al*. 1999; Kawamura *et al*. 2007; Laepple *et al*. 2011).

5 – 2.2 Hypothesis testing

Based on the Milankovitch cycles (Milanković 1941) we expect latitudinally and seasonally varying temperature trends, with the strongest cooling to be found in summer-sensitive proxies from high latitude, and the least cooling to be found in the annual temperature sensitive proxies from lower latitudes (Berger and Loutre 1991; Laskar *et al*. 2004). To assess the long-term trends preserved in an individual tree-ring record, the statistical significance of the slope of least-squares linear regressions through each proxy record (at 50-year resolution) was evaluated, and the fraction of records that exhibit a significant or insignificant cooling trend over the pre-industrial period (1-1800 CE), and a warming trend over the industrial (post 1800 CE) period were recorded. Those records with significant warming and cooling trends were further analysed with respect to proxy type (archive), latitude, and temperature sensitive seasonality. Assuming the longer proxy records more likely exhibit a significant long-term cooling trend, the minimum considerable length for a tree-ring proxy was set to 800 years (PAGES 2k Consortium 2013).

Of the original 415 tree-ring datasets a subset of 70 tree-ring collections, each at least 800 years-long, was drawn from the International Tree-ring Databank (ITRDB), or kindly provided by the original authors, and used to test the influence of three different tree-ring detrending methods on removing non-climatic age trends from the raw measurements (Cook *et al*. 2017). The tree-ring detrending methods applied are the calculation of residuals from individually fit (i) cubic smoothing splines with a 50% frequency-response cutoff at 100 years (SPL; Cook 1985), (ii) negative exponential functions (NEG), and (iii) from regional growth curves (RCS; Esper *et al*. 2003). The individual series detrending methods (i & ii) emphasize annual to centennial trends in the resulting index chronologies (Cook and Peters 1981) by removing long-term trends that exceed the lengths of sampled trees. By contrast, RCS (iii) (Briffa *et al*. 1992) attempts to preserve low-frequency climate variability through its address of the so called "segment length curse" (Cook *et al*. 1995; Briffa and Melvin 2011). However, RCS is best applied to large datasets with a homogenous age-structure through time to guarantee a proper representation of the population growth curve used to detrend the data (Esper *et al*. 2003), and most tree-ring measurements in the 2k database do not satisfy this criterion. Prior to detrending, a data adaptive power transformation was applied to all measurements to mitigate the heteroscedastic nature of the tree-ring series (Cook and Peters 1997), and chronologies calculated using the bi-weight robust means of tree-ring indices in each calendar year. In addition, the average correlation coefficient among the individual series (Rbar; Wigley *et al*. 1984) was used to stabilize the variance of the chronologies (Frank *et al*. 2007). The resulting chronologies produced from each of the three methodologies i, ii, and iii were then z-transformed and averaged over 50-year bins to produce

three unique composite chronologies. The 50-year binned composites were compared with the PAGES 2k subset composite that includes the same 70 records to investigate the influence of tree-ring standardization on millennial scale temperature trends.

The nature of the climate signal encoded in each tree-ring record was assessed by Pearson correlation coefficients between all 415 z-transformed tree-ring chronologies, and both the 1° and 5° gridded CRU TS 4.01 (Harris *et al*. 2014) monthly June-September temperatures from 1950-1980. The relatively short interval of 31 years was selected for computing correlations in response to the sparse station data availability, especially in Asia, and the decline in the quality of interpolated observational temperature data prior to 1950 (Cook *et al*. 2012; Krusic *et al*. 2015). For each re-standardized and z-transformed chronology, the highest monthly maximum correlation coefficient was extracted and plotted with respect to the trees' location as provided in the metadata table (PAGES 2k Consortium 2017). The use of extended calibration periods (prior to 1950 and post 1980), and annual temperatures, yielded no meaningful differences in the calibration results. The stability of the growth-climate relationship was assessed by first smoothing the tree-ring and corresponding CRU temperatures using 10-year splines, to emphasize decadal and, using these splines to high-pass filter the data to accentuate inter-annual variances. The tree-ring records were ranked according to the strength of their maximum monthly temperature response between June and September, and averaged into 50-year binned composites to evaluate the importance of changing signal strength on any preserved millennial-scale trend.

5 – 3 Results

5 – 3.1 Latitude and season

In total, 66.3% of the tree-ring, 93.8% of the glacier ice, 75.0% of the marine and 79.3% of the lake sediment records, longer than 800 years, reveal a millennial-scale cooling over the period 1-1800 CE (Figure 5–5a). Substantial proxy differences appear when comparing the fraction of records with a significant overall cooling trend ($p < 0.05$): 68.8% of the glacier ice, 54.5% of the marine and 37.9% of the lake sediment records, but only 11.2% of the tree-ring records. Separating the data by latitude reveals that the fraction of significantly cooling tree-ring records decreases from 25.0% at 60-90°N to 8.7% at 30-60°N, which, though the percentages are fairly small, supports the theory that the signature of orbital forcing in tree-rings has a meridionally declining spatial signature. In contrast, the cooling trends in glacier ice, marine and lake sediment records reach their maximum in the mid-latitudes, from 30-60°N, which contradicts this explanation. The overall number of summer temperature sensitive proxy records showing long-term cooling is similar to the number of annual temperature sensitive proxies showing long-term cooling, suggesting that the orbitally forced reduction in summer insolation over the past 2k has no substantial effect on the expression of long-term trends. Over the industrial

period 1800-2000 CE (Figure 5–5b), glacier ice, marine and lake sediments, and the tree-ring records particularly, consistently show a temperature increase.

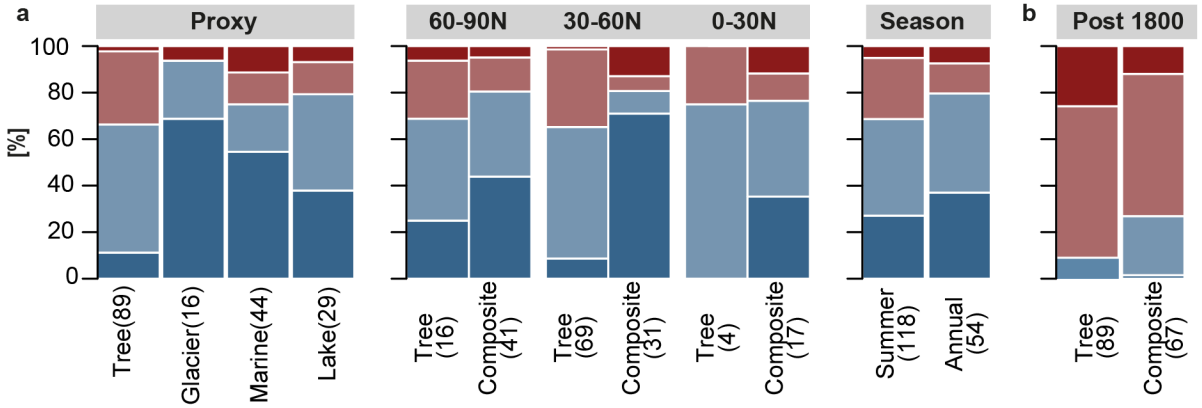

Figure 5–5 | Effects of orbital forcing on low-frequency temperature trends. Summary of NH long-term temperature trends from tree-ring, glacier ice, marine and lake sediment records longer than 800 years. The fraction of 50-year binned records that exhibit a significant negative (dark blue) and non-significant cooling (blueish) trend or significant (red) and non-significant (reddish) warming trend at $p < 0.05$ over **a** the pre-industrial (1-1800 CE) and **b** industrial (post 1800 CE) period derived from the statistical significance of the slope of least-squares linear regressions through each individual 50-year binned proxy record. Pre-industrial summaries are split by proxy, latitude, and seasonality. The category composite includes glacier, marine and lake sediments, and brackets indicate the number of records per category.

5 – 3.2 Tree-ring detrending

We applied three different detrending methods with varying ability to preserve low-frequency information on a subset of 70 of the 415 datasets in the PAGES 2k database. Together, these 70 collections include 7572 series. The single best replicated collection is the Torneträsk (Sweden) TRW dataset containing 650 measurement series and the least replicated is a dataset from southern China containing just 10 measurement series. This huge range of underlying data points to potential weaknesses in our application of RCS, which specifically requires high sample replication (Briffa *et al*. 1992; Esper *et al*. 2003). Comparisons between of the SPL, NEG, RCS, and the PAGES 2k subset composites reveals how there is substantially more low-frequency variability present in the RCS composite chronology (Figure 5–6). Extended cool periods are seen in the intervals from 300-750 CE, 1450-1500 CE and 1600-1800 CE, and prolonged warm periods between 850-1200 CE and 1800-2000 CE. As expected (Cook *et al*. 1995), the SPL composite lacks any long-term cool or warm periods. In the NEG and PAGES 2k subset composite, pre-industrial temperature variations are restricted to multi-decadal scales, indicating cool conditions from 250-300 CE and 1450-1500 CE, warm conditions from 550-600 CE, and a more persistent warming from 1850 CE to present. Comparison of the RCS detrended composite against the PAGES 2k tree-ring composite reveals substantial

differences in long-term trends in the first millennium. This demonstrable difference is a consequence of the pronounced cooling from 300-750 CE, a feature lacking in the both the PAGES 2k subset (Figure 5–6) as well as entire PAGES 2k tree-ring composite (Figure 5–2), but conserved in the RCS mean chronology. From 300-750 CE, the average standard deviation in the RCS composite is -0.32, which compares to -0.03 in the PAGES 2k subset. Good agreement exists in the second millennium, as the magnitude, timing and strength of warm and cool intervals largely overlap. The best fit over the entire Common Era exists among the NEG and PAGES 2k subset composites, suggesting the PAGES 2k database includes a sizable amount of NEG detrended records. However, even with the application of RCS, which is arguably the current best method for conserving low-frequency trends in tree-rings, the pre-industrial cooling trend in the PAGES 2k tree-ring dataset differs significantly from those found in glacier ice, marine and lake sediment records (Figure 5–2 and Figure 5–6).

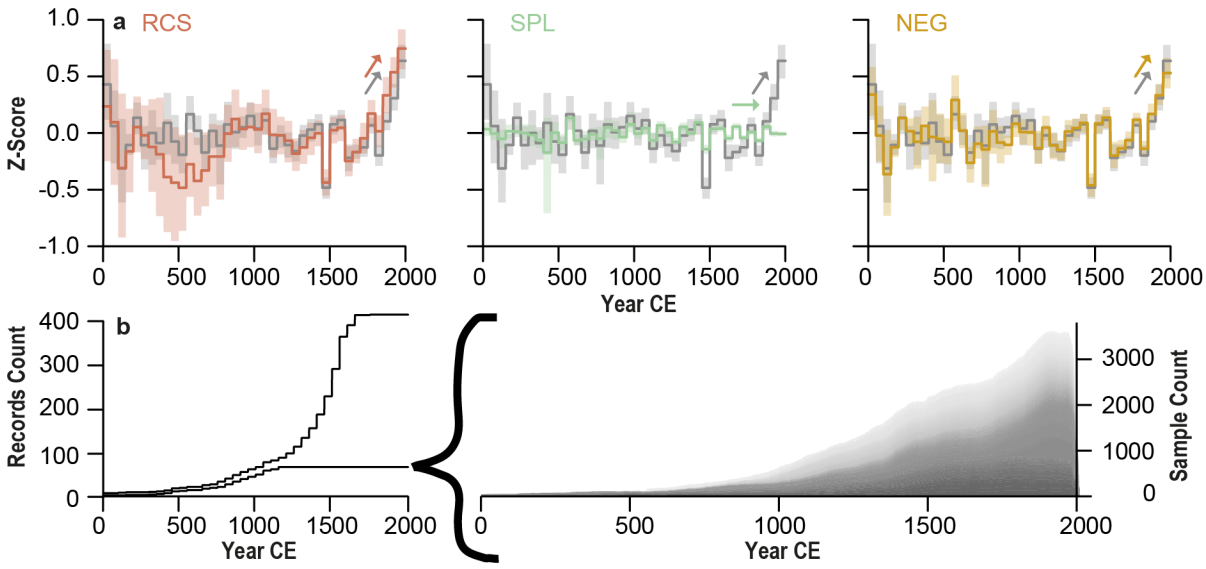

Figure 5–6 | Effects of tree-ring detrending on low frequency temperature trends. **a** 50-year binned composites from 70 RCS (red), 100-year SPL (green) and NEG (gold) standardized datasets. The PAGES 2k composite (dark grey) includes the corresponding chronology versions that are provided in the 2.0.0 database. Shadings indicate 95% bootstrap confidence intervals with 500 replicates, and the arrows indicate the direction of the post-1800 temperature trend. **b** Temporal distribution of the samples included in the whole database (415) relative to the detrended subset (70) and distribution of individual samples from records included in the subset (grey shadings).

5 – 3.3 Climate signal strength

Pearson correlation analyses between the tree-ring proxy records and their respective local temperature grids reveals considerable inter-continental differences in the proxy's response to maximum monthly June-September temperature (Figure 5–7a). The median correlation coefficients differ substantially by region, reaching r = 0.6 in the Arctic, r = 0.21 in Asia, r = 0.54 in Europe and r = 0.38 in North

America. In the Arctic 87.5%, Asia 21.1%, Europe 75.0% and North America 61.33% of the maximum monthly June-September correlation coefficients are significant ($p < 0.05$), indicating a more stable growth-climate relationships in the Arctic and Europe, compared to Asia and North America. However, these differences might be an artefact of different sampling strategies. In the first case (Arctic and Europe), only 16 and 8 highly temperature sensitive records are considered, but the second case (Asia and North America) has 228 and 150 records. The differences among the continents, as demonstrated by the distributions of their June-September correlation coefficients, remains fairly stable in the different frequency domains, as well as for the records longer than 800 years (Figure 5–7b). To account for seasonal responses beyond June-September, and potential influences of the calibration period, the analysis was repeated for all months, varying warm season means, and extended the calibration periods (1950 to the end dates of the individual chronologies). Consequently, no substantial changes were recorded (not shown). Despite significant differences in high-to-low-frequency temperature signals we find that none of the composites, integrating the good, medium and poorly calibrating records, contain a significant millennial-scale cooling (Figure 5–7c and Figure 5–7d). This result suggests climate signal strength has no influence on the expression of low-frequency trends.

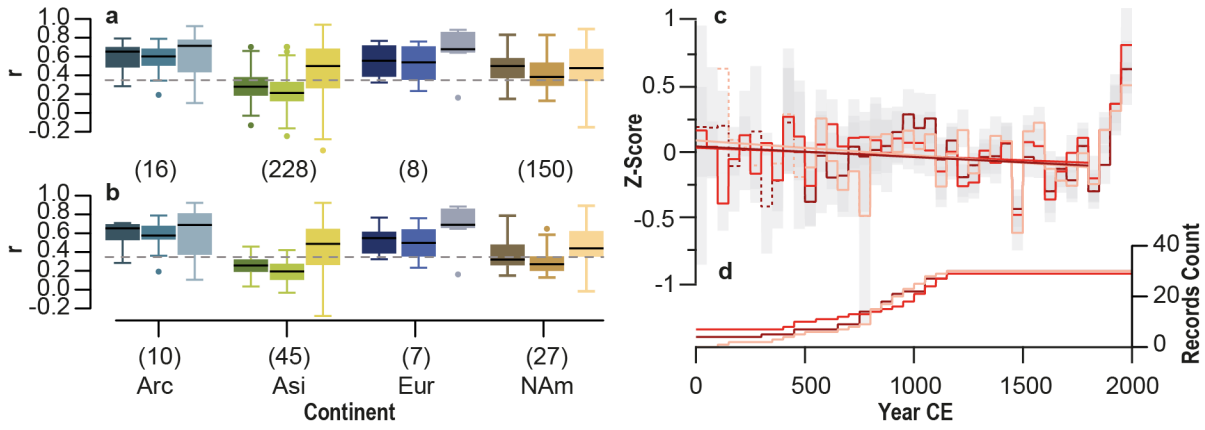

Figure 5–7 | Effects of tree-ring calibration on low-frequency temperature trends. **a** Maximum correlation coefficients between NH individual site-level tree-ring records and 1x1° CRU TS 4.01 June-September monthly temperature data over the period 1950-1980, divided by region, using 10-year high-pass filtered data (left box), original data (central box), 10-year smoothed data (right box). Dashed line indicates the $p < 0.05$ threshold. **b** Same as Figure 5–7a using only records longer than 800 years, and corresponding **c** 50-year binned composites divided by climate signal strength including records with the lowest (n= 30; rose), medium (n= 31; red) and highest (n= 30; dark red) climate sensitivity. Light grey shadings indicate 95% bootstrap confidence intervals with 500 replicates and **d** temporal distribution of the records.

5 – 4 Discussion

5 – 4.1 Orbital signatures in regional and large-scale records

The signature of orbital forcing has been described in regional studies from the Arctic and Antarctica (Kawamura *et al*. 2007; Kaufman *et al*. 2009; Esper *et al*. 2012), as well as in one Holocene climate reconstruction based on a multiproxy collection from the northern high- and mid-latitudes; the latter attributing a distinct value to the orbital cooling effect of 0.5 °C since the Holocene Thermal Maximum (Marcott *et al*. 2013). However, in the case of Marcott *et al*. (2013), it has been shown that NH cooling is only apparent in high-latitude North Atlantic proxies, and that the trend would not exist without them (Marsicek *et al*. 2018). Previous studies have also reported that it is difficult to reconcile the negative orbital forcing trends preserved in proxy data with simulated temperatures which show a strong warming of about 0.5 °C over the Holocene (Laepple *et al*. 2011; Liu *et al*. 2014). Our results demonstrate that millennial-scale trends in NH proxy records are inconsistent between proxies. From a theoretical perspective, independent of the proxy type, we would expect a stronger cooling trend in summer temperature proxies and an increase in the strength of the trend from the mid to the high latitudes (e.g. Kaufman *et al*. 2009; Esper *et al*. 2012). The absence of a clear meridional and seasonal pattern demonstrates the importance of internal climate variability (Schneider and Kinter 1994; Deser *et al*. 2010) and other external forcing factors (Vieira *et al*. 2011; Sigl *et al*. 2015) on proxy records. We conclude that although tree-rings are systematically limited in their low-frequency amplitude, they deviate from forcing expectations in the same way as all other proxies. We conclude that the reduced low-frequency variability in tree-ring data cannot be explained by an overrepresentation of the mid-latitudes in the global mean composite.

Despite the insignificant pre-industrial temperature changes in 86.5% of the tree-ring records, compared to other proxies, the post 1800 CE warming trend in tree-rings is significant (25.8% versus 11.9%). Consequently, large-scale multiproxy climate reconstructions that include long tree-ring records (> 800 years), or solely tree-ring based reconstructions developed from the PAGES 2k database, will likely show a stronger post-1800 warming than multiproxy reconstructions that deliberately exclude (long) tree-ring records (Figure 5–2 and Figure 5–6). The selection of the proxy type has major implications on the reconstructed warmest interval over the Common Era. Using marine data, the warmest period is 151-200 CE and the pre-industrial Era is dominated by a strong cooling trend, suggesting the magnitude of the current warming is not outstanding. By contrast, in lake sediments, ice cores, and tree-ring data, the most recent period is exceptionally warm (Figure 5–2). This finding highlights the importance of tree-ring data in any effort to determine whether twentieth-century temperatures are unprecedented in both their magnitude and rate of warming during the past two millennia (Büntgen *et al*. 2011; Foley *et al*. 2013).

5 – 4.2 The impact of detrending on temperature trends

The degree of similarity between the NEG tree-ring chronology produced here and the corresponding PAGES 2k version suggests that the current PAGES 2k tree-ring collection is not the most ideal for studying millennial scale trends. This is in large part due to the limitations of individual series detrending (Cook *et al*. 1995). Even with the application of RCS (Briffa *et al*. 1992; Esper *et al*. 2003), currently the most widely accepted method to preserve low-frequency variance in tree-ring chronology development, detection of a millennial-scale cooling trend is still elusive. These findings clearly demonstrate that the limited low-frequency variance in tree-ring chronologies is not solely an artefact of inappropriate detrending, previously identified as main explanation for the observed lack of long-term oscillations in large-scale temperature reconstructions (Mann *et al*. 1999; Esper *et al*. 2002). Our reassessment of tree-ring chronologies also highlights the importance of the detrending methodology in reconstructing centennial scale temperature variability, as evidenced by the performance of the RCS chronology. In the RCS chronology we are able to clearly identify the Late Antique Little Ice Age (LALIA) (Büntgen *et al*. 2016), a cool period from 300-750 CE that is absent in the PAGES 2k version, albeit with slightly greater uncertainty about the mean. The Büntgen *et al*. (2016) analysis and the dataset used in this study only share four tree-ring records in common, thus our analysis provides independent confirmation of the existence of LALIA and cooler conditions during the Migration period (Büntgen *et al*. 2011). In contrast, the PAGES 2k tree-ring time series suggest an alternation of warmer and cooler decades, but no persistent cooling at large spatial scales, during LALIA.

5 – 4.3 Temperature sensitivity and the link to long-term trends

Temperature sensitivity was key criterion for the inclusion of data into the PAGES 2k database (PAGES 2k Consortium 2017) and was assessed by the PAGES community through comparison with gridded HadCRUT 4.2 temperatures (Morice *et al*. 2012). However, this analysis has shown the PAGES 2k database includes many tree-ring records that have a weak relationship with local temperature at high-to-low frequencies. The monthly maximum correlation coefficients between 1x1° CRU TS 4.01, June-September temperature data falls below 0.2 in 126 cases. The lowest correlation coefficient is -0.25 (unfiltered data). Such week temperature sensitivities amongst the tree-rings is likely related to confounding non-climatic (Johnson *et al*. 2010; Konter *et al*. 2015) or hydroclimatic (Ljungqvist *et al*. 2016) growth controls, or to the circumstance that some records are by nature less sensitive to summer temperature than others (St. George 2014). Further contributions to the range of climate signal strength found in the tree-ring proxies are related to the fact that MXD are more sensitive to temperature than TRW records (Büntgen *et al*. 2009). At the same time, some records might be more temperature sensitive than they appear due to their calibration against noisy or inappropriate temperature targets (Böhm *et al*. 2009; Cook *et al*. 2012). The re-calibration against instrumental temperatures showed that temperature sensitivity and absolute climate signal strength are of limited importance for the preservation of millennium scale cooling trends in tree-ring records.

Even the best calibrated records ($r > 0.6$; 1950-1980) convey a different low-frequency signature compared to the glacier ice, marine, and lake sediment records. This observation is relevant to the current debate in paleoclimatology on developing basic strategies for compiling proxy datasets to represent past natural temperature variability; is it best to include (a) a large number of proxy records, including those possessively a relatively weak temperature signal, or (b) a small number of only the very best calibrated proxies (Christiansen and Ljungqvist 2017).

5 – 5 Conclusion

The community-sourced database of 692 different temperature-sensitive proxy records in the PAGES 2k initiative provides unprecedented opportunities to study long-term temperature trends at regional to global scales. The synthesis of glacier ice, marine and lake sediment records that span the Common Era reveals a persistent, millennial-scale cooling over the pre-industrial period that is missing in the tree-ring data. This analysis has shown that the observed discrepancies in long-term trends do not arise from the latitudinal and seasonally varying imprints of orbital forcing or the limited temperature sensitivity of tree-ring records. Despite application of the most suitable tree-ring detrending, one that can potentially support the preservation of low-frequency signals at millennial scale temperature trends, substantial long-term trend differences between proxies remain. On centennial scales, due to inappropriate detrending, some of the tree-ring records in the PAGES 2k database are limited in their low-frequency variance. However, when a more low-frequency conserving tree-ring detrending method is applied to the subset of suitable records new corroborating evidence for the existence of the LALIA appears. This lack of low-frequency variance needs to be considered when combining proxies in large-scale temperature reconstructions to avoid the underrepresentation of late Holocene cooling trends prior to post-industrial warming in hemispheric and global mean temperature reconstructions.

5 – 6 Acknowledgements

This research was supported by the German Science Foundation, grants # Inst 247/665-1 FUGG and ES 161/9-1, and the Alexander von Humboldt Foundation. We thank Alexander Kirdyanov, Hans Linderholm, Fredrick C. Ljungqvist, Alma Piermattei, Denis Scholz, and Eduardo Zorita for discussion and helpful comments. The authors declare no conflict of interest.

5 – 7 References

Baltensweiler W, Weber UM, and Cherubini P. 2008. Tracing the influence of larch–bud–moth insect outbreaks and weather conditions on larch tree–ring growth in Engadine (Switzerland). *Oikos* **117**: 161–172.

Berger A. 1978. Long–term variations of daily insolation and quaternary climatic changes. *J. Atmos. Sci.* **35**: 2362–2367.

Berger A, Loutre MF. 1991. Insolation values for the climate of the last 10 million years. *Quat. Sci. Rev.* **10**: 297–317.

Björklund JA, Gunnarson BE, Seftigen K, Esper J, Linderholm HW. 2014. Blue intensity and density from northern Fennoscandian tree rings, exploring the potential to improve summer temperature reconstructions with earlywood information. *Clim. Past* **10**: 877–885.

Böhm R, Jones PD, Hiebl J, Frank D, Brunetti M, Maugeri M. 2009. The early instrumental warm–bias: a solution for long central European temperature series 1760–2007. *Clim. Chang.* **101**: 41–67.

Braconnot P, Harrison SP, Kageyama M, Bartlein PJ, Masson–Delmotte V, Abe–Ouchi A, Otto–Bliesner B, Zhao Y. 2012. Evaluation of climate models using palaeoclimatic data. *Nat. Clim. Chang.* **2**: 417–424.

Bräker OU. 1981. Der Alterstrend bei Jahrringdichten und Jahrringbreiten von Nadelhölzern und sein Ausgleich. *Mitt. Forstl. Bundes–Vers.anst. Wien* **142**: 75–102.

Briffa KR, Jones PD, Bartholin TS, Eckstein D, Schweingruber FH, Karlen W, Zetterberg P, Eronen M. 1992. Fennoscandian summers from AD 500 – temperature changes on short and long timescales. *Clim. Dyn.* **7**: 111–119.

Briffa KR. 2000. Annual climate variability in the Holocene: interpreting the message of ancient trees. *Quat. Sci. Rev.* **19**: 87–105.

Briffa KR, Melvin TM. 2011. A closer look at regional curve standardization of tree–ring records: Justification of the need, a warning of some pitfalls, and suggested improvements in its application. In *Dendroclimatology*, Hughes MK, Swetnam TW, Diaz HF (eds). Springer, Dordrecht, Netherlands, pp. 113-145.

Briffa KR, Melvin TM, Osborn TJ, Hantemirov RM, Kirdyanov AV, Mazepa VS, Shiyatov SG, Esper J. 2013. Reassessing the evidence for tree–growth and inferred temperature change during the Common Era in Yamalia, northwest Siberia. *Quat. Sci. Rev.* **72**: 83–107.

Büntgen U, Frank D, Trouet V, Esper J. 2009. Diverse climate sensitivity of Mediterranean tree–ring width and density. *Trees* **24**: 261–273.

Büntgen U, Tegel W, Nicolussi K, McCormick M, Frank D, Trouet V, Kaplan JO, Herzig F, Heussner KU, Wanner H, Luterbacher J, Esper J. 2011. 2500 years of European climate variability and human susceptibility. *Science* **331**: 578–582.

Büntgen U, Myglan VS, Ljungqvist FC, McCormick M, Di Cosmo N, Sigl M, Jungclaus J, Wagner S, Krusic PJ, Esper J, Kaplan JO, de Vaan MAC, Luterbacher J, Wacker L, Tegel W, Kirdyanov AV. 2016. Cooling and societal change during the Late Antique Little Ice Age from 536 to around 660 AD. *Nat. Geosci.* **9**: 231–236.

Büntgen U, Krusic PJ, Verstege A, Sangüesa–Barreda G, Wagner S, Camarero JJ, Ljungqvist FC, Zorita E, Oppenheimer C, Konter O Tegel W, Gärtner H, Cherubini P, Reinig F, Esper J. 2017. New tree–ring

evidence from the Pyrenees reveals western Mediterranean climate variability since medieval times. *J. Clim.* **30**: 5295–5318.

Christiansen B, Ljungqvist FC. 2011. Reconstruction of the extratropical NH mean temperature over the last millennium with a method that preserves low–frequency variability. *J. Clim.* **24**: 6013–6034.

Christiansen B, Ljungqvist FC. 2012. The extra–tropical Northern Hemisphere temperature in the last two millennia: reconstructions of low–frequency variability. *Clim. Past* **8**: 765–786.

Christiansen B, Ljungqvist FC. 2017. Challenges and perspectives for large–scale temperature reconstructions of the past two millennia. *Rev. Geophys.* **55**: 40–96.

Cook ER, Peters K. 1981. The smoothing spline: a new approach to standardizing forest interior tree–ring width series for dendroclimatic studies. *Tree–Ring Bulletin* **41**: 45—53.

Cook ER. 1985. *A time series analysis approach to tree ring standardization (PhD thesis)*. University of Arizona: Tucson, USA.

Cook E. 1990. *Methods of dendrochronology: Applications in the environmental sciences*. Kluwer: Dordrecht, Netherlands.

Cook E, Briffa KR, Meko DM, Graybill D, Funkhouser G. 1995. The 'segment length curse' in long tree–ring chronology development for palaeoclimatic studies. *Holocene* **5**: 229–237.

Cook E, Peters K. 1997. Calculating unbiased tree–ring indices for the study of climatic and environmental change. *Holocene* **7**: 361–370.

Cook E, Krusic PJ, Anchukaitis KJ, Buckley BM, Nakatsuka T, Sano M. 2012. Tree–ring reconstructed summer temperature anomalies for temperate East Asia since 800 C.E. *Clim. Dyn.* **41**: 2957–2972.

Cook E, Krusic PJ, Peters K, Holmes RL. 2017. Program ARSTAN version48d2, Autoregressive tree–ring standardization program. Tree–Ring Laboratory of Lamot–Doherty Earth Observatory. http://www.ldeo.columbia.edu/tree–ring–laboratory/resources/software.

D'Arrigo R, Wilson R, Jacoby G. 2006. On the long–term context for late twentieth century warming. *J. Geophys. Res.* **111**: D03103, doi: 10.1029/2005JD006352.

Deser C, Phillips A, Bourdette V, Teng H. 2012. Uncertainty in climate change projections: the role of internal variability. *Clim. Dyn.* **38**: 527–546.

Douglass AE. 1919. *Climatic Cycles and Tree Growth Volume I*. Carnegie Institution of Washington: Washington, USA.

Esper J, Cook ER, Schweingruber FH. 2002. Low–frequency signals in long tree–ring chronologies for reconstructing past temperature variability. *Science* **295**: 2250–2253.

Esper J, Cook ER, Krusic PJ, Peters K, Schweingruber FH. 2003. Tests of the RCS method for preserving low–frequency variability in long tree–ring chronologies. *Tree–Ring Res.* **59**: 81–98.

Esper J, Frank D, Wilson R. 2004. Climate reconstructions: Low-frequency ambition and high-frequency ratification. *EOS* **85**: 113–130.

Esper J, Frank DC, Timonen M, Zorita E, Wilson RJS, Luterbacher J, Holzkämper S, Fischer N, Wagner S, Nievergelt D, Verstege A, Büntgen U. 2012. Orbital forcing of tree–ring data. *Nat. Clim. Chang.* **2**: 862–866.

Esper J, Düthorn E, Krusic PJ, Timonen M, Büntgen U. 2014. Northern European summer temperature variations over the Common Era from integrated tree–ring density records. *J. Quat. Sci.* **29**: 487–494.

Esper J, Konter O, Krusic PJ, Saurer M, Holzkämper S, Büntgen U. 2015. Long–term summer temperature variations in the Pyrenees from detrended stable carbon isotopes. *Geochronometria* **42**: 53–59.

Esper J, Krusic PJ, Ljungqvist FC, Luterbacher J, Carrer M, Cook E, Davi NK, Hartl–Meier C, Kirdyanov A, Konter O, Myglan V, Timonen M, Treydte K, Trouet V, Villalba R, Yang B, Büntgen U. 2016. Ranking of tree–ring based temperature reconstructions of the past millennium. *Quat. Sci. Rev.* **145**: 134–151.

Fernández–Donado L, González–Rouco JF, Raible CC, Ammann CM, Barriopedro D, García–Bustamante E, Jungclaus JH, Lorenz SJ, Luterbacher J, Phipps SJ, Servonnat J, Swingedouw D, Tett SFB, Wagner S, Yiou P, Zorita E. 2013. Large–scale temperature response to external forcing in simulations and reconstructions of the last millennium. *Clim. Past* **9**: 393–421.

Foley SF, Gronenborn D, Andreae MO, Kadereit JW, Esper J, Scholz D, Pöschl U, Jacob DE, Schöne BR, Schreg R, Vött A, Jordan D, Lelieveld J, Weller CG, Alt KW, Gaudzinski–Windheuser S, Bruhn KC, Tost H, Sirocko F, Crutzen PJ. 2013. The Palaeoanthropocene – The beginnings of anthropogenic environmental change. *Anthropocene* **3**: 83–88.

Frank D, Esper J, Cook ER. 2007. Adjustment for proxy number and coherence in a large–scale temperature reconstruction. *Geophys. Res. Lett.* **34**: L16709, doi: 10.1029/2007GL030571.

Frank D, Esper J, Zorita E, Wilson R. 2010. A noodle, hockey stick, and spaghetti plate: a perspective on high–resolution paleoclimatology. *Nat. Clim. Chang.* **1**: 507–516.

Fritts HC. 1976. *Tree rings and climate*. Blackburn Press: Caldwell, USA.

Harris I, Jones PD, Osborn TJ, Lister DH. 2014. Updated high–resolution grids of monthly climatic observations – the CRU TS3.10. *Int. J. Clim.* **34**: 623–642.

Hartl–Meier CTM, Büntgen U, Smerdon JE, Zorita E, Krusic PJ, Ljungqvist FC, Schneider L, Esper J. 2017. Temperature covariance in tree ring reconstructions and model simulations over the past millennium. *Geophys. Res. Lett.* **44**: 9458–9469.

Hegerl GC, Crowley TJ, Allen M, Hyde WT, Pollack HN, Smerdon J, Zorita E. 2007. Detection of human influence on a new, validated 1500–year temperature reconstruction. *J. Clim.* **20**: 650–666.

Helama S, Arppe L, Timonen M, Mielikäinen K, Oinonen, M. 2015. Age–related trends in subfossil tree–ring δ13C data. *Chem. Geol.* **416**: 28–35.

Horiuchi K, Uchida T, Sakamoto Y, Ohta A, Matsuzaki H, Shibata Y, Motoyama, H. 2008. Ice core record of 10Be over the past millennium from Dome Fuji, Antarctica: A new proxy record of past solar activity and a powerful tool for stratigraphic dating. *Quat. Geochron.* **3**: 253–261.

Huybers P, Curry W. 2006. Links between annual, Milankovitch and continuum temperature variability. *Nature* **441**: 329–332.

Johnson DM, Büntgen U, Frank DC, Kausrud K, Haynes KJ, Liebhold AM, Esper J, Stenseth NC. 2010. Climatic warming disrupts recurrent Alpine insect outbreaks. *PNAS* **107**: 20576–20581.

Jones PD, Briffa KR, Barnett TP, Tett SFB. 1998. High–resolution palaeoclimatic records for the last millennium: interpretation, integration and comparison with General Circulation Model control–run temperatures. *Holocene* **8**: 455–471.

Jones PD, Briffa KR, Osborn TJ, Lough JM, van Ommen TD, Vinther BM, Luterbacher J, Wahl ER, Zwiers F W, Mann ME, Schmidt GA, Ammann CM, Buckley BM, Cobb KM, Esper J, Goosse H, Graham N, Jansen E, Kiefer T, Kull C, Kuttel M, Mosley–Thompson E, Overpeck JT, Riedwyl N, Schulz M, Tudhope AW, Villalba R, Wanner H, Wolff E, Xoplaki E. 2009. High–resolution palaeoclimatology of the last millennium: a review of current status and future prospects. *Holocene* **19**: 3–49.

Juckes MN, Allen MR, Briffa KR, Esper J, Hegerl GC, Moberg A, Osborn TJ, Weber SL. 2007. Millennial temperature reconstruction intercomparison and evaluation. *Clim. Past* **3**: 591–609.

Kaufman DS, Schneider DP, McKay NP, Ammann CM, Bradley RS, Briffa KR, Miller GH, Otto–Bliesner BL, Overpeck JT, Vinther BM, Arctic Lakes 2k Project Members. 2009. Recent warming reverses long–term arctic cooling. *Science* **325**: 1236–1239.

Kawamura K, Parrenin F, Lisiecki L, Uemura R, Vimeux F, Severinghaus JP, Hutterli MA, Nakazawa T, Aoki S, Jouzel J, Raymo ME, Matsumoto K, Nakata H, Motoyama H, Fujita S, Goto–Azuma K, Fujii Y, Watanabe O. 2007. Northern Hemisphere forcing of climatic cycles in Antarctica over the past 360,000 years. *Nature* **448**: 912–916.

Klippel L, Krusic PJ, Konter O, St. George S, Trouet V, Esper J. 2018. A 1200+ year reconstruction of temperature extremes for the northeastern Mediterranean region. *Int. J. Climatol.* **39**: 2336–2350.

Konter O, Esper J, Liebhold A, Kyncl T, Schneider L, Düthorn E, Büntgen U. 2015. Tree–ring evidence for the historical absence of cyclic larch budmoth outbreaks in the Tatra Mountains. *Trees* **29**: 809–814.

Krusic PJ, Cook ER, Dukpa D, Putnam AE, Rupper S, Schaefer J. 2015. Six hundred thirty-eight years of summer temperature variability over the Bhutanese Himalaya. *Geophys. Res. Lett.* **42**: 2988-2994.

Laepple T, Werner M, Lohmann G. 2011. Synchronicity of Antarctic temperatures and local solar insolation on orbital timescales, *Nature* **471**: 91–94.

Laskar J, Robutel P, Joutel F, Gastineau M, Correia ACM, Levrard B. 2004. A long–term numerical solution for the insolation quantities of the Earth. *A&A* **428**: 261–285.

Linderholm HW, Björklund J, Seftigen K, Gunnarson BE, Fuentes M. 2014. Fennoscandia revisited: a spatially improved tree–ring reconstruction of summer temperatures for the last 900 years. *Clim. Dyn.* **45**: 933–947.

Liu Z, Zhu J, Rosenthal Y, Zhang X, Otto–Bliesner BL, Timmermann A, Smith RS, Lohmann G, Zheng W, Elison Timm O. 2014. The Holocene temperature conundrum. *PNAS* **111**: 3501–3505.

Ljungqvist FC, Krusic PJ, Brattstrom G, Sundqvist HS. 2012. Northern Hemisphere temperature patterns in the last 12 centuries. *Clim. Past* **8**: 227–249.

Ljungqvist FC, Krusic PJ, Sundqvist HS, Zorita E, Brattstrom G, Frank D. 2016. Northern Hemisphere hydroclimate variability over the past twelve centuries. *Nature* **532**: 94–98.

Luckman BH, Wilson RJS. 2005. Summer temperatures in the Canadian Rockies during the last millennium: a revised record. *Clim. Dyn.* **24**: 131–144.

Mann ME, Bradley RS, Hughes MK. 1999. Northern hemisphere temperatures during the past millennium: Inferences, uncertainties, and limitations. *Geophys. Res. Lett.* **26**: 759–762.

Mann ME, Zhang Z, Hughes MK, Bradley RS, Miller SK, Rutherford S, Ni F. 2008. Proxy–based reconstructions of hemispheric and global surface temperature variations over the past two millennia. *PNAS* **105**: 13252–13257.

Marcott SA, Shakun JD, Clark PU, Mix AC. 2013. A reconstruction of regional and global temperature for the past 11,300 years. *Science* **339**: 1198–1201.

Marsicek J, Shuman BN, Bartlein PJ, Shafer SL, Brewer S. 2018. Reconciling divergent trends and millennial variations in Holocene temperatures. *Nature* **554**: 92–96.

Martín–Chivelet J, Muñoz–García MB, Edwards RL, Turrero MJ, Ortega AI. 2011. Land surface temperature changes in Northern Iberia since 4000yrBP, based on δ13C of speleothems. *Glob. Planet. Chang.* **77**: 1–12.

Masson–Delmotte V, Schulz M, Abe–Ouchi A, Beer J, Ganopolski A, González Rouco JF, Jansen E, Lambeck K, Luterbacher J, Naish T, Osborn T, Otto–Bliesner B, Quinn T, Ramesh R, Rojas M, Shao X, Timmermann A. 2013. Information from paleoclimate archives. In *Climate Change 2013: The physical science basis. Contribution of Working Group I to the Fifth Assessment Report of the Intergovernmental Panel on Climate Change*, Stocker TF, Qin D, Plattner GK, Tignor M, Allen SK, Boschung J, Nauels A, Xia Y, Bex V, Midgley PM (eds). Cambridge University Press, Cambridge, pp. 383–464.

Melvin TM, Grudd H, Briffa KR. 2013. Potential bias in 'updating' tree–ring chronologies using regional curve standardisation: Re–processing 1500 years of Torneträsk density and ring–width data. *Holocene* **23**: 364–373.

Milanković M. *Kanon der Erdbestrahlung und seine Anwendung auf das Eiszeitproblem*: Königlich Serbische Akademie.

Moore JJ, Hughen KA, Miller GH, Overpeck JT. 2001. Little Ice Age recorded in summer temperature reconstructions from varved sediments of Donard Lake, Baffin Island, Canada. *J. Paleolimnol.* **25**: 503–517.

Morice CP, Kennedy JJ, Rayner NA, Jones PD. 2012. Quantifying uncertainties in global and regional temperature change using an ensemble of observational estimates: The HadCRUT4 data set. *J. Geophys. Res.* **117**: D08101, doi:10.1029/2011JD017187.

Nieto–Moreno V, Martínez–Ruiz F, Willmott V, García–Orellana J, Masqué P, Sinninghe Damsté JS. 2013. Climate conditions in the westernmost Mediterranean over the last two millennia: An integrated biomarker approach. *Org. Geochem.* **55**: 1–10.

PAGES 2k Consortium. 2013. Continental–scale temperature variability during the past two millennia. *Nat. Geosci.* **6**: 339–346.

PAGES 2k Consortium. 2017. A global multiproxy database for temperature reconstructions of the Common Era. *Nat. Sci. Data.* **4**: 1–33.

Petit JR, Jouzel J, Raynaud D, Barkov NI, Barnola JM, Basile I, Bender M, Chappellaz J, Davis M, Delaygue G, Delmotte M, Kotlyakov VM, Legrand M, Lipenkov VY, Lorius C, Pépin L, Ritz C, Saltzman E, Stievenard M. 1999. Climate and atmospheric history of the past 420 000 years from the Vostok ice core, Antarctica. *Nature* **399**: 429-436.

Pfister C, Brazdil R, Glaser R, Barriendos M, Camuffo D, Deutsch M, Dobrovolný P, Enzi S, Guidoboni E, Kotyza O, Militzer S, Racz L, Rodrigo FS. 1999. Documentary evidence on climate in sixteenth–century Europe. *Clim. Chang.* **43**: 55–110.

Rosenheim BE. 2005. Salinity change in the subtropical Atlantic: Secular increase and teleconnections to the North Atlantic Oscillation. *Geophys. Res.* **32**: L02603, doi:10.1029/2004GL021499.

Schneider EK, Kinter JL. 1994. An examination of internally generated variability in long climate simulations. *Clim. Dyn.* **10**: 181–204.

Schneider L, Smerdon JE, Büntgen U, Wilson RJS, Myglan VS, Kirdyanov AV, Esper J. 2015. Revising midlatitude summer temperatures back to A.D. 600 based on a wood density network. *Geophys. Res. Lett.* **42**: 4556–4562.

Seim A, Büntgen U, Fonti P, Haska H, Herzig F, Tegel W, Trouet V. Treydte K. 2012. Climate sensitivity of a millennium–long pine chronology from Albania. *Clim. Res.* **51**: 217–228.

Shi F, Yang B, Mairesse A, von Gunten L, Li J, Bräuning A, Yang F, Xiao X. 2013. Northern Hemisphere temperature reconstruction during the last millennium using multiple annual proxies. *Clim. Res.* **56**: 231–244.

Sigl M, Winstrup M, McConnell JR, Welten KC, Plunkett G, Ludlow F, Büntgen U, Caffee M, Chellman N, Dahl–Jensen D, Fischer H, Kipfstuhl S, Kostick C, Maselli OJ, Mekhaldi F, Mulvaney R, Muscheler R, Pasteris DR, Pilcher JR, Salzer M, Schupbach S, Steffensen JP, Vinther BM, Woodruff TE. 2015. Timing and climate forcing of volcanic eruptions for the past 2,500 years. *Nature* **523**: 543–549.

Solomina ON, Bradley RS, Jomelli V, Geirsdottir A, Kaufman DS, Koch J, McKay NP, Masiokas M, Miller G, Nesje A, Nicolussi K, Owen LA, Putnam AE, Wanner H, Wiles G, Yang B. 2016. Glacier fluctuations during the past 2000 years. *Quat. Sci. Rev.* **149**: 61-90.

Steig EJ, Ding Q, White JWC, Küttel M, Rupper SB, Neumann TA, Neff PD, Gallant AJE, Mayewski PA, Taylor KC, Hoffmann G, Dixon DA, Schoenemann SW, Markle BR, Fudge TJ, Schneider DP, Schauer AJ, Teel RP, Vaughn BH, Burgener L, Williams J, Korotkikh E. 2013. Recent climate and ice–sheet changes in West Antarctica compared with the past 2,000 years. *Nat. Geosci.* **6**: 372–375.

St. George S. 2014. An overview of tree–ring width records across the Northern Hemisphere. *Quat. Sci. Rev.* **95**: 132–150.

Stoffel M, Khodri M, Corona C, Guillet S, Poulain V, Bekki S, Guiot J, Luckman BH, Oppenheimer C, Lebas N, Beniston M, Masson–Delmotte V. 2015. Estimates of volcanic–induced cooling in the Northern Hemisphere over the past 1,500 years. *Nature Geosci.* **8**: 784–788.

Vieira LE, Solanki SK, Krivova NA, Usoskin I. 2011. Evolution of the solar irradiance during the Holocene. *A&A* **531**: 1–20.

Wang J, Emile–Geay J, Guillot D, Smerdon JE, Rajaratnam B. 2014. Evaluating climate field reconstruction techniques using improved emulations of real–world conditions. *Clim. Past* **10**: 1–19.

Wanner H, Beer J, Bütikofer J, Crowley TJ, Cubasch U, Flückiger J, Goosse H, Grosjean M, Joos F, Kaplan JO, Küttel M, Müller SA, Prentice IC, Solomina O, Stocker TF, Tarasov P, Wagner M, Widmann M. 2008. Mid– to Late Holocene climate change: an overview. *Quat. Sci. Rev.* **27**: 1791–1828.

Wanner H, Mercolli L, Grosjean M, Ritz SP. 2015. Holocene climate variability and change; a data–based review. *J. Geol. Soc.* **172**: 254–263.

Wigley T, Briffa KR, Jones PD. 1984. On the average of correlated time series, with applications in dendroclimatology and hydrometeorology. *J. Clim. Appl. Meteorol.* **23**: 201–213.

Wilson R, Anchukaitis K, Briffa KR, Büntgen U, Cook E, D'Arrigo R, Davi N, Esper J, Frank D, Gunnarson B, Hegerl G, Helama S, Klesse S, Krusic PJ, Linderholm HW, Myglan V, Osborn TJ, Rydval M, Schneider L, Schurer A, Wiles G, Zhang P, Zorita E. 2016. Last millennium northern hemisphere summer temperatures from tree rings: Part I: The long term context. *Quat. Sci. Rev.* **134**: 1–18.

Young GHF, Demmler JC, Gunnarson BE, Kirchhefer AJ, Loader NJ, McCarroll D. 2011. Age trends in tree ring growth and isotopic archives: A case study of Pinus sylvestris L. from northwestern Norway. *Glob. Biogeochem. Cycles* **25**: GB2020, doi:10.1029/2010GB003913.

5 – 8 Supplement

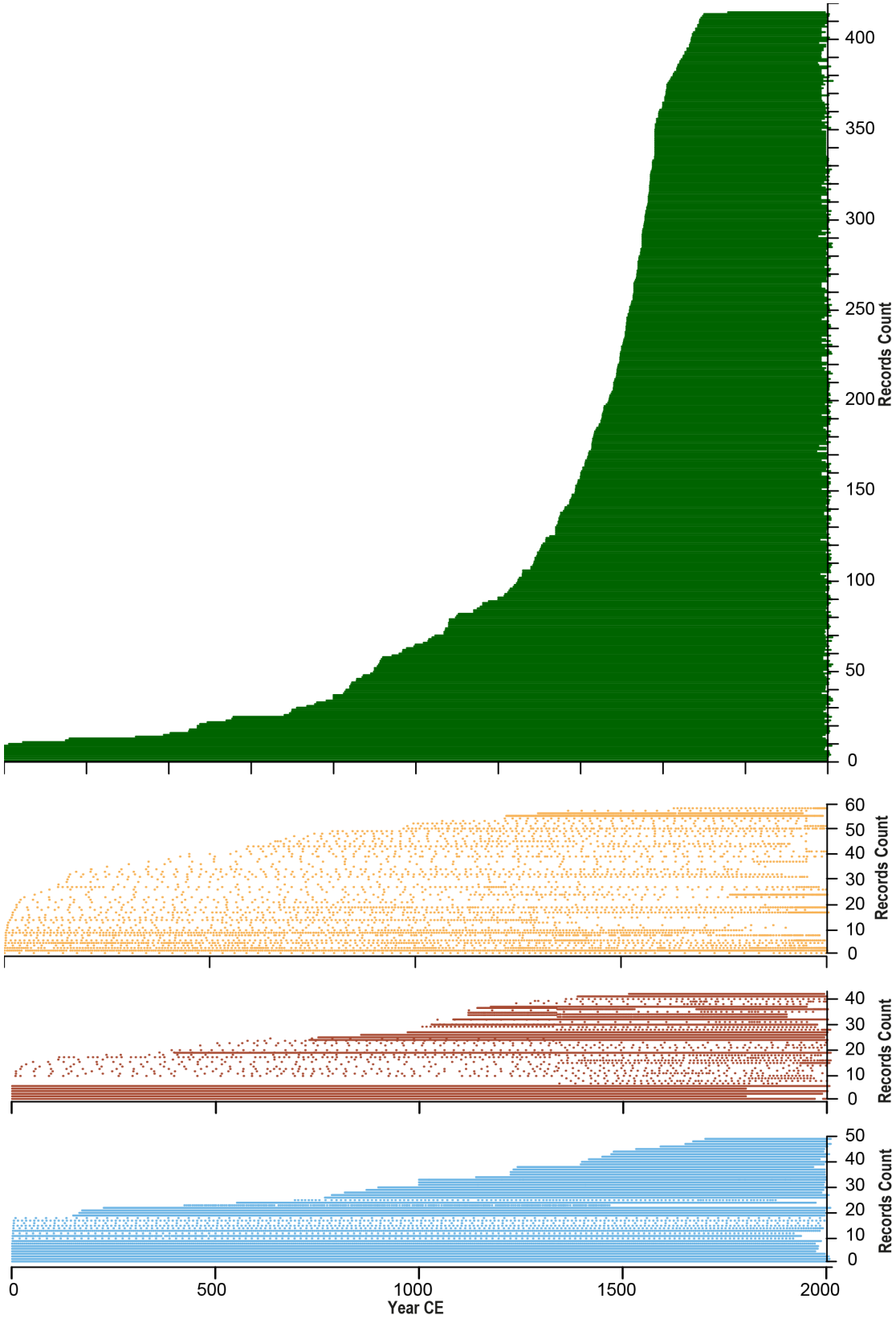

Figure 5–S1 | Temporal distribution and resolution of the tree-ring (green), lake sediment (red), marine sediment (orange) and glacier ice (blue) proxy records from the PAGES 2k 2.0.0 database. (Dashed) lines indicate proxy resolution ranging between sub-annual and 145 years.

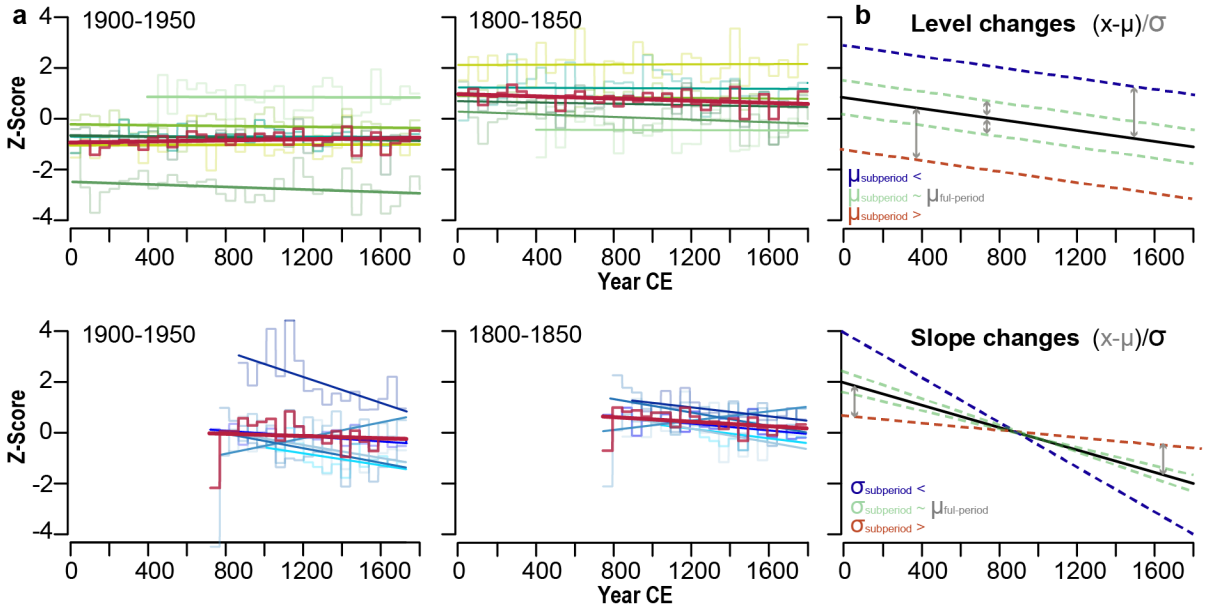

Figure 5–S2 | a Differently normalized tree-ring records (green, blue), their chronology means (red) and corresponding pre-industrial temperature trends (1-1800 CE) and **b** explanation, why level and slope change dependent on the period chosen for tree-ring normalization.

6 | Conclusions and perspectives

Paleoclimate data provide perspectives on global temperature changes over the past centuries to millennia and enable evaluation of the 20th century warming trend against the context of natural climate variability (Büntgen *et al*. 2011). However, proxies are an imperfect realization of past climate, because they store multiple environmental impacts, thus temperature reconstructions will naturally integrate a certain amount of noise and uncertainty (Christiansen and Ljungqvist 2017). An improved signal-to-noise ratio in large-scale temperature reconstructions can be achieved through proper calibration against reliable instrumental temperatures, and through the continued development of new, high-quality reconstructions from climate-sensitive proxy datasets.

In this thesis, an important step towards the improvement of the European 2k reconstruction network is undertaken. The two new millennial-length reconstructions for southeastern Europe, one targeting temperature and the other drought, offer new insights into the frequency, intensity, and magnitude of temperature and precipitation extremes in the eastern Mediterranean, and extend the annually-resolved regional climate history by roughly 800 years. Analysis of the dendroclimatic potential in *P. heldreichii* is analysed in a step-wise procedure:

First, this thesis explores climate signals inherent in eastern Mediterranean high-elevation *P. heldreichii* trees growing at the tree line of Mt. Smolikas. The exploration of site-specific climate sensitivity patterns is the first important step towards the development of long climate reconstructions (chapter 2). TRW formation is significantly controlled by temperature in April and precipitation in June-July which emphasizes the overall importance of an early growth onset and subsequent moisture conditions. Inter-site differences in climate signal strength are related to slope exposure and meltwater supply. TRW contains only a weak and temporally unstable temperature signal, making a robust reconstruction challenging. A stable precipitation signal in the high-frequency domain, however, points toward the potential of the TRW data to be used for hydroclimate climate reconstruction.

Based on this calibration study, in a second step, a June-July drought reconstruction using TRW and the Standardized Precipitation Index (SPI) is established for the Balkan Peninsula over the period 730-2015 (chapter 3). The driest year during the 1286 year-long period proves to be 1660 and the wettest year is 1482. Comparison with shorter reconstructions and documentary evidence validates the new reconstruction and gives additional insight into socioeconomic impacts and spatial patterns of extreme events. The new reconstruction reveals long-term changes in the number of extremes, including substantially fewer drought and pluvial events in the 20th century.

P. heldreichii MXD measurements have previously only spanned the past 500 years, limiting the analysis of long-term temperature variability patterns (Trouet *et al*. 2012; Klesse *et al*. 2015). In the following section, the first millennium-length reconstruction of late summer (August-September) temperature extremes for the Mediterranean region based on MXD measurements is presented

(chapter 4). Analysis of temperature extremes reveals the coldest summers occurring in 1035, 1117, 1217, 1884 and 1959 and the coldest decades being 1061-1070 and 1811-1820. The dominant mode that drives annual-decadal temperature variability along the northeastern Mediterranean is associated with the position of the North Atlantic Jetstream (NAJ) which, in its northward position, generates extremely cold summer temperatures in the region, whereas it brings extremely warm summer temperatures in an anomalous southward position.

Besides the development of long high-quality proxy data and climate reconstructions, the evaluation of current climate reconstructions and proxy datasets is vital to reduce uncertainties in climate reconstruction efforts. An important question that has to be answered within this context concerns the establishment of tree-ring and multiproxy reconstructions that represent temperature variability at all frequencies (Franke *et al*. 2013), since many large-scale temperature reconstructions underestimate low-frequency variability to some extent (Christiansen and Ljungqvist 2017). In this thesis, a first step is undertaken to identify drivers that cause the absence of a long-term cooling trend over the Common Era (until ~1800) in a combined Northern Hemisphere tree-ring data composite that includes 415 records released by the PAGES 2k initiative (chapter 5). From a forcing perspective, cooling trends across the Northern Hemisphere summers, particularly the high latitudes, are expectable in all proxies due to orbitally driven changes in solar irradiance. However, long-term cooling trends are only retained in ice cores, glacier ice, and marine sediments, but not in tree-rings. Following analyses reveal no systematic increase of cooling trends towards high latitudes in response to increased orbital forcing towards the northern tree line. Besides, differences in seasonality as well as regional variations in climate sensitivity do not correlate with the cooling trends, or lack thereof, throughout the Northern Hemisphere. Tests of different detrending methods reveal substantial effects on the reconstructed magnitude of the Late Antique Little Ice Age during the first millennium CE because of their varying ability to preserve low-frequency information in tree-rings. However, none of the applied dendrochronological methods indicate retention of millennial-scale cooling trends in the tree-ring based reconstructions.

The thesis has diverse benefits and its results serve as a base for multiple open research questions. During the last decade, the dendroclimatic community frequently emphasized the need to sample new or, at least, update old millennial length temperature-sensitive tree-ring archives in the extratropical Northern and Southern Hemisphere (Wilson *et al*. 2016). With this dissertation, new millennial-length tree-ring MXD and TRW records as well as one June-July hydroclimate reconstruction and one August-September temperature reconstruction are made publicly available. The data fill a spatial and temporal gap in the European network of millennium-length, annually-resolved tree-ring proxy network. However, both reconstructions presented here focus on the high-frequency spectrum only. An evaluation of cool/warm and dry/wet intervals including the timing and expression of the MWP and LIA and associated atmospheric settings is still pending. Initial analyses have shown that medieval

warming is delayed, supporting the theory of the absence of a global MWP (PAGES 2k Consortium 2013) and demonstrating the need for further analysis.

Additional research needs to be carried out in order to advance our understanding of atmospheric dynamical processes associated with climate variability in (southeastern) Europe. Trouet *et al*. (2018) used the link between MXD formation in the northeastern Mediterranean and British Isles and Northern Hemisphere polar jet stream anomalies to reconstruct North Atlantic Jetstream (NAJ) variability back to 1725. The new millennium-long MXD chronology bears the potential to reconstruct the NAJ over longer timescales. Further, a special characteristic of the dataset introduced here is that TRW and MXD respond to different climate parameters. Potential is given to include other measures such as isotopes (Treydte *et al*. 2007) and wood anatomical features (von Arx and Carrer 2014), to extend the spectrum of climatic and environmental information that can be extracted from *P. heldreichii* tree growth.

This analysis of missing long-term temperature trends in Northern Hemisphere tree-ring records draws attention to the circumstance that the usage of tree-rings in multiproxy reconstructions might contribute to an underestimation of long-term trends and that this characteristic is not caused by an inappropriate tree-ring detrending as previously suggested (Esper *et al*. 2004). The thesis illustrates the need for the community to re-evaluate strategies regarding the best use of climate information from tree-rings for (multi-) proxy climate reconstructions.

References

Abram NJ, McGregor HV, Tierney JE, Evans MN, McKay NP, Kaufman DS, PAGES 2k Consortium. 2016. Early onset of industrial-era warming across the oceans and continents. *Nature* **536**: 411-418.

Akkemik U, Aras A. 2005. Reconstruction (1689-1994 AD) of April-August precipitation in the southern part of central Turkey. *Int. J. Climatol.* **25**: 537-548.

Akkemik U, D'Arrigo R, Cherubini P, Köse N, Jacoby GC. 2008. Tree-ring reconstructions of precipitation and streamflow for north-western Turkey. *Int. J. Climatol.* **28**: 173-183.

Anchukaitis KJ, Wilson R, Briffa KR, Büntgen U, Cook ER, D'Arrigo R, Davi N, Esper J, Frank D, Gunnarson BE, Hegerl G, Helama S, Klesse S, Krusic PJ, Linderholm HW, Myglan V, Osborn TJ, Zhang P, Rydval M, Schneider L, Schurer A, Wiles G, Zorita E. 2017. Last millennium Northern Hemisphere summer temperatures from tree rings: Part II, spatially resolved reconstructions. *Quat. Sci. Rev.* **163**: 1-22.

Böhm R, Jones PD, Hiebl J, Frank D, Brunetti M, Maugeri M. 2009. The early instrumental warm-bias: a solution for long central European temperature series 1760-2007. *Clim. Chang.* **101**: 41-67.

Braconnot P, Harrison SP, Kageyama M, Bartlein PJ, Masson-Delmotte V, Abe-Ouchi A, Otto-Bliesner B, Zhao Y. 2012. Evaluation of climate models using palaeoclimatic data. *Nat. Clim. Chang.* **2**: 417-424.

Briffa KR. 2000. Annual climate variability in the Holocene: interpreting the message of ancient trees. *Quat. Sci. Rev.* **19**: 87-105.

Büntgen U, Frank DC, Nievergelt D, Esper J. 2006. Summer temperature variations in the European Alps, AD 755-2004. *J. Clim.* **19**: 5606-5623.

Büntgen U, Frank D, Grudd H, Esper J. 2008. Long-term summer temperature variations in the Pyrenees. *Clim. Dyn.* **31**: 615-631.

Büntgen U, Tegel W, Nicolussi K, McCormick M, Frank D, Trouet V, Kaplan JO, Herzig F, Heussner KU, Wanner H, Luterbacher J, Esper J. 2011. 2500 years of European climate variability and human susceptibility. *Science* **331**: 578-82.

Büntgen U, Frank D, Neuenschwander T, Esper J. 2012. Fading temperature sensitivity of Alpine tree growth at its Mediterranean margin and associated effects on large-scale climate reconstructions. *Clim. Chang.* **114**: 651-666.

Büntgen U, Kyncl T, Ginzler C, Jacks DS, Esper J, Tegel W, Heussner KU, Kyncl J. 2013. Filling the Eastern European gap in millennium-long temperature reconstructions. *PNAS* **110**: 1773-1778.

Cherubini P, Gärtner H, Esper J, Dobbertin MK, Kaiser KF, Rigling A, Treydte K, Zimmermann NE, Bräker OU. 2004. Jahrringe als Archive für interdisziplinäre Umweltforschung | Annual rings as an archive for interdisciplinary environmental research. *Schweiz. Z. Forstwes.* **155**: 162-168.

Christiansen B, Ljungqvist FC. 2011. Reconstruction of the extratropical NH mean temperature over the last millennium with a method that preserves low-frequency variability. *J. Clim.* **24**: 6013-6034.

Christiansen B, Ljungqvist FC. 2012. The extra-tropical Northern Hemisphere temperature in the last two millennia: reconstructions of low-frequency variability. *Clim. Past* **8**: 765-786.

Christiansen B, Ljungqvist FC. 2017. Challenges and perspectives for large-scale temperature reconstructions of the past two millennia. *Rev. Geophys.* **55**: 40-96.

Cooper TF, O'Leary RA, Lough JM. 2012. Growth of Western Australian corals in the anthropocene. *Science* **335**: 593-596.

Crowley TJ, Lowery TS. 2000. How warm was the Medieval Warm Period? *Ambio* **29**: 51-54.

Crutzen PJ. 2002. Geology of mankind. *Nature* **415**: 23.

D'Arrigo R, Wilson R, Jacoby G. 2006. On the long-term context for late twentieth century warming. *J. Geophys. Res.* **111**: D03103, doi: 10.1029/2005JD006352.

Deser C, Phillips A, Bourdette V, Teng H. 2012. Uncertainty in climate change projections: the role of internal variability. *Clim. Dyn.* **38**: 527-546.

Dobrovolný P, Moberg A, Brázdil R, Pfister C, Glaser R, Wilson R, van Engelen A, Limanówka D, Kiss A, Halícková M, Macková J, Riemann D, Luterbacher J, Böhm R. 2010. Monthly, seasonal and annual temperature reconstructions for Central Europe derived from documentary evidence and instrumental records since AD 1500. *Clim. Chang.* **101**: 69-107.

Esper J, Cook ER, Schweingruber FH. 2002. Low-frequency signals in long tree-ring chronologies for reconstructing past temperature variability. *Science* **295**: 2250-2253.

Esper J, Treydte K, Frank DC, Gärtner H, Büntgen U. 2004. Temperaturvariationen und Jahrringe | Temperature variation and tree rings. *Schweiz. Z. Forstwes.* **155**: 213-221.

Esper J, Büntgen U, Timonen M, Frank DC. 2012. Variability and extremes of northern Scandinavian summer temperatures over the past two millennia. *Glob. Planet. Chang.* **88-89**: 1-9.

Esper J, Büntgen U, Luterbacher J, Krusic PJ. 2013a. Testing the hypothesis of post-volcanic missing rings in temperature sensitive dendrochronological data. *Dendrochronologia* **31**: 216-222.

Esper J, Schneider L, Krusic PJ, Luterbacher J, Büntgen U, Timonen M, Sirocko F, Zorita E. 2013b. European summer temperature response to annually dated volcanic eruptions over the past nine centuries. *Bull. Volcanol.* **75**: 736.

Esper J, St. George S, Anchukaitis KJ, D'Arrigo R, Ljungqvist FC, Luterbacher J, Schneider L, Stoffel M, Wilson R and Büntgen U. 2018. Large-scale, millennial-length temperature reconstructions from tree-rings. *Dendrochronologia* **50**: 81-90.

Franke J, Frank D, Raible CC, Esper J, Bronnimann S. 2013. Spectral biases in tree-ring climate proxies. *Nat. Clim. Chang.* **3**: 360-364.

Fritts HC. 1976. *Tree rings and climate*. Blackburn Press: Caldwell, USA.

Grissino-Mayer HD, Fritts HC. 1997. The International Tree-Ring Data Bank: An enhanced global database serving the global scientific community. *Holocene* **7**: 235-238.

Gunnarson BE, Linderholm HW, Moberg A. 2011. Improving a tree-ring reconstruction from west-central Scandinavia: 900 years of warm-season temperatures. *Clim. Dyn.* **36**: 97-108.

Hartmann DL, Klein Tank AMG, Rusticucci M, Alexander LV, Brönnimann S, Charabi Y, Dentener FJ, Dlugokencky EJ, Easterling DR, Kaplan A, Soden BJ, Thorne PW, Wild M, Zhai, PM. 2013. Observations: Atmosphere and Surface. In *Climate Change 2013: The Physical Science Basis. Contribution of Working Group I to the Fifth Assessment Report of the Intergovernmental Panel on Climate Change,* Stocker TF, Qin D, Plattner GK, Tignor M, Allen SK, Boschung J, Nauels A, Xia Y, Bex V, Midgley PM (eds). Cambridge University Press, Cambridge, pp. 159-254.

Hegerl GC, Crowley TJ, Allen M, Hyde WT, Pollack HN, Smerdon J, Zorita E. 2007. Detection of human influence on a new, validated 1500-year temperature reconstruction. *J. Clim.* **20**: 650-666.

Jones PD, Briffa KR, Barnett TP, Tett SFB. 1998. High-resolution palaeoclimatic records for the last millennium: interpretation, integration and comparison with General Circulation Model control-run temperatures. *Holocene* **8**: 455-471.

Jones PD, Briffa KR, Osborn TJ, Lough JM, van Ommen TD, Vinther BM, Luterbacher J, Wahl ER, Zwiers F W, Mann ME, Schmidt GA, Ammann CM, Buckley BM, Cobb KM, Esper J, Goosse H, Graham N, Jansen E, Kiefer T, Kull C, Kuttel M, Mosley-Thompson E, Overpeck JT, Riedwyl N, Schulz M, Tudhope AW, Villalba R, Wanner H, Wolff E, Xoplaki E. 2009. High-resolution palaeoclimatology of the last millennium: a review of current status and future prospects. *Holocene* **19**: 3-49.

Juckes MN, Allen MR, Briffa KR, Esper J, Hegerl GC, Moberg A, Osborn TJ, Weber SL. 2007. Millennial temperature reconstruction intercomparison and evaluation. *Clim. Past* **3**: 591-609.

Kinnard C, Zdanowicz CM, Fisher DA, Isaksson E, de Vernal A, Thompson LG. 2011. Reconstructed changes in Arctic sea ice over the past 1,450 years. *Nature* **479**: 509-512.

Klesse S, Ziehmer M, Rousakis G, Trouet V, Frank D. 2015. Synoptic drivers of 400 years of summer temperature and precipitation variability on Mt. Olympus, Greece. *Clim. Dyn.* **45**: 807-824.

Lenz O, Schär E, Schweingruber FH. 1976. Methodische Probleme bei der radiographisch-densitometrischen Bestimmung der Dichte und der Jahrringbreiten von Holz. *Holzforschung* **30**: 114-123.

Leonelli G, Coppola A, Salvatore MC, Baroni C, Battipaglia G, Gentilesca T, Ripullone F, Borghetti M, Conte E, Tognetti R, Marchetti M, Lombardi F, Brunetti M, Maugeri M, Pelfini M, Cherubini P, Provenzale A, Maggi V. 2017. Climate signals in a multispecies tree-ring network from central and southern Italy and reconstruction of the late summer temperatures since the early 1700s. *Clim. Past* **13**: 1451-1471.

Ljungqvist FC. 2010. A new reconstruction of temperature variability in the extra-tropical Northern Hemisphere during the last two millennia. *Geografiska Annaler Series* **92A**: 339-351.

Loehle C. 2007. A 2000-year global temperature reconstruction based on non tree-ring proxies. *Energy Environ.* **18**: 1049-1058.

Mann ME, Bradley RS, Hughes MK. 1999. Northern hemisphere temperatures during the past millennium: Inferences, uncertainties, and limitations. *Geophys. Res. Lett.* **26**: 759-762.

Mann ME, Jones PD. 2003. Global surface temperatures over the past two millennia. *Geophys. Res. Lett.* **30**: 1820, doi:10.1029/2003GL017814.

Mann ME, Zhang Z, Hughes MK, Bradley RS, Miller SK, Rutherford S, Ni F. 2008. Proxy-based reconstructions of hemispheric and global surface temperature variations over the past two millennia. *PNAS* **105**: 13252-13257.

Martín-Chivelet J, Muñoz-García MB, Edwards RL, Turrero MJ, Ortega AI. 2011. Land surface temperature changes in Northern Iberia since 4000yrBP, based on δ13C of speleothems. *Glob. Planet. Chang.* **77**: 1-12.

McGregor HV, Evans MN, Goosse H, Leduc G, Martrat B, Addison JA, Mortyn PG, Oppo DW, Seidenkrantz MS, Sicre MA, Phipps SJ, Selvaraj K, Thirumalai K, Filipsson HL, Ersek V. 2015. Robust global ocean cooling trend for the pre-industrial Common Era. *Nat Geosci.* **8**: 671-677.

Melvin TM, Grudd H, Briffa KR. 2013. Potential bias in 'updating' tree-ring chronologies using regional curve standardisation: Re-processing 1500 years of Torneträsk density and ring-width data. *Holocene* **23**: 364-373.

Moberg A, Sonechkin DM, Holmgren K, Datsenko NM, Karlen W, Lauritzen SE. 2005. Highly variable Northern Hemisphere temperatures reconstructed from low- and high-resolution proxy data. *Nature* **433**: 613-617.

Morice CP, Kennedy JJ, Rayner NA, Jones PD. 2012. Quantifying uncertainties in global and regional temperature change using an ensemble of observational estimates: The HadCRUT4 data set. *J. Geophys. Res.* 117: D08101, doi:10.1029/2011JD017187.

Neukom R, Gergis J, Karoly DJ, Wanner H, Curran M, Elbert J, Gonzalez-Rouco F, Linsley BK, Moy AD, Mundo I, Raible CC, Steig EJ, van Ommen T, Vance T, Villalba R, Zinke J, Frank D. 2014. Inter-hemispheric temperature variability over the past millennium. *Nat. Clim. Chang.* **4**: 362-367.

Nieto-Moreno V, Martínez-Ruiz F, Willmott V, García-Orellana J, Masqué P, Sinninghe Damsté JS. 2013. Climate conditions in the westernmost Mediterranean over the last two millennia: An integrated biomarker approach. *Org. Geochem.* **55**: 1-10.

PAGES 2k Consortium. 2013. Continental-scale temperature variability during the past two millennia. *Nat. Geosci.* **6**: 339-346.

PAGES 2k PMIP3 group. 2015. Continental-scale temperature variability in PMIP3 simulations and PAGES 2k regional temperature reconstructions over the past millennium. *Geophys. Res. Lett.* **11**: 1673-1699.

PAGES 2k Consortium. 2017. A global multiproxy database for temperature reconstructions of the Common Era. *Nat. Sci. Data.* **4**: 1-33.

Pfister C, Brazdil R, Glaser R, Barriendos M, Camuffo D, Deutsch M, Dobrovolný P, Enzi S, Guidoboni E, Kotyza O, Militzer S, Racz L, Rodrigo FS. 1999. Documentary evidence on climate in sixteenth-century Europe. *Clim. Chang.* **43**: 55-110.

Plomion C, Leprovost G, Stokes A. 2001. Wood formation in trees. *Plant Physiol.* **127**: 1513-1523.

Popa I, Kern Z. 2009. Long-term summer temperature reconstruction inferred from tree-ring records from the Eastern Carpathians. *Clim. Dyn.* **32**: 1107-1117.

Rossi S, Deslauriers A, Anfodillo T, Carraro V. 2007. Evidence of threshold temperatures for xylogenesis in conifers at high altitudes. *Oecologia* **152**: 1-12.

Schneider L, Smerdon JE, Büntgen U, Wilson RJS, Myglan VS, Kirdyanov AV, Esper J. 2015. Revising midlatitude summer temperatures back to A.D. 600 based on a wood density network. *Geophys. Res. Lett.* **42**: 4556-4562.

Schweingruber FH, Bartholin T, Schaur E, Briffa KR. 1988. Radiodensitometric-dendroclimatological conifer chronologies from Lapland (Scandinavia) and the Alps (Switzerland). *Boreas* **17**: 559-566.

Seim A, Büntgen U, Fonti P, Haska H, Herzig F, Tegel W, Trouet V, Treydte K. 2012. Climate sensitivity of a millennium-long pine chronology from Albania. *Clim. Res.* **51**: 217-228.

Shi F, Yang B, Mairesse A, von Gunten L, Li J, Bräuning A, Yang F, Xiao X. 2013. Northern Hemisphere temperature reconstruction during the last millennium using multiple annual proxies. *Clim. Res.* **56**: 231-244.

Stoffel M, Khodri M, Corona C, Guillet S, Poulain V, Bekki S, Guiot J, Luckman BH, Oppenheimer C, Lebas N, Beniston M, Masson-Delmotte V. 2015. Estimates of volcanic-induced cooling in the Northern Hemisphere over the past 1,500 years. *Nature Geosci.* **8**: 784-788.

Tejedor E, de Luis M, Cuadrat JM, Esper J, Saz MA. 2016. Tree-ring-based drought reconstruction in the Iberian Range (east of Spain) since 1694. *Int. J. Biometeorol.* **60**: 361-72.

Touchan R, Funkhouser G, Hughes MK, Erkan N. 2005. Standardized precipitation index reconstructed from Turkish tree-ring widths. *Clim. Chang.* **72**: 339-353.

Treydte K, Frank D, Esper J, Andreu L, Bednarz Z, Berninger F, Boettger T, D'Alessandro CM, Etien N, Filot M, Grabner M, Guillemin MT, Gutierrez E, Haupt M, Helle, Hilasvuori E, Jungner H, Kalela-Brundin M, Krapiec M, Leuenberger M, Loader NJ, Masson-Delmotte V, Pazdur A, Pawelczyk S, Pierre M, Planells O, Pukiene R, Reynolds-Henne CE, Rinne KT, Saracino A, Saurer M, Sonninen E, Stievenard M, Switsur VR, Szczepanek M, Szychowska-Krapiec E, Todaro L, Waterhouse JS, Weigl M, Schleser GH. 2007. Signal strength and climate calibration of a European tree-ring isotope network. *Geophys. Res. Lett.* **34**: L24302, doi:10.1029/2007GL031106.

Trouet V, Panayotov MP, Ivanova A, Frank D. 2012. A pan-European summer teleconnection mode recorded by a new temperature reconstruction from the northeastern Mediterranean (AD 1768-2008). *Holocene* **22**: 887-898.

Trouet V. 2014. A tree-ring based late summer temperature reconstruction (AD 1675-1980) for the northeastern Mediterranean. *Radiocarbon* **56**: 69-78.

Trouet V, Babst F, Meko M. 2018. Recent enhanced high-summer North Atlantic Jet variability emerges from three-century context. *Nat. Commun.* **9**, 180-189.

Wanner H, Beer J, Bütikofer J, Crowley TJ, Cubasch U, Flückiger J, Goosse H, Grosjean M, Joos F, Kaplan JO, Küttel M, Müller SA, Prentice IC, Solomina O, Stocker TF, Tarasov P, Wagner M, Widmann M. 2008. Mid- to Late Holocene climate change: an overview. *Quat. Sci. Rev.* **27**: 1791-1828.

Wilson R, Anchukaitis K, Briffa KR, Büntgen U, Cook E, D'Arrigo R, Davi N, Esper J, Frank D, Gunnarson B, Hegerl G, Helama S, Klesse S, Krusic PJ, Linderholm HW, Myglan V, Osborn TJ, Rydval M, Schneider L, Schurer A, Wiles G, Zhang P, Zorita E. 2016. Last millennium northern hemisphere summer temperatures from tree rings: Part I: The long term context. *Quat. Sci. Rev.* **134**: 1-18.

von Arx G, Carrer M. 2014. ROXAS - A new tool to build centuries-long tracheid-lumen chronologies in conifers. *Dendrochronologia* **32**: 290-293.

Zhao S, Pederson N, D'Orangeville L, HilleRisLambers J, Boose E, Penone C, Bauer B, Jiang Y, Manzanedo Rubén D. 2018. The International Tree-Ring Data Bank (ITRDB) revisited: Data availability and global ecological representativity. *J. Biogeogr.* **46***:* 355-368.

List of figures

List of tables

Curriculum vitae

Not available online